UCRL-20390

OPTICALLY DETECTED MAGNETIC RESONANCE OF MOLECULES IN EXCITED TRIPLET STATES

Michael J. Buckley
(Ph. D. Thesis)

February 1971

AEC Contract No. W-7405-eng-48

LAWRENCE RADIATION LABORATORY
UNIVERSITY of CALIFORNIA BERKELEY

UCRL-20390

DISCLAIMER

PAGES i to ii

WERE INTENTIONALLY

LEFT BLANK

TABLE OF CONTENTS

OPTICALLY DETECTED MAGNETIC RESONANCE OF MOLECULES IN EXCITED TRIPLET STATES

Michael J. Buckley

Department of Chemistry, University of California, and
Inorganic Materials Research Division, Lawrence Radiation Laboratory,
Berkeley, California 94720

ABSTRACT

The sensitivity of optically detected magnetic resonance (ODMR) as a function of the intramolecular energy transfer processes is developed along with the explicit form of the spin Hamiltonian used in ODMR with zero external magnetic field. The main features of the optically detected ESR and ENDOR spectra in zero field for molecules with one $I = 1$ or $I = 3/2$ nuclear spin is presented.

The optically detected ESR spectra of the $^3\pi\pi^*$ state of 8-chloroquinoline, the $^3n\pi^*$ state of pyrazine and the $^3\pi\pi^*$ state of paradichlorobenzene are reported. In addition the ^{35}Cl and ^{37}Cl ENDOR spectra are reported for the excited triplet states of 8-chloroquinoline and paradichlorobenzene. The observed ODMR spectra are interpreted in terms of a spin Hamiltonian incorporating the electron spin-spin, nuclear quadrupole and nuclear-electron hyperfine interactions.

The $^3\pi\pi^*$ state of 8-chloroquinoline is found to have essentially the same values for the electron spin-spin interaction as the $^3\pi\pi^*$ state of

quinoline. The chlorine nuclear quadrupole coupling constant of the $^3\pi\pi^*$ state of 8-chloroquinoline is approximately the same as the values reported for the ground state of similar molecules, indicating that the chlorine electric field gradient is not significantly changed upon excitation.

The large electron spin-spin interaction measured for the $^3n\pi^*$ state of pyrazine is explained in terms of the one-center contribution to the interaction. Analysis of the nitrogen hyperfine interaction gives the approximate values for the spin density of 0.28 and 0.35 for the nitrogen π^* and n orbitals respectively.

The ODMR and phosphorescence microwave double resonance (PMDR) spectra of paradichlorobenzene are consistent with the hypothesis that the excited state is a $^3\pi\pi^*$ state and that the symmetry of the excited state is B_{2u}. From the assigned orientation of the electron spin-spin tensor, the spin density appears to be localized primarily on the four carbon atoms that are not bonded to the chlorines. The small value of the chlorine out-of-plane hyperfine element leads to the conclusion that the chlorines do not participate significantly in the excitation. On the basis of the PMDR spectra and the reduced value of the chlorine nuclear quadrupole coupling constant as compared to the value for the ground state, it is further hypothesized that the C-Cl bonds are bent and that the molecule possesses C_{2h} rather than D_{2h} spacial symmetry in the excited state.

I. INTRODUCTION

Since the success of optically detected magnetic resonance (ODMR) of the lowest triplet state of organic molecules is highly dependent on the nature of the triplet state, a short review of some of the most important properties of the triplet state is given in this section. There are several very good review articles on the triplet state to which the reader is referred for a more complete discussion.[1-3] The second half of this section is devoted to the historical development of ODMR and a survey of previous experimental results.

A. The Excited Triplet State in Organic Molecules

The ground state of most organic molecules consists of a singlet electron configuration in which all the electrons have their spins paired. The molecule may be excited to a higher energy electron configuration by the application of electromagnetic radiation of the appropriate energy. We will primarily be concerned with the excited electron configurations produced when one electron in the highest bonding molecular orbital (ϕ_A) is promoted to the lowest non-bonding molecular orbital (ϕ_B). Since electrons have a spin of $\frac{1}{2}$, there are four possible orientations for the two unpaired electrons, which, if we let α equal spin up and β equal spin down, may be represented as,

$$\begin{array}{lll} \alpha(1)\ \alpha(2) & S_z = 1 & S^2 = 1 \\ \alpha(1)\ \beta(2) & S_z = 0 & S^2 = 0 \\ \beta(1)\ \alpha(2) & S_z = 0 & S^2 = 0 \\ \beta(1)\ \beta(2) & S_z = -1 & S^2 = 1 \end{array} \qquad (1)$$

This representation, however, is not satisfactory since the electrons obey Fermi-Dirac statistics and therefore the total wave function (orbital times spin) must be antisymmetric with respect to electron exchange. In addition, we would like the spin functions to be eigenstates of S^2 and Sz. The spin functions $\alpha(1)\ \alpha(2)$ and $\beta(1)\ \beta(2)$ are clearly eigenstates of S^2 and Sz since $S^2 = 1$ for both and Sz = +1 and -1 respectively. We can generate the Sz = 0 component of the triplet spin state by applying the lowering operator to the $\alpha(1)\ \alpha(2)$ state which gives us the desired spin function,

$$^3\psi_o = [1/\sqrt{2}]\ [\alpha(1)\ \beta(2) + \beta(1)\ \alpha(2)] \quad (2)$$

The remaining spin function is a singlet

$$^1\psi = [1/\sqrt{2}][\alpha(1)\ \beta(2) - \beta(1)\ \alpha(2)] \quad (3)$$

and, in contrast to the triplet spin functions, is antisymmetric with respect to electron exchange.

The spacial part of the excited state electron wavefunction may be respesented as a symmetric (+) and antisymmetric (-) linear combination of ϕ_A and ϕ_B as:

$$\psi_\pm = [1/\sqrt{2}][\phi_A(1)\ \phi_B(2) \pm \phi_A(2)\ \phi_B(1)] \quad (4)$$

Since the total wavefunction must be antisymmetric, there are only four allowed representations of the total wavefunction; a singlet state with a symmetric spacial function and an antisymmetric spin function,

$$^1\underline{\psi} = \left([1/\sqrt{2}][\phi_A(1)\phi_B(2) + \phi_A(2)\phi_B(1)]\right)\left([1/\sqrt{2}][\alpha(1)\alpha(2) - \beta(1)\beta(2)]\right) \quad (5)$$

and a triplet state with an antisymmetric spacial function and a symmetric spin function

$$^3\underline{\Psi} = [1/\sqrt{2}][\phi_A(1)\phi_B(2) - \phi_A(2)\phi_B(1)]\cdot \begin{Bmatrix} \alpha(1)\alpha(2) \\ [1/\sqrt{2}][\alpha(1)\beta(2) + \beta(1)\alpha(2)] \\ \beta(1)\beta(2) \end{Bmatrix} \quad (6)$$

The repulsive electrostatic interaction between the two unpaired electrons gives rise to a term in the total Hamiltonian equal to e^2/r_{12}, where e is the electron charge and r_{12} is the vector connecting the two electrons. This term removes the degeneracy of the singlet and triplet states and results in the singlet state going to higher energy while the triplet state is shifted to lower energy with an energy separation between the two states of

$$^1E - {}^3E = 2\delta_{12} \quad (7)$$

where δ_{12} is the exchange integral given by

$$\delta_{12} = \langle \phi_A(1)\phi_B(2) | e^2/r_{12} | \phi_A(2)\phi_B(1) \rangle \quad (8)$$

For most organic molecules $2\,\delta_{12}$ is 5000 to 10000 cm^{-1}. As will be discussed in the section on the spin Hamiltonian, the inclusion of the magnetic dipole-dipole interaction in the Hamiltonian removes the three fold degeneracy of the triplet state. This splitting is usually referred to as the zero field splitting and is on the order of 0.1 cm^{-1}.

An additional contribution to the zero field splitting arises from the coupling of the spin and orbital electron angular momentum and is of the form $A(L\cdot s)$ where L and s are the spin and orbital angular momentum quantum numbers and A is a constant that depends on

the particular molecule being considered. The effect of the spin orbit Hamiltonian is to mix states of different multiplicity and, therefore, to give singlet character to triplet states and vice versa. The most important effect of this is to permit the triplet state to undergo weak electric dipole radiation to the ground state (phosphorescence), the intensity from each of the three triplet sublevels being a function of the spin orbit coupling to both the excited and the ground singlet states.

Since the sensitivity of ODMR depends upon the number of molecules in their triplet state, an important consideration is intramolecular energy transfer processes. Following excitation, a molecule may lose energy by radiative or non-radiative pathways as shown in Figure 1. Phosphorescence ($T_1 \rightarrow S_0$) and fluorescence ($S_1 \rightarrow S_0$) comprise the radiative pathways and proceed with rate constants on the order of 10^4 to 10^{-2} sec^{-1} and 10^6 to 10^9 sec^{-1}, respectively. The longer lifetime for phosphorescence results from the fact that the triplet state is spin-forbidden for electric dipole radiation to the ground state.

The molecule may also lose energy through three non-radiative pathways.

1) Vibrational Relaxation -- or passage from a non-equilibrium vibrational energy distribution in a given electronic state to the Boltzmann energy distribution relative to the zero point energy of that same state. This proceeds primarily by a non-radiative mechanism with a rate constant of approximately 10^{12} $sec.^{-1}$

2) Internal Conversion -- or radiationless passage between two electronic states of the same spin multiplicity. The pathway also has a fast rate constant of approximately 10^{12} $sec.^{-1}$

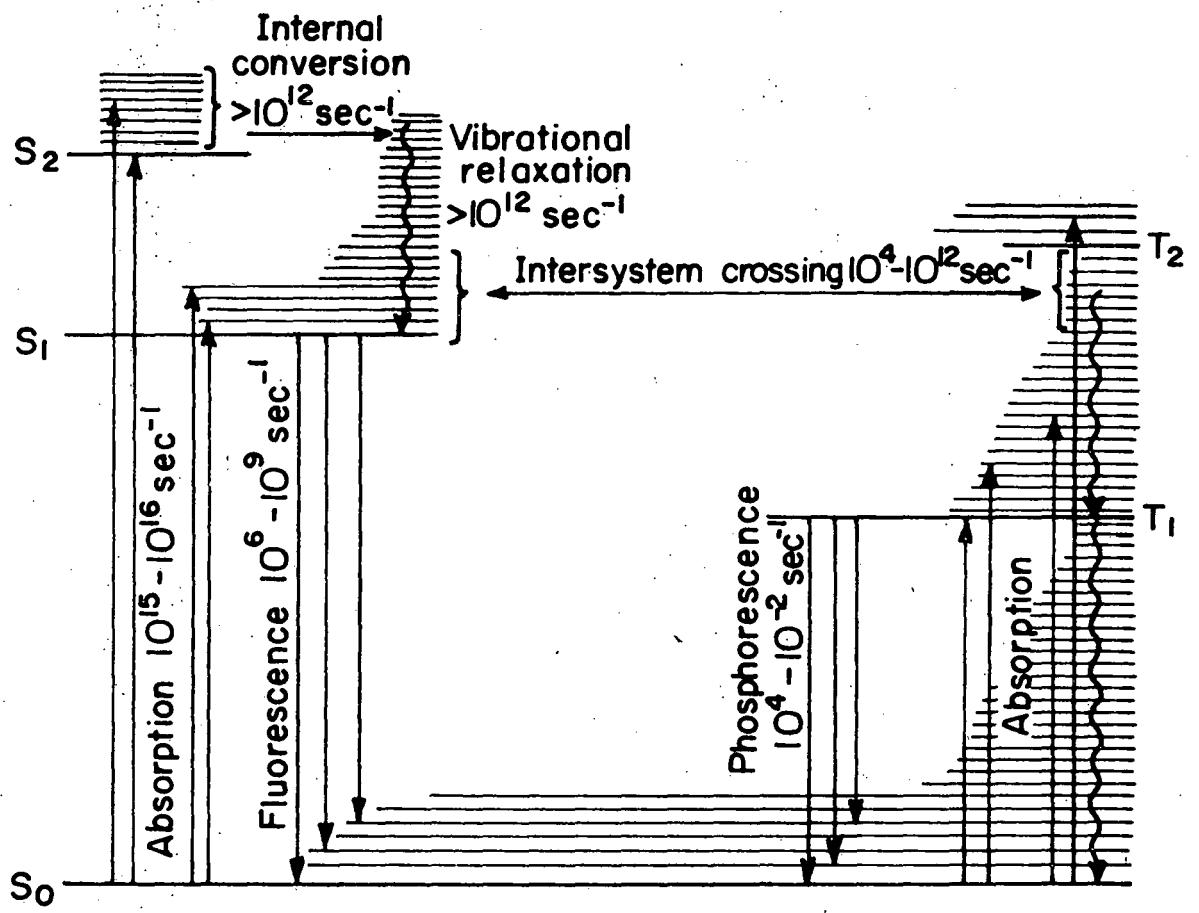

XBL 7012-7263

Figure 1

Intramolecular Energy Transfer Pathways and Rate Constants

3) Intersystem Crossing -- or radiationless passage from an electronic state in the singlet manifold to an electronic state in the triplet manifold or vice versa. This pathway is slower than the other two and is on the order of 10^4 to 10^{12} $sec.^{-1}$

The lowest triplet state may be populated either by direct excitation into the triplet manifold followed by vibrational relaxation to the lowest vibrational level of T_1 or by excitation into the singlet manifold followed by intersystem crossing into the triplet manifold. The latter is usually more efficient due to its larger cross section.

Although the exact mechanisms of intersystem crossing are not completely understood, it is generally found that at liquid helium temperatures (4.20° K) the triplet sublevels of the lowest triplet state have unequal populations and consequently, a state of alignment exists for the electron spins.[4]

The various rate constants for energy transfer, the existence of spin alignment, and the spin lattice relaxation rate between the triplet spin sublevels are all important factors in determining the sensitivity of ODMR as will be shown in section II.

B. The Historical Development of ODMR

The development of any field of science is difficult to trace since every advancement is dependent on the work of many previous researchers; however, we will choose for the starting point of this discussion the extensive study of the phosphorescence of organic molecules by Lewis and Kasha[5,6] in 1944. In their series of papers it was proposed that the

phosphorescent state of these molecules corresponded to their lowest triplet state. This hypothesis was strongly supported shortly thereafter by magnetic susceptibility measurements[7,8] which showed that small changes in the susceptibility were observed upon irradiation of the samples.

As with any major change in the existing paradigm of science, this hypothesis was not universally accepted.[9] The most distressing aspect of the hypothesis was the failure to observe the predicted electron spin resonance (ESR) of the phosphorescent state. The problem was resolved in 1958 when Hutchison and Mangum[10,11] succeeded in observing the ESR of naphthalene in its phosphorescent state and showed conclusively that the phosphorescent state was a triplet state. The experiment was performed by using conventional techniques in that the absorption of the microwave energy was monitored while varying the applied magnetic field. The sample, consisting of a single crystal of durene containing 2 to 5 mole percent naphthalene, was maintained at liquid nitrogen temperature while irradiating with a mercury arc lamp. The resonance signal was observed to decay with the same lifetime as the phosphorescence upon extinguishing the exciting light, proving that the phosphorescent state was being detected. The observed resonance spectra showed that the triplet state was already split into three levels in the absence of a magnetic field which explained the failure of previous experiments using randomly oriented samples to detect the resonance.

Subsequently, the triplet state ESR of many organic compounds was observed; however, most of the work was done on randomly oriented samples. Since only one parameter can usually be measured with randomly oriented

samples, the separation of the three levels of the triplet could not be determined. In certain cases[12,13] the three levels can be assigned but the assignment is difficult and the method has not been used often.

The limited sensitivity of ESR and the difficulty of preparing single crystal samples has restricted the number of molecules investigated. Only 14 molecules have been reported to date using conventional methods and they are all characterized by relatively long lived π-π^* triplet states (see Table 1).

The next major change in the existing paradigm occurred in 1965 when Geschwind, Devlin, Cohen and Chinn[14] reported the optical detection of the ESR of the excited metastable $\bar{E}$ (2E) state of Cr^{+3} in Al_2O_3. In this classic experiment they showed that the optical rf double resonance techniques first suggested by Brossel and Kastler[15] and widely used in gases[16] could also be applied to solids. The experiment was performed using a high resolution optical spectrometer to monitor the change in intensity of one of the Zeeman components of the fluorescent light [$\bar{E}$ (2E) $\rightarrow$ $^4A_2$] as $\bar{E}$ was saturated with microwaves when the magnetic field was swept through resonance. The resonance signal was observed by modulating the microwave field and detecting the resultant modulation of the optical emission. Since optical rather than microwave photons are detected, the sensitivity may be increased several orders of magnitude over conventional techniques. As an example, at temperatures below the λ point of helium the resonance could be observed directly on an oscilloscope without the need for phase sensitive detection. The success in optically detecting the electron spin resonance of a metastable state

led several research groups to attempt to apply the same principles to the optical detection of the ESR of organic molecules in their lowest triplet state.

In 1967 the first successful experiment was reported by Sharnoff for the $\Delta M = 2$ transition of naphthalene.[17] In this experiment a single crystal of biphenyl containing 0.1 mole percent naphthalene was placed in a microwave cavity where it was immersed in liquid helium maintained at 1.8° K. The crystal was irradiated with the appropriately filtered light from a mercury arc lamp and the phosphorescence isolated with a detector consisting of a linear polarizer and a low resolution spectrometer. The microwave field was modulated at 40 Hz and the signal detected by feeding the output of the photomultiplier into a phase sensitive amplifier. In this experiment it was shown that the radiative matrix elements connecting any triplet sublevel with the ground singlet electronic level are functions of the magnetic quantum numbers of that sublevel.

At this point the development of ODMR of the lowest triplet state of organic molecules entered a new phase. Now that this new method was shown to be applicable to these molecules the research centered around improving the basic techniques and using this new tool to gain information on the various phenomena associated with the triplet state.

Shortly after Sharnoff's paper, Kwiram[18] reported the optical detection of the $\Delta M = 1$ and $\Delta M = 2$ transitions of phenanthrene in its triplet state. In this investigation the experimental methods were the same as those used by Sharnoff except that the microwave field was not modulated while the exciting and emitted light was chopped antisynchronously at 50 Hz.

The 50 Hz output of the photomultiplier was converted to DC by a phase sensitive detector and fed into a signal averager. The observed change in intensity of the phosphorescence at the three transition frequencies was used to assign the spacial symmetry of the triplet state.

Schmidt, Hesselmann, De Groot and van der Waals also reported the optical detection of quinoxaline (d_6) in 1967. Their experimental procedure was basically the same as that used by Sharnoff, except that they modulated the magnetic field with and without amplitude modulation of the microwave field. They were able to show (1) that the emission originates from the top spin component (out-of-plane), and (2) from phosphorescence decay studies, that entry into the triplet state by intersystem crossing is also to the top spin component.

In 1968 Schmidt and van der Waals[20] extended the almost zero field work (3G) of Hutchison's group[21] by optically detecting the zero-field transitions of molecules in their triplet state at zero external magnetic field. Since it is necessary to vary the microwave frequency in order to observe the resonance in zero external magnetic field, a helix was used to couple the microwave power to the sample. The observed signals were extremely sharp and in the case of quinoxaline (d_6), showed fine structure which was tentatively explained on the basis of a first order nitrogen nuclear quadrupole and second order nitrogen hyperfine interactions. The structure was explained quantitatively in a later paper[22] in terms of a Hamiltonian incorporating these interactions.

Tinti, El-Sayed, Maki and Harris[23] extended the method of optical detection in zero field by incorporating a high resolution spectrometer

and studying the effect of the microwave field on the individual lines of the phosphorescence spectrum of 2,3-dichloroquinoxaline. They showed that the use of a high resolution spectrometer will give better sensitivity in cases where there is mixed polarization of the phosphorescence, since if the total emission is monitored, the change in intensity due to the microwave field may be partially cancelled. The sensitivity was excellent, and in fact, a very strong signal was observed using C. W. conditions for both the microwave and optical radiations. The observed structure of the zero-field transitions was explained quantitatively in a later paper[24] in which the first optically detected electron nuclear double resonance (ENDOR) for nitrogen was also reported. Several other papers followed on the observation and interpretation of nitrogen ENDOR in zero field[25,26] and was extended to ^{35}Cl and ^{37}Cl by Buckley and Harris[27]. Optical detection of electron-electron double resonance (EEDOR) was reported by Kuan, Tinti and El-Sayed[28] and was demonstrated to be a method of improving the signal strength of weak zero-field transitions if emission is from only one of the triplet sublevels.

Several interesting physical phenomena have been reported recently, including such areas as level anticrossing, [51] transferred hyperfine and nuclear quadrupole interactions from host to guest molecules[52] and the prediction of microwave modulation of the phosphorescence.[53]

As a consequence of the newness of this field most of the ODMR studies to date have been on molecules previously reported using conventional techniques (see Table 2). However, molecules with short triplet lifetimes which cannot be observed by conventional methods have received considerable

attention and the resonances of several new molecules have been reported (see Table 3).

One of the most promising new applications of magnetic resonance is the investigation of exciton interactions in crystals. Wolf and his co-workers using conventional ESR techniques have observed energy exchange between pairs of naphthalene (h_8) molecules as nearest neighbors in an isotopically dilute system,[29] and triplet excitons in pure crystals of naphthalene and anthracene single crystals.[54] Sharnoff has reported the ODMR of triplet exitons in a single crystal of benzophenone[34-35]; however, his results have been questioned[51] and to date no other reports have been published of the ODMR of excitons in molecular crystals.*

In conclusion, ODMR has developed into three basic areas: 1) the study of the electron distribution of organic molecules in their triplet state by analysis of the zero field, nuclear quadrupole and hyperfine interactions, 2) investigations into the intramolecular as well as intermolecular pathways and rates of energy transfer in trap molecules by analysis of the ODMR signal as a function of time for various vibronic bands in the phosphorescence spectrum, and 3) as a tool to investigate the energy levels and dynamic properties of exciton bands in molecular crystals.

* Recently, however, Francis and Harris[76] have used this technique to measure the density of states functions of triplet Frenkel excitons in molecular crystals and have observed coherent migration.

Table 1

Single Crystal ESR Studies

Molecule	Host Crystal	T(°K)	D(GHz)*	E(GHz)*	Ref.
Anthracene	Diphenyl	77	+2.1453	- .253	55
Benzene	Benzene-d_6	1.95	+4.740	- .192	93
Diphenylmethylene	Benzophenone	77	±12.1430	∓ .5750	46-48
Diphenylmethylene	1,1-Diphenylethylene	77	±11.8837	∓ .4473	46-48
Fluorene	Fluroene		± 2.9140	∓1.3341	41
Fluorenylidene	Diazafluorene	77	±12.2683	∓ .8478	47,48
Isoquinoline	Durene	77	± 3.0099	∓ .3508	43
Mesitylene	B-Trimethylborazole	77	± 1.8586	∓ .7195	78
Naphthalene-h_8	Durene	77	+ 3.0069	- .4107	10,11,40,41
Naphthalene-h_8	Biphenyl	77	+ 2.9739	- .4632	10,11,40,41
			+ 2.9799	- .4617	10,11,40,41
Naphthalene-d_8	Durene-d_{14}	77	+ 3.03807	- .4176	10,11,40,41
			+ 3.0279	- .4017	10,11,40,41
Phenanthrene	Biphenyl	78	± 3.01079	∓1.3963	21
			± 3.0111	∓1.3961	10,11,40,41
			± 3.0219	∓1.4000	10,11,40,41
Phenanthrene	Fluorene		± 3.0129	∓1.4000	10,11,40,41
Phenazine	Diphenyl	90	+ 2.2304	- .3298	49
Pyrene-h_{10}	Fluorene	100	± 2.0326	∓ .9479	44
Pyrene-d_{10}	Fluorene	room temp	± 1.9717	∓ .9479	45
Quinoxaline	Durene	77	± 3.0189	∓ .5456	42
Quinoline	Durene	77	± 3.0878	∓ .4857	43
Tetramethylpyrazine	Durene	77	± 2.9679	∓ .1289	50

* The zero field splitting parameters D and E are discussed in Section III, pp. 33-40.

Table 2

ODMR of Molecules Previously Observed by Conventional Techniques

Molecule	Reference
Naphthalene	17
Quinoxaline	19
Quinoline	39
Phenanthrene	18
Isoquinoline	39
Tetramethylpyrazine	20

Table 3

New Molecules Observed using ODMR

Molecule	Host	T(°K)	D(GHz)	E(GHz)	Ref.
Benzophenone[a]	------	4.2	+ 4.557	- .630	34
			+ 4.4309	- .4977	35
2,3 dichloroquinoxaline	Durene	1.6	+ 2.9849	- .5271	24
8-chloroquinoline	Durene	1.7	+ 2.9550	- .4295	26
		1.6	+ 2.9526[b]	- .4248[b]	36
Pyrazine - h_4	Paradichloro-benzene	1.3	+ 9.264	- .180	37
		4.2	+10.170	- .216	38
Pyrazine - d_4	Paradichloro-benzene	4.2	+10.204	-.206	38

[a] Pure crystal

[b] For the second trap

II. SENSITIVITY CONSIDERATIONS IN OPTICAL DETECTION

In this section the basic proceduresused in the optical detection of ESR and ENDOR in zero magnetic field are reviewed. Quantitative expressions are derived for the change in phosphorescence intensity as a function of the various relaxation rate constants for the triplet state and the strength of the applied microwave field.

A. ESR

The experiments were all performed under conditions of continuous optical excitation while monitoring the change in intensity of the phosphorescence as a function of the applied microwave field. Only the case in which the triplet state is populated by excitation of the sample into the first excited singlet state followed by intersystem crossing into the triplet state will be considered. For molecules with reasonably high symmetry (i.e., D_{2h}, C_{2h}, and C_{2v}) different methods of populating the triplet state may produce different spin alignments; however, the same considerations apply in calculating the sensitivity achieved using ODMR.[63,66,67]

The radiative and non-radiative pathways for energy transfer are depicted in Figure 2, where S_1 is the population of the lowest excited singlet state, N_χ ($\chi = x,y,z$) is the steady state population of the corresponding triplet levels, $K_{1\chi}$ is the non-radiative relaxation rate constant for relaxation to S_o, K_χ is the radiative or phosphorescence rate constant for relaxation to S_o, $W_{\chi_1\chi_2}$ ($\chi_1 \neq \chi_2$) is the spin lattice relaxation rate constant and $P_{\chi_1\chi_2}$ ($\chi_1 \neq \chi_2$) is the induced rate constant due

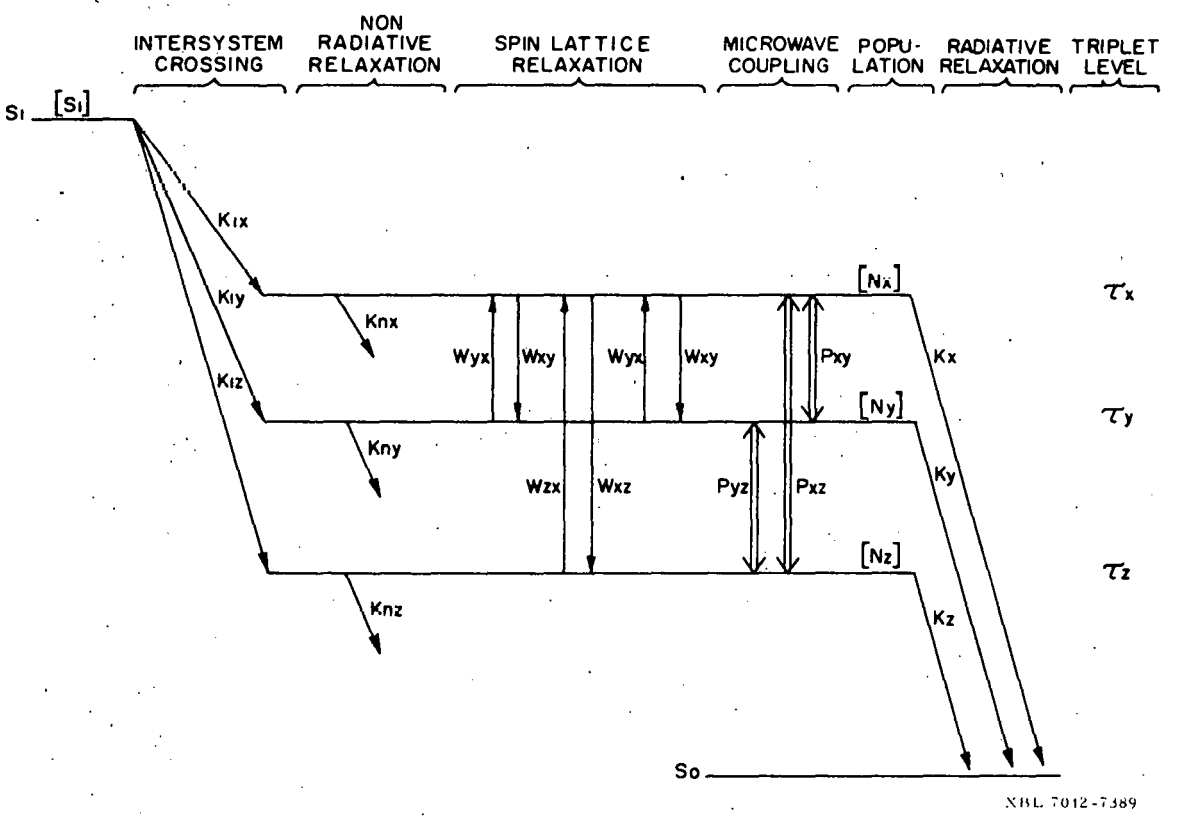

Figure 2

Relaxation Pathways and Rate Constants for the Triplet State

to the applied microwave field (H_1).

When the microwave field does not connect any two of the zero field levels of the triplet, the steady state population is given by setting $P_{\chi_1\chi_2} = 0$. The application of the microwave field at a frequency corresponding to the energy separation of two of the levels (i.e., $\nu = E_x - E_y/h$) will introduce a new pathway for relaxation causing redistribution of the population which in most cases results in a change in the phosphorescence intensity.

Since optical, rather than microwave, photons are detected, one would expect the sensitivity to be improved in proportion to the ratio of the energies of the photons, which, for a typical molecule, is approximately 3×10^5. The actual change in the phosphorescence intensity, however, is a complex function of the various relaxation rate constants. Therefore, the actual improvement in sensitivity (if there is an improvement) will depend on the molecule under study.

In order to derive a reasonably simple quantitative expression for the change in intensity of the phosphorescence, the three following assumptions will be made:

1) The splitting of the three triplet zero field levels by nuclear quadrupole and nuclear hyperfine interactions will be neglected,

2) Only the two levels connected by the H_1 field (τ_x and τ_y) will be considered, and

3) Only the steady state condition $dN_x/dt = dN_y/dt = 0$ will be considered for both the case when $H_1 = 0$ and $H_1 \neq 0$.

The first assumption will predict too great a change in intensity if the individual triplet levels are split by more than the frequency

width of the H_1 field, since in this case the H_1 field will induce an additional relaxation pathway for only a fraction of the population of each triplet level at any given frequency.

The second assumption will introduce an error in the expression for the percentage change in intensity since the intensity contribution from the level not connected by the H_1 field (τ_z) is neglected. This assumption also requires that the spin lattice relaxation rate between τ_z and τ_x and between τ_z and τ_y be neglected. This is usually valid since the experiments are performed at or below 4.20°K.

The third assumption requires that the experiment be performed using C. W. microwave conditions or modulating the microwave field with a frequency lower than the total rate constant of the system.

The differential equations describing the population of the levels shown in Figure 3 are

$$\frac{dN_x}{dt} = S_1 K_{1x} - N_x [K_{nx} + K_x + W_{xy} + P_{xy}] + N_y [W_{yx} + P_{xy}] \qquad (1)$$

$$\frac{dN_y}{dt} = S_1 K_{1y} - N_y [K_{ny} + K_y + W_{yx} + P_{xy}] + N_x [W_{xy} + P_{xy}] \qquad (2)$$

With the definitions

$$\begin{aligned} A &= K_{nx} + K_x + W_{xy} + P_{xy} \\ B &= W_{yx} + P_{xy} \\ C &= K_{ny} + K_y + W_{yx} + P_{xy} \\ D &= W_{xy} + P_{xy} \end{aligned} \qquad (3)$$

Equations 1 and 2 may be rewritten

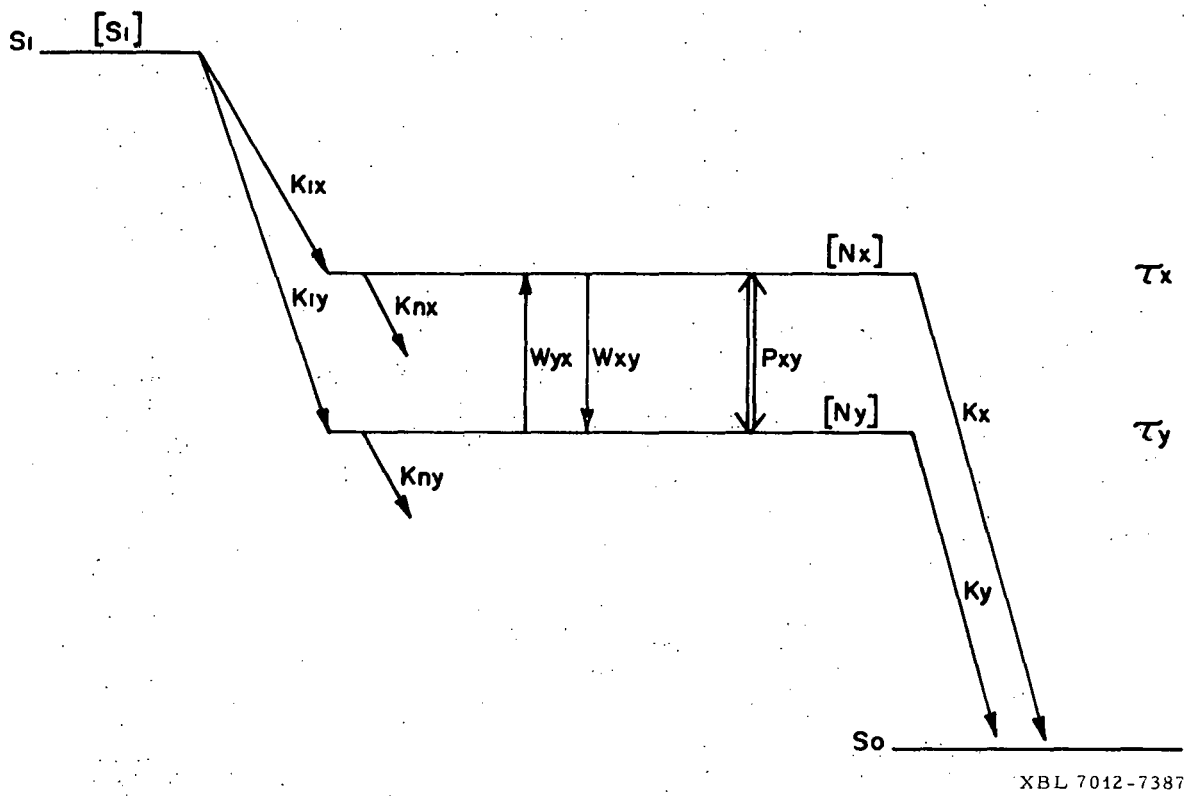

Figure 3

Relaxation Pathways and Rate Constants for only Two of the Three Triplet Levels (See Text)

$$\frac{dN_x}{dt} = S_1 K_{1x} - N_x A + N_y B \tag{4}$$

$$\frac{dN_y}{dt} = S_1 K_{1y} - N_y C + N_x D \tag{5}$$

The steady state assumption allows us to write

$$\frac{dN_x}{dt} = S_1 K_{1x} - N_x A + N_y B = 0 \tag{6}$$

$$\frac{dN_y}{dt} = S_1 K_{1y} - N_y C + N_x D = 0 \tag{7}$$

Upon solving Equations (6) and (7) for the population of the triplet levels, we have

$$N_x = \frac{S_1 [CK_{1x} + BK_{1y}]}{AC - BD} \tag{8}$$

and

$$N_y = \frac{S_1 [AK_{1y} + DK_{1x}]}{AC - BD} \tag{9}$$

The intensity of the phosphorescence detected with an optical spectrometer may be written

$$I = \alpha_1 N_x K_x + \alpha_2 N_y K_y \tag{10}$$

where α_1 and α_2 are constants that depend on the polarization of the emission, the orientation of the sample, and the efficiency of the detection system. The assumption will be made that $\alpha_1 = \alpha_2$, which allows the fractional change in the intensity of the phosphorescence upon application of the H_1 field to be written

$$\Delta I = \frac{I - I_o}{I_o} = \frac{I}{I_o} - 1 \tag{11}$$

where I_o is the intensity of the phosphorescence when $P_{xy} = 0$. With this condition, it is convenient to define the parameters given in Equation 3 as

$$\begin{aligned} a &= K_{nx} + K_x + W_{xy} \\ b &= W_{yx} \\ c &= K_{ny} + K_y + W_{yx} \\ d &= W_{xy} \end{aligned} \tag{12}$$

If both of the triplet levels are monitored, the fractional change in intensity of the emission is given by

$$\Delta I = \frac{[K_{1y}(AK_y + BK_x) + K_{1x}(CK_x + DK_y)][ac - bd]}{[K_{1y}(aK_y + bK_x) + K_{1x}(cK_x + dK_y)][AC - BD]} - 1 \quad . \tag{13}$$

In some cases it is possible to monitor only one of the triplet levels connected by the H_1 field, in which case the changes in intensity of emmission from the τ_x and τ_y levels are given by

$$\Delta I_x = \frac{[CK_{1x} + BK_{1y}][ac - bd]}{[cK_{1x} + bK_{1y}][AC - BD]} - 1 \tag{14}$$

and

$$\Delta I_y = \frac{[AK_{1y} + DK_{1x}][ac - bd]}{[aK_{1y} + dK_{1x}][AC - BD]} - 1 \tag{15}$$

Three limiting cases will now be discussed in order to examine the effect of the magnitude of the various rate constants on the sensitivity of the experiment.

Case #1, The Effect of the Radiative Rate Constants

For this case the additional assumption is made that the nonradiative and spin lattice relaxation may be neglected. The parameters defined in Equations 3 and 12 become

$$\begin{aligned} A &= K_x + P_{xy} & a &= K_x \\ B &= P_{xy} & b &= 0 \\ C &= K_y + P_{xy} & c &= K_y \\ D &= P_{yx} & d &= 0 \end{aligned} \tag{16}$$

In the absence of the H_1 field the steady state populations are given by

$$\begin{aligned} N_x^{\,o} &= S_1(K_{1x}/K_x) \\ N_y^{\,o} &= S_1(K_{1y}/K_y) \end{aligned} \tag{17}$$

The steady state population of τx is given by Equation 8 which for this example becomes

$$N_x = \frac{S_1[K_{1x}K_y + P_{xy}(K_{1x} + K_{1y}]}{[K_xK_y + P_{xy}(K_x + K_y)]} \tag{18}$$

In the limit that P_{xy} is much larger than any of the relaxation rate constants, the populations of τx and τy are equalized and the

transition is saturated. Clearly, the power required to equalize the populations is directly proportional to the relaxation rate of the system and inversely proportional to the lifetime of the excited state.

The population of τ_x at saturation is given by

$$N_x^s = \frac{S_1[K_{1x} + K_{1y}]}{[K_x + K_y]} \tag{19}$$

and the corresponding population of τ_y is given by

$$N_y^s = \frac{S_1[K_{1x} + K_{1y}]}{[K_x + K_y]} \quad . \tag{20}$$

and therefore, $N_x^s = N_y^s$.

The change in population of τ_x upon saturation is given by

$$\Delta N_x = N_x^s - N_x^o = \frac{K_x K_{1y} - K_y K_{1x}}{K_{1x}(K_x + K_y)} \quad . \tag{21}$$

Therefore, if $K_x K_{1y} = K_y K_{1x}$, there is no change in population.

If the emissions from τ_x and τ_y are monitored simultaneously, the fractional change in intensity is given by Equation 13 which, for this example, reduces to

$$\Delta I = \frac{[K_{1y}(AK_y + BK_x) + K_{1x}(CK_x + DK_y)]}{[K_{1y}(AC - BD)]} - 1 \tag{22}$$

$$= \frac{[K_{1x} + K_{1y}][P_{xy}(K_x + K_y) + K_x K_y]}{[K_{1x} + K_{1y}][P_{xy}(K_x + K_y) + K_x K_y]} - 1 \tag{23}$$

And therefore, $\Delta I = 0$ and no change in the intensity of emission will be observed.

However, if a high resolution optical spectrometer is used, it is often possible to monitor the emission from just one of the triplet levels via its selective emission to the origin or a vibration of the ground state singlet manifold. Consider for example, τ_x, in which case, the change in intensity given by Equation 14 becomes

$$\Delta I_x = \frac{K_x}{K_{1x}} \left[\frac{P_{xy}(K_{1x} + K_{1y}) + K_x K_y}{P_{xy}(K_x + K_y) + K_x K_y} \right] - 1 \quad . \tag{24}$$

In the limiting case where intersystem crossing proceeds primarily to τ_x ($K_{1x} \gg K_{1y}$) Equation 24 reduces to

$$\Delta I_x = \frac{P_{xy} K_x + K_x K_y}{P_{xy}(K_x + K_y) + K_x K_y} - 1 \tag{25}$$

At saturation we have

$$\Delta I_x^s = \frac{K_x}{K_x + K_y} - 1 \tag{26}$$

The effect of the ratio of the radiative rate constants (K_x/K_y) on the maximum change in intensity of the emission may be illustrated with the following examples:

K_x/K_y	$\Delta I(\%)$
0.1	91
1	50
10	9

Therefore, the maximum sensitivity is achieved if the level with the fast intersystem crossing rate constant has the slower phosphorescence rate constant. Unfortunately, the opposite is generally found to be the case.

Case #2, The Effect of Spin Lattice Relaxation

The two rate constants for spin lattice relaxation are not independent and may be related directly to the spin lattice relaxation time T_1 for any given temperature.[64,65]

The interaction between the energy and the lattice may be represented schematically as

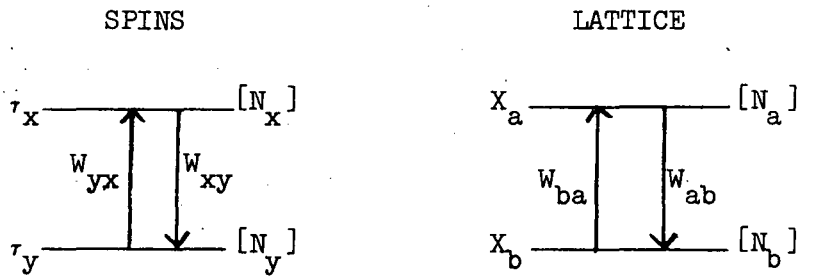

The conservation of energy requires that for each transition from τ_x to τ_y there be a corresponding lattice transition from X_b to X_a and vice versa. The transition rate for the lattice may be written

$$W_{ab} = N_a A$$
$$W_{ba} = N_b A \qquad (27)$$

where A is the transition probability and N_a and N_b are the populations of X_a and X_b respectively.

The spin lattice relaxation rate constants may be written in terms of the population of the lattice as

$$\begin{aligned} W_{xy} &= W_{ba} = N_b A \\ W_{yz} &= W_{ab} = N_a A \end{aligned} \tag{28}$$

Since the lattice is at the temperature of the bath (liquid helium), the normalized population of the lattice is given by

$$N_a = \frac{e^{-\delta/2kt}}{e^{-\delta/2kt} + e^{\delta/2kt}} - f \tag{29}$$

$$N_b = \frac{e^{\delta/2kt}}{e^{-\delta/2kt} + e^{\delta/2kt}} = 1 - f$$

where $\delta = (Ex - Ey)/2$ and Ex and Ey are the energies of the τ_x and τ_y levels respectively. The spin lattice relaxation rates may now be written

$$\begin{aligned} W_{xy} &= (1 - f)\, A \\ W_{yx} &= (f)A \end{aligned} \tag{30}$$

The spin lattice relaxation time is defined by the expression

$$T_1 = \frac{1}{W_{xy} + W_{yx}} = \frac{1}{A} \tag{31}$$

Therefore, W_{xy} and W_{yx} may be expressed in terms of T_1 and f as

$$\begin{aligned} W_{xy} &= \frac{1 - f}{T_1} \\ W_{yx} &= \frac{f}{T_1} \end{aligned} \tag{32}$$

In the derivation of equation 32 it is assumed that only a direct process of energy transfer between the spin system and the lattice exists which is usually the case at the temperatures of the experiments (4.2° to 1.3°K). In the case that Raman or Orbach processes are present, only the explicit temperature dependence of the relaxation must be corrected so that the spin lattice relaxation may always be defined for a two level system in terms of only T_1 at a given temperature.

A short T_1 relaxation time will tend to produce a Boltzmann population distribution between the spin sublevels and will therefore generally reduce the spin alignment. This can be seen by considering the simple case where there is only intersystem crossing to τ_y and emission from τ_x and τ_y. Again the non-radiative relaxation rate constants K_{1x} and K_{1y} are assumed to be negligible.

The parameters defining this model are

$$\begin{aligned} A &= K_x + W_{xy} + P_{xy} & a &= K_x + W_{xy} \\ B &= W_{yx} + P_{xy} & b &= W_{yx} \\ C &= K_y + W_{yx} + P_{xy} & c &= K_y + W_{yx} \\ D &= W_{xy} + P_{xy} & d &= W_{xy} \end{aligned} \tag{33}$$

and the populations of τ_x and τ_y when $P_{xy} = 0$ are given by

$$N_x^o = \frac{S_1[(K_y + W_{yx})K_{1x}]}{K_xK_y + K_yW_{xy} + K_xW_{yx}} \tag{34}$$

and

$$N_y^o = \frac{S_1[(W_{xy})K_{1x}]}{K_xK_y + K_yW_{xy} + K_xW_{yx}}$$

In the limit that $W_{xy} = W_{yx} = 0$ this reduces to

$$N_x^o = \frac{S_1[K_{1x}]}{K_x}$$
$$N_y^o = 0 \qquad (35)$$

At high temperatures when $W_{xy} \approx W_{yx} \gg K_x$, K_y, K_{1x}, Equation 34 becomes

$$N_x^o = \frac{S_1[K_{1x}]}{K_x + K_y}$$
$$N_y^o = \frac{S_1[K_{1x}]}{K_x + K_y} \qquad (36)$$

Since the change in population is monitored, it is clearly advantageous to perform the experiments at the lowest possible temperature in order to decrease the thermalization of the spin levels and the resulting loss in sensitivity.

Case #3, The Effect of Non-Radiative Relaxation

The final case to be considered is the effect of the non-radiative relaxation rate constants K_{1x} and K_{1y} on the sensitivity of the experiment. It is obvious that since only the radiative emission is detected, a large rate of depopulation by non-radiative relaxation is not desirable. In the case of a sample that relaxes primarily through non-radiative pathways, the sensitivity may be improved by using conventional ESR techniques and monitoring the absorption of microwave power, or in extreme cases by monitoring the change in

temperature of the sample. A quantitative measure of the decrease in sensitivity may be calculated by substituting the appropriate rate constants into Equations 13, 14 and 15; however the expressions are rather complex and therefore not particularly useful.

B. ENDOR

The sensitivity of this experiment may be simply estimated if the assumption is made that there is no nuclear polarization. Since this assumption has yet to be thoroughly investigated, it is reasonable to expect that in some cases it will not be valid. Nuclear polarization may arise through cross relaxation between the electron and nuclear spin systems (the Overhauser effect), or it may be induced by saturation of "forbidden" transitions (simultaneous electron nuclear flips). It is also possible that selective intersystem crossing may preferentially populate a particular nuclear spin level if there is strong hyperfine coupling of the electron and nuclear wavefunctions.

In the absence of nuclear polarization, the sensitivity of the optically detected ENDOR signal may be understood by referring to Figure 4 in which the τ_x and τ_y triplet levels are now each composed of two levels. This splitting of the triplet levels is due to nuclear quadrupole and hyperfine interactions as will be discussed in the section on the spin Hamiltonian.

The results obtained by considering the triplet levels as being split into only two nuclear sublevels are independent of the number of sublevels if the ESR transition connects only one nuclear sublevel in

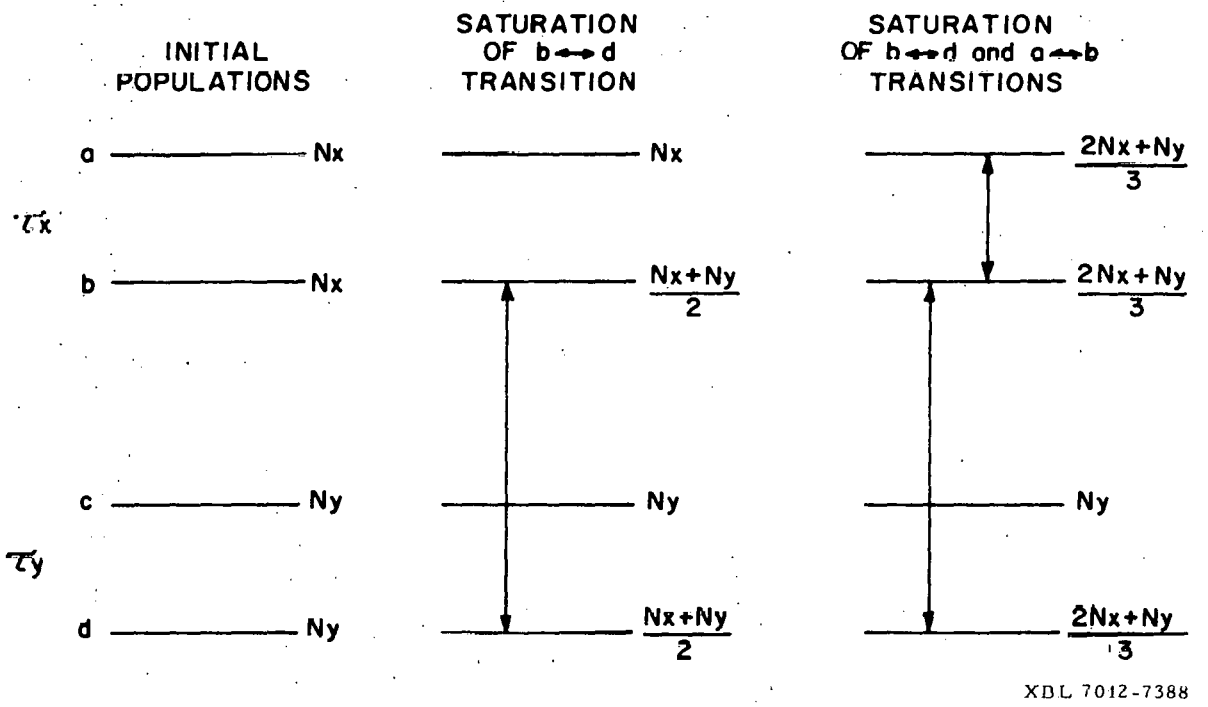

Figure 4

Population Change Predicted for ESR (b ↔ d) and ENDOR (a ↔ b) Transitions

each of the two triplet levels, and the ENDOR transition connects only two nuclear sublevels in one of the triplet levels.

As has already been discussed, the sensitivity of the optical detection technique is dependent on the various relaxation pathways from the triplet state. The same considerations apply in an ENDOR experiment. Since the sensitivity of the ENDOR experiment will be referenced to the sensitivity of the ESR experiment, the explicit dependence of the triplet state populations on the various rate constants need not be specified. For the system shown in Figure 4, the phosphorescence intensity may then be written

$$I_o = 2(N_x K_x + N_y K_y) \tag{37}$$

Upon saturation of the electron spin transition ($b \leftrightarrow d$), this becomes

$$I_s = \left(\frac{3N_x + N_y}{2}\right) K_x + \left(\frac{3N_y + N_x}{2}\right) K_y \tag{38}$$

with the change in intensity given by

$$\Delta I = I_s - I_o = \tfrac{1}{2}(N_x - N_y)(K_y - K_x) \, . \tag{39}$$

If the ENDOR transition ($a \leftrightarrow b$) is also saturated, the intensity is given by

$$I_E = \frac{2}{3}\left[(2N_x + N_y)K_x + (2N_y + N_x)K_y\right] \, . \tag{40}$$

Since the ENDOR signal is detected by monitoring the change in intensity of the ESR transition, the signal strength is given by

$$\Delta I_E = I_E - I_S \tag{41}$$

$$= \frac{1}{6}\left[(N_x - N_y)(K_y - K_x)\right] \tag{42}$$

and the fractional change in intensity of the ESR signal upon saturation of the ENDOR transition is

$$\delta I = \Delta I_E / \Delta I_S = \frac{1}{3} \quad . \tag{43}$$

If the ENDOR transition (c↔d) is saturated instead of the transition from (a↔b), the same expression is obtained for the change in intensity (Equations 42 and 43).

It is interesting to note from Equations 39 and 42 that the ESR signal and the ENDOR signal always affect the intensity of the phosphorescence in the same direction.

If the forbidden ESR transition from (b↔c) is saturated and if the two ENDOR transitions (a↔b) and (c↔d) occur at the same frequency, the change in phosphorescence intensity is given by

$$\Delta I_E = \frac{1}{2}\left[(N_x - N_y)(K_y - K_x)\right] \tag{44}$$

and the fractional change in intensity of the ESR signal is unity.

As a final note, if the ESR transitions from (a↔c) and (b↔d) occur at the same frequency, the ENDOR transitions from (a↔b) and (c↔d) must also occur at the same frequency causing the change in intensity of the ESR signal to be twice as large (Equation 39).

$$\Delta I = (N_x - N_y)(K_y - K_x) \tag{45}$$

while the ENDOR transitions will not be observed since the populations of the nuclear sublevels are already equal.

III. The Spin Hamiltonian

The observed magnetic resonance spectra of the excited triplet state of organic molecules in zero external magnetic field may be understood in terms of a Hamiltonian of the form,

$$H = H_{SS} + H_Q + H_{HF}$$

where H_{SS} is the spin-spin or zero field interaction between the two unpaired electrons, H_Q is the nuclear quadrupole interaction, and H_{HF} is the nuclear electron hyperfine interaction.

This section is devoted to a review of the explicit form of each term of the Hamiltonian and the resulting energy levels and transition probabilities.

A. H_{SS} -- The Spin-Spin or Zero Field Splitting Hamiltonian

H_{SS} is primarily due to the magnetic dipole-dipole interaction between the unpaired electrons in the excited triplet state. There can also be a contribution from the spin-orbit coupling between the lowest triplet and other excited states; however, the contribution from the interaction between other excited triplet states will shift the three levels equally, and may therefore be neglected.[56]

If the radiative lifetime for fluorescence and phosphorescence is known, the magnitude of the spin-orbit contribution to the zero field splitting may be estimated by choosing a simple model in which the transition probability for phosphorescence is due only to the spin-orbit coupling of one spin sublevel with the nearest excited singlet state. In the framework of this model the transition probability for phosphorescence may be expressed as

$$P_P \approx |\langle {}^3\psi_1 |\ e\vec{r}\ | {}^1\psi_o \rangle|^2 = \frac{1}{\tau_P} \tag{1}$$

where $e\vec{r}$ is the electron dipole moment transition operator, ${}^3\psi_1$ is the first triplet state, ${}^1\psi_o$ is the ground singlet state, and τ_P is the phosphorescence radiative lifetime. The wave function for the phosphorescent triplet state is actually a linear combination of the pure triplet state, which is spin forbidden for electric dipole radiation to the ground state, and an admixture of singlet character due to spin orbit coupling. ${}^3\psi_1$ may therefore be represented as a linear combination of ${}^3\psi_1$ and ${}^1\psi_1$ as

$$ {}^3\psi_1 = C_1\, {}^3\psi_1 + C_2\, {}^1\psi_1 \tag{2}$$

where ${}^3\psi_1$ and ${}^1\psi_1$ are the wave functions for the first excited singlet and triplet states respectively in the absence of spin-orbit coupling.

In organic molecules the spin orbit matrix element is generally small so $C_1 \approx 1$ while C_2 is given from second order perturbation theory by;

$$C_2 = \frac{\langle {}^1\psi_1 |\ H_{SO}|\ {}^3\psi_1 \rangle}{|{}^1E_1 - {}^3E_o\ |} = \frac{\delta}{|{}^1E_1 - {}^3E_1|} \tag{3}$$

where ${}^1E_1$ is the energy of ${}^1\psi_1$ and ${}^3E_o$ is the energy of ${}^3\psi_1$. The phosphorescence transition probability (Equation 1) may now be written

$$\frac{1}{\tau_P} = |\langle C_1\, {}^3\psi_o + C_2\, {}^1\psi_1 |e\vec{r}| {}^1\psi_o \rangle|^2 \tag{4}$$

$$= C_2^2\ |\ \langle {}^1\psi_1 |e\vec{r}| {}^1\psi_o|^2$$

while the fluorescence transition probability is given by

$$P_F \approx |\langle {}^1\psi_1 | e\vec{r} | {}^1\psi_o \rangle|^2 = \frac{1}{\tau_F} \quad . \tag{5}$$

Substituting Equation 5 into Equation 4 , we have

$$C_2^2 = \frac{\tau_F}{\tau_P} = \frac{\delta^2}{|{}^1E_1 - {}^3E_o|^2} \quad . \tag{6}$$

Within the limits of the model, the spin-orbit matrix element is given by

$$\delta = \left(\frac{\tau_F}{\tau_P}\right)^{\frac{1}{2}} \left({}^1E_1 - {}^3E_o\right) \quad . \tag{7}$$

Also from second order perturbation theory the shift in energy of the triplet zero field level coupled to ${}^1\psi_1$ may be written

$$\Delta = \frac{\delta^2}{|{}^1E_1 - {}^3E_o|} = \left(\frac{\tau_F}{\tau_P}\right) \left({}^1E_1 - {}^3E_o\right) \quad . \tag{8}$$

As an example, for benzene,[68] τ_P = 30 sec., $\tau_F = 3 \times 10^{-8}$ sec., and $|{}^1E_1 - {}^3E_o| = 6000\ cm^{-1}$. Therefore,

$$\Delta = \frac{3 \times 10^{-8}\ \text{sec.}}{30\ \text{sec.}} \cdot (6000\ cm^{-1})$$

$$= 6 \times 10^{-5} cm^{-1} \quad .$$

Compared to the measured zero field splittings of benzene[56] of 0.1644 cm^{-1}, 0.1516 cm^{-1}, and 0.0128 cm^{-1}, the spin-orbit coupling contribution to the zero field splitting is clearly negligible.

The addition of a heavy atom will increase the spin orbit coupling matrix element.[69,70] An example of the magnitude of the effect is given by

paradichlorobenzene[70,71] for which τ_P = 16 ms., $\tau_F = 3 \times 10^{-8}$ sec., and $|^1E_1 - {}^3E_0| = 7800\ cm^{-1}$. Substituting these values into Equation 8, we find that $\Delta = 1.5 \times 10^{-2}\ cm^{-1}$. This is still small compared to the observed zero field splittings of 0.1787 cm^{-1}, 0.1201 cm^{-1}, and 0.0584 cm^{-1}. In addition, since we used the measured lifetime of the phosphorescence which includes both the radiative and non-radiative transition probabilities, the actual contribution of spin orbit coupling to the zero field splitting is certainly smaller.

For organic molecules in their excited triplet state, the splitting of the zero field levels due to spin orbit coupling accounts for only a small percentage of the observed zero field splitting and therefore, we will consider only the magnetic dipole-dipole interaction in explaining the observed spectra.

The Hamiltonian for the magnetic dipole-dipole interaction between two unpaired electrons may be written as[77]

$$H_{SS} = g_e^2 \beta_e^2 \left\{ \frac{S_1 \cdot S_2}{r^3} - \frac{3(S_1 \cdot r)(S_2 \cdot r)}{r^5} \right\} \qquad (9)$$

where g_e is the anomalous electron g factor, which has been found to be basically isotropic for aromatic triplet states and equal to the free electron value of 2.00232, β_e is the Bohr magneton ($eh/2mc$), and r is the vector connecting the two electron spins S_1 and S_2.

The Hamiltonian is of the same form as any dipole-dipole interaction, and in the case of the interaction between the two triplet state electrons may be expressed as

$$H_{SS} = S \cdot D \cdot S \qquad (10)$$

which may be written in a Cartesian axis system as

$$\begin{aligned} H_{SS} = {} & D_{xx}S_x^2 + D_{xy}S_xS_y + D_{xz}S_xS_z + \\ & D_{yx}S_yS_x + D_{yy}S_y^2 + D_{yz}S_yS_z + \\ & D_{zx}S_zS_x + D_{zy}S_zS_y + D_{zz}S_z^2 \end{aligned} \tag{11}$$

The values of the D_{ij} (i, j = x, y, z) are given by averages over the triplet state electronic wave function[57]

$$\begin{aligned} D_{xx} &= \frac{1}{2} g_e^2 \beta^2 \left\langle \frac{r^2 - 3x^2}{r^5} \right\rangle \\ D_{xy} &= \frac{1}{2} g_e^2 \beta^2 \left\langle \frac{-3xy}{r^5} \right\rangle \end{aligned} \tag{12}$$

and so on. D is a symmetrical tensor ($D_{xy} = D_{yx}$, etc.); therefore, in the principal axis system which diagonalizes the zero field tensor, the Hamiltonian becomes

$$H_{SS} = -XS_x^2 - YS_y^2 - ZS_z^2 \tag{13}$$

where $X = -D_{xx}$, $Y = -D_{yy}$, and $Z = -D_{zz}$

Since the Hamiltonian satisfies LaPlace's equation, X + Y + Z = 0, only two independent parameters are needed to describe the interaction. In conventional ESR the Hamiltonian in the principal axis system is usually rewritten by defining

$$D = \frac{1}{2}(X + Y) - Z \quad \text{and} \quad E = -\frac{1}{2}(X - Y) \tag{14}$$

with the axis convention that $|X| \leq |Y| \leq |Z|$. Therefore, the three components of the Hamiltonian are given by

$$\begin{aligned} X &= D/3 - E \\ Y &= D/3 + E \\ Z &= -2/3D \quad . \end{aligned} \tag{15}$$

The Hamiltonian may be rewritten by substituting the definitions of D and E (Equation 14) into the Hamiltonian (Equation 13),

$$\begin{aligned} H_{SS} &= -(D/3 - E)\, S_x^2 - (D/3 + E)\, S_y^2 + 2/3\, D\, S_z^2 \\ &= D(2/3\, S_z^2 - 1/3(S_x^2 + S_y^2)) + E(S_x^2 - S_y^2) \quad . \end{aligned} \tag{16}$$

since $S_x^2 + S_y^2 = S^2 - S_z^2$, (17)

we may write

$$H_{SS} = D(S_z^2 - 1/3\, S^2) + E(S_x^2 - S_y^2) \quad . \tag{18}$$

However, for the triplet state $S^2 = 2$; therefore,

$$H_{SS} = D(S_z^2 - 2/3) + E(S_x^2 - S_y^2) \quad . \tag{19}$$

The Hamiltonian may also be expressed in equivalent form using the raising and lowering operators as

$$H_{SS} = D(S_z^2 - 2/3) + E/2\, (S+^2 - S-^2) \quad . \tag{20}$$

The D and E parameters are defined by the average over the triplet state wave function

$$D = 3/4\, g_e^2\, \beta^2 \left\langle \frac{r^2 - 3z^2}{r^5} \right\rangle \tag{21}$$

$$E = 1/4\ g_e^2 \beta^2 \left\langle \frac{3y^2 - 3x^2}{r^5} \right\rangle . \qquad \text{(21 Cont.)}$$

The Hamiltonian in matrix form with the basis states chosen to be eigenvalues of Sz may now be expressed as

$$H_{SS} = \begin{array}{c|c|c} |1> & |0> & |-1> \\ \hline D/3 & 0 & E \\ \hline 0 & -2/3D & 0 \\ \hline E & 0 & D/3 \end{array} \qquad (22)$$

This form is generally applicable and may be used with any interacting nuclear spin. In certain cases the simpler form may be used in which the basis states are eigenfunctions for both the Hamiltonian and Sx, Sy and Sz.

$$H_{SS} = \begin{array}{c|c|c} |x> & |y> & |z> \\ \hline -X & 0 & 0 \\ \hline 0 & -Y & 0 \\ \hline 0 & 0 & -Z \end{array} \qquad (23)$$

where

$$\begin{aligned} |x> &= 1/\sqrt{2}\ (|-1> - |1>) \\ |y> &= i/\sqrt{2}\ (|-1> + |1>) \\ |z> &= |0> \end{aligned} \qquad (24)$$

This form of the Hamiltonian is directly related to the chosen axis system of the molecule and presents a clear picture of the orientational dependence of the energy.

The resulting energy level diagram and nomenclature for both representations are shown in Figure 5 .

The usual selection rule in ESR of $\Delta S_z = \pm 1$ is not valid in zero magnetic field since the triplet sublevels are not eigenfuctions of Sz. The nonvanishing matrix elements for magnetic dipole transitions between the triplet magnetic sublevels are given by

$$\begin{aligned} P_{y \rightarrow z} &= |\langle Y| \; S_x \; |Z\rangle|^2 = 1 \\ P_{x \rightarrow z} &= |\langle X| \; S_y \; |Z\rangle|^2 = 1 \\ P_{x \rightarrow y} &= |\langle X| \; S_z \; |Y\rangle|^2 = 1 \quad . \end{aligned} \tag{25}$$

Therefore the three microwave transitions are polarized along the x, y and z directions as shown in Figure 2.

B. H_Q -- The Nuclear Quadrupole Hamiltonian

A nucleus with a spin ≥ 1 will have a non-spherical charge distribution and therefore an electric quadrupole moment. The quadrupole moment of the nucleus may be positive or negative depending on whether the charge distribution is elongated or flattened along the spin axis. Each allowed nuclear orientation along the spin axis will have associated with it a potential energy due to the surrounding electric field. In the case of a free molecule, the electric field is due to non-s electrons which produce a field gradient at the nucleus defined by

$$V_{i,j} = \frac{\partial^2 V}{\partial_i, \partial_j} \quad (i, \; j = x, y, z) \tag{26}$$

The Hamiltonian is derived by expanding the expression for the

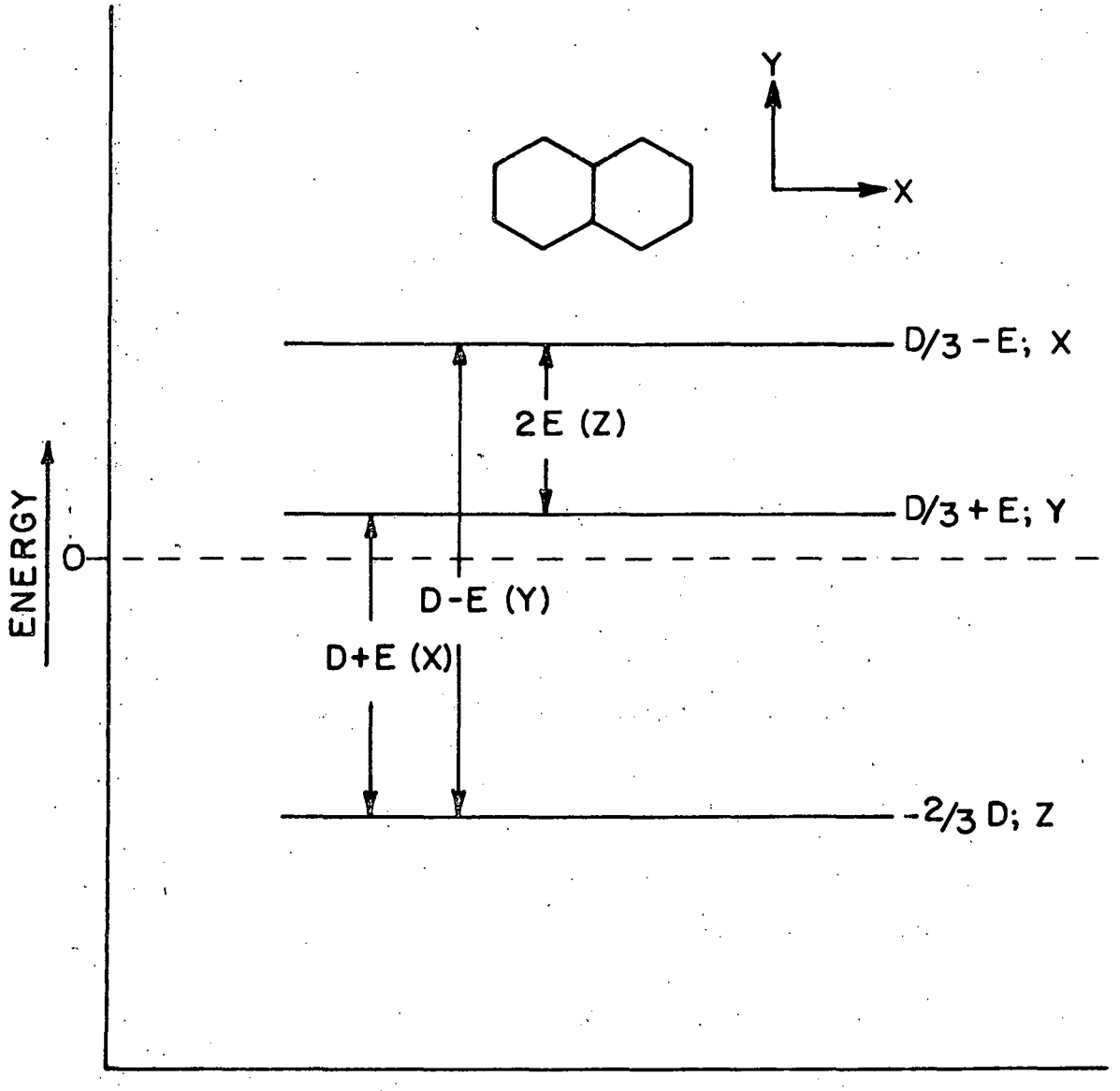

XBL 7012-7266

Figure 5

Energy Levesl and ESR Transitions for the Triplet State

electrostatic potential energy of a nucleus of finite dimensions in the field of its surrounding electrons in terms of the nuclear multipole moments. The electrostatic dipole moment vanishes by symmetry and the first term in the expansion giving rise to deviations from a simple point charge interaction is the quadrupole term. The explicit derivation of the Hamiltonian is given in several sources and will not be repeated here.[58-62]

In an arbitrary axis system the Hamiltonian may be written as

$$H_Q = B \left\{ V_{zz}(3I_z^2 - I^2) + (V_{zx} + i\,V_{zy})(I_-I_z + I_zI_-) + (V_{zx} - i\,V_{zy})(I_+I_z + I_zI_+) + [1/2(V_{xx} - V_{yy}) + i\,V_{xy}]\,I_+^2 + [1/2(V_{xx} - V_{yy}) - i\,V_{xy}]\,I_-^2 \right\} \quad (27)$$

where $B = \frac{eQ}{4I(2I-1)}$

e = the electron charge (esu)

Q = the quadrupole mement (cm^2)

and I = the nuclear spin quantum number.

The Hamiltonian is a symmetric tensor and by transforming to an axis system such that $V_{i,j} = 0$ for $i \neq j$, the Hamiltonian may be re-written as:

$$H_Q = B \left\{ V_{zz}(3I_z^2 - I^2) + [1/2(V_{xx} - V_{yy})(I_+^2 + I_-^2)] \right\} . \quad (28)$$

Since the Hamiltonian only includes interactions due to charges external to the nucleus, the LaPlace equation is satisfied and therefore:

$$V_{xx} + V_{yy} + V_{zz} = 0 \quad . \quad (29)$$

and it is only necessary to specify two independent parameters to describe the interaction. The conventional nomenclature in nuclear quadrupole resonance spectroscopy defines the field gradient, q, and the asymmetry parameter η by the relations

$$eq = V_{zz}$$
$$\eta = \frac{V_{xx} - V_{yy}}{V_{zz}} \tag{30}$$

with the convention

$$|V_{xx}| \leq |V_{yy}| \leq |V_{zz}| \tag{31}$$

The three components of the field gradient are then given by

$$V_{zz} = eq$$
$$V_{xx} = \frac{-V_{zz}(1 - n)}{2} \tag{32}$$
$$\text{and } V_{yy} = \frac{-V_{zz}(1 + n)}{2} .$$

The asymmetry parameter η may take on values from 0 to 1 and in the case where $\eta = 0$, the field gradient has axial symmetry and,

$$V_{xx} = V_{yy} = -1/2\ V_{zz} . \tag{33}$$

When η has its maximum value of 1,

$$V_{xx} = 0$$
$$V_{yy} = -V_{zz} \tag{34}$$

The asymmetry parameter will vanish by symmetry whenever the nucleus is at a sight of three-fold or higher symmetry since this requires that $V_{xx} = V_{yy}$.

The standard form of the Hamiltonian, Equation 28 , may now be written as

$$H_Q = A\left[(3I_z^2 - I^2) + \eta/2\,(I_+^2 + I_-^2)\right] \tag{35}$$

where $A = \frac{e^2qQ}{4I(2I - 1)}$.

This may also be written in the completely equivalent form

$$H_Q = A\left[(3I_z^2 - I^2) + \eta(I_x^2 - I_y^2)\right] \quad . \tag{36}$$

The Hamiltonian matrix therefore consists of diagonal terms and off diagonal terms connecting states differing in I_z by $\pm$ 2.

At this point we will consider the explicit form of the Hamiltonian matrix for I = 1 and I = 3/2 since interactions due to both spins were observed in the course of this work.

The Hamiltonian for an I = 1 nucleus may be expressed in matrix form as

$$H_Q = A \cdot \begin{array}{c|c|c|c} & |1> & |0> & |-1> \\ \hline |1> & 1 & 0 & \eta \\ \hline |0> & 0 & -2 & 0 \\ \hline |-1> & \eta & 0 & 1 \end{array} \tag{37}$$

where $A = \frac{e^2qQ}{4}$.

A more convenient form of the Hamiltonian is obtained by transforming the Hamiltonian to the representation in which the energy is diagonal. In this

representation the Hamiltonian is in the same form as the spin-spin Hamiltonian, Equation 13 , and in matrix form, may be written;

$$H_Q = A \cdot \begin{array}{c|c|c|c} & |X> & |Y> & |Z> \\ \hline -X & -X & 0 & 0 \\ \hline Y & 0 & -Y & 0 \\ \hline Z & 0 & 0 & -Z \end{array} \qquad (38)$$

The energy is given by

$$\begin{aligned} X &= -A(1+\eta) \\ Y &= -A(1-\eta) \\ Z &= -2A \end{aligned} \qquad (39)$$

and the eigenstates are

$$\begin{aligned} |X> &= (1/\sqrt{2})(|1> + |-1>) \\ |Y> &= (i/\sqrt{2})(|1> - |-1>) \\ |Z> &= |0> \quad . \end{aligned} \qquad (40)$$

This form of the Hamiltonian is particularly convenient since it may be written in terms of the nuclear angular momentum operators as

$$H_Q = -xI_x^2 - yI_y^2 - zI_z^2 \qquad (41)$$

which is in the same form as the zero field Hamiltonian.

In Figure 6a, the energies and polarizations of the pure nuclear quadrupole transitions, for a spin 1 nucleus, are given. The three magnetic dipole transitions are polarized along the X, Y and Z axis as are the zero field transitions.

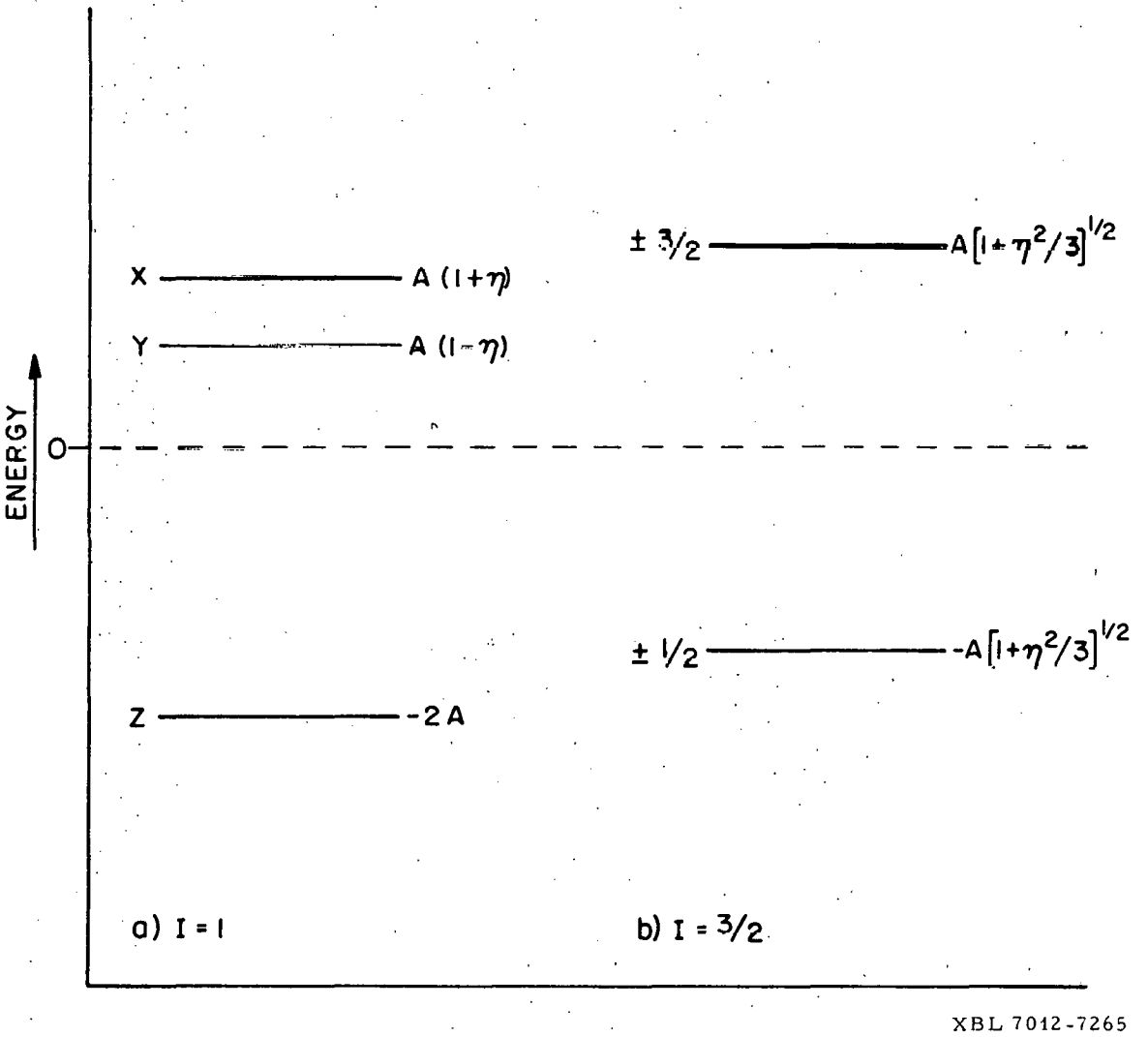

Figure 6

Nuclear Quadrupole Energy Level Diagram for a) I = 1 and b) I = 3/2 Nuclear Spins

The Hamiltonian matrix for I = 3/2 may be written as

$$H_Q = \frac{e^2qQ}{4} \cdot$$

$\|3/2>$	$\|1/2>$	$\|-1/2>$	$\|-3/2>$
1	0	$\eta/\sqrt{3}$	0
0	-1	0	$\eta/\sqrt{3}$
$\eta/\sqrt{3}$	0	-1	0
0	$\eta/\sqrt{3}$	0	1

(42)

The matrix may be rewritten as two separate 2 x 2 matrices by rearranging the order of the basis states as

$$H_Q = \frac{e^2qQ}{4} \cdot$$

$\|3/2>$	$\|-1/2>$	$\|1/2>$	$\|-3/2>$
1	$\eta/\sqrt{3}$	0	0
$\eta/\sqrt{3}$	-1	0	0
0	0	-1	$\eta/\sqrt{3}$
0	0	$\eta/\sqrt{3}$	1

(43)

The eigenvalues of the Hamiltonian may now be obtained by diagonalizing each of the 2 x 2 matrices with the result that there are only two energy levels, both of which are doubly degenerate (see Figure 6b).

$$E_{\pm 3/2} = \frac{e^2qQ}{4}\left(1 + \eta/3\right)^{1/2}$$
$$E_{\pm 1/2} = \frac{-e^2qQ}{4}\left(1 + \eta/3\right)^{1/2} \qquad (44)$$

The eigenstates are

$$|3/2>' = a|3/2> + b|-1/2>$$
$$|-1/2>' = a|-1/2> - b|3/2>$$
$$|1/2>' = a|1/2> - b|-3/2> \qquad (45)$$
$$|-3/2>' = a|-3/2> + b|1/2>$$

where

$$a = \frac{1 + \sqrt{1 + x^2}}{[2(1 + x^2 + \sqrt{1 + x^2})]^{1/2}}$$

$$b = x/\left[2(1 + x^2 + \sqrt{1 + x^2}\right]^{1/2} \qquad (46)$$

and $$x = \eta/3$$

In contrast to a nucleus with spin I = 1, we cannot determine both e^2qQ and η by measuring only the transition energy since the levels are twofold degenerate. It is therefore necessary to apply a perturbation such as a Zeeman field to remove the degeneracy of the ± levels in order to completely measure the nuclear quadrupole interaction. It should be noted, however, that the transition frequency is not particularly sensitive to η. The assumption that $\eta = 0$ and therefore that the transition energy is equal to $(1/2)e^2qQ$ will produce only a small error for small values of η as shown in Figure 7. Furthermore, an oscillating magnetic field along the Z axis will not induce magnetic dipole transitions between the ± 3/2 and ± 1/2 nuclear levels if $\eta = 0$.

C. H_{HF} -- The Nuclear Electron Hyperfine Interaction

A nucleus with a spin ≥ 1/2, like an electron, will have a magnetic moment. The interaction of this nuclear magnetic moment, with the electron magnetic moment, will lead to both an anisotropic dipole-dipole interaction and the Fermi contact interaction due to a finite electron spin density at the nucleus.

The component of the hyperfine interaction, due to the interaction of the nuclear and electron magnetic moments, is entirely analogous to the

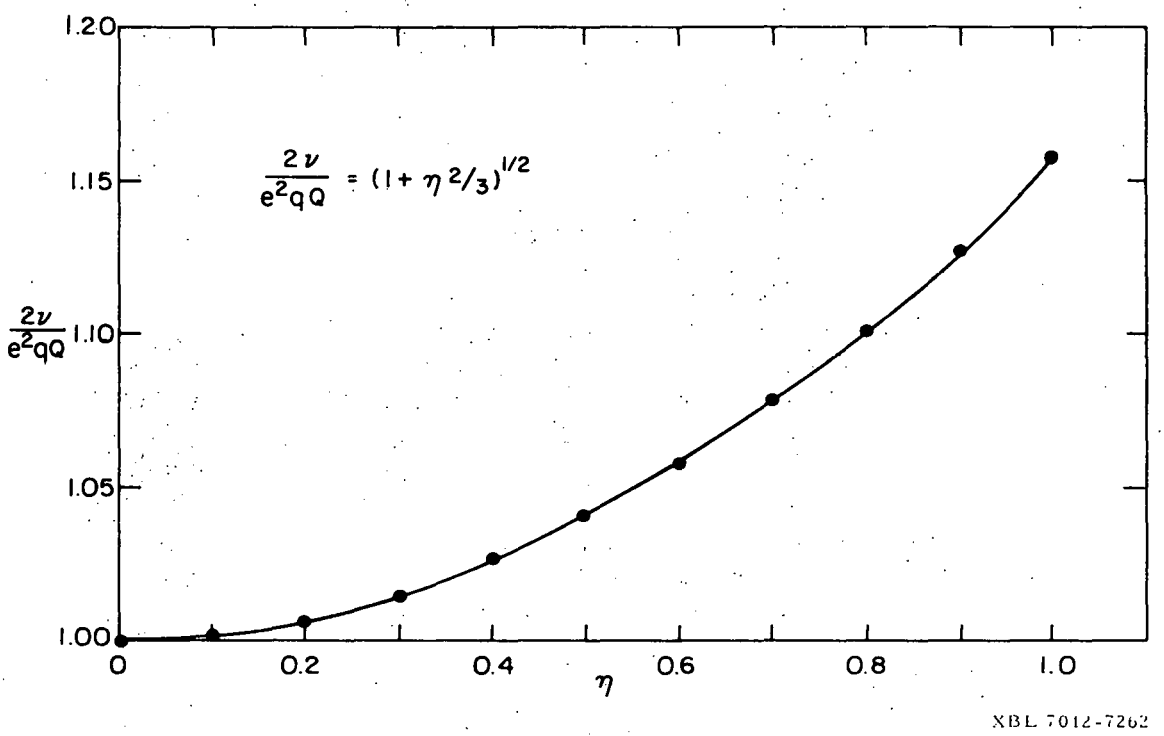

Figure 7

Plot of the Ratio of the Observed NQR Transition Frequency to the Nuclear Quadrupole Coupling Constant versus the Asymmetry Parameter

zero field Hamiltonian with the replacement of one of the electron spins with a nuclear spin and the appropriate change of constants. The Hamiltonian may be written as

$$H_{HF}^{DD} = - g_e\beta_e g_n\beta_n \left[\frac{I\cdot S}{r^3} - \frac{3(I\cdot r)(S\cdot r)}{r^5} \right] \tag{47}$$

where g_n is the nuclear g factor and β_n is the nuclear magneton.

Since this is identical in form to Equation 9 for the zero field Hamiltonian, Equation 47 may be expressed as

$$H_{HF}^{DD} = S\cdot A\cdot I \tag{48}$$

which may be expanded in tha same manner as Equation 11 . The A matrix is symmetric and therefore, in its principle axis system, may be written as,

$$H_{HF}^{DD} = A_{xx}S_x I_x + A_{yy}S_y I_y + A_{zz}S_z I_z \tag{49}$$

where the hyperfine elements are given by the average over the spatial distribution of the unpaired spins

$$A_{\chi\chi} = -g_e g_n\beta_e\beta_n \left\langle \frac{r^2 - 3\chi^2}{r^5} \right\rangle \tag{50}$$

where $\chi = x, y, z$.

The LaPlace equation is again satisfied and therefore,

$$A_{xx} + A_{yy} + A_{zz} = 0 \tag{51}$$

The unpaired spin density at the nucleus will produce an additional

contribution to the hyperfine Hamiltonian called the Fermi contact term. This will arise only from spin density in s orbitals since the other orbitals have a vanishing probability of being at the nucleus. The Fermi contact contribution is usually considered to be isotropic and may therefore be written as

$$H_{HF}^{F} = C(S_x I_x + S_y I_y + S_z I_z) \tag{52}$$

where

$$C = (8\pi/3)\gamma_e \gamma_n \hbar^2 |\psi_s(0)|^2 \tag{53}$$

and $|\psi_s(0)|^2$ is the s electron spin density at the nucleus.

The total hyperfine Hamiltonian may now be written as

$$H_{HF} = A'_{xx} S_x I_x + A'_{yy} S_y I_y + A'_{zz} S_z I_z \tag{54}$$

where

$$A'_{xx} = A_{xx} + C, \text{ etc.} \tag{55}$$

Therefore, if the three components of the total hyperfine Hamiltonian are measured, the contribution due to the anisotropic and isotropic components can be separated; however, the absolute signs will not generally be obtained. It should be pointed out that since the nuclei in which we are interested also have quadrupole moments, the Fermi contact term will not be strictly isotropic since the nuclei are distorted, and consequently, the dipole-dipole and contact terms are not completely separable.

D. The Total Hamiltonian, Energy Levels and Transition Probabilities

In this section the total Hamiltonian for two molecules which are examples of the triplet state electrons interacting with an I=1 and an I=3/2 nuclear spin will be considered. In order to simplify the discussion we will make the following assumptions for both cases:

1) The principal axis system of H_{SS}, H_Q and H_{HF} are coincident,
2) Only the out-of-plane component of the hyperfine Hamiltonian need be considered, and
3) The hyperfine interaction due to protons may be neglected.

Assumptions 1 and 2 can be, in many cases, justified on the basis of the single crystal ESR spectra,[43] and assumption 3 on the fact that resolved proton hyperfine splitting has not been observed in zero field ESR.

Example #1, I=1

An example of a molecule which is characterized by the interaction of one (I=1) nuclear spin with the triplet electrons is the $\pi\pi^*$ state of quinoline (1-azanaphthalene). The spin Hamiltonian for this molecule may be written for the axis system given in Fig. 8 as[22,24]

$$H = H_{SS} + H_Q + H_{HF} \tag{56}$$

where

$$\begin{aligned} H_{ZF} &= -XS_x^2 - YS_y^2 - ZS_z^2 \\ H_Q &= -xI_x^2 - yI_y^2 - zI_z^2 \end{aligned} \tag{57}$$

and

$$H_{HF} = A_{xx} S_x I_x$$

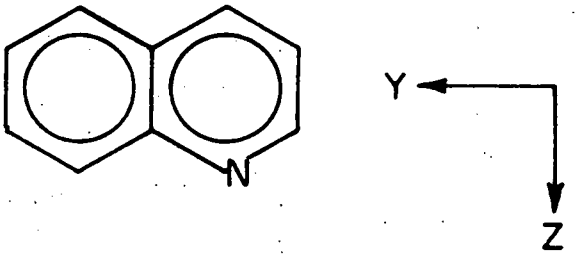

XX	XY	XZ	YX	YY	YZ	ZX	ZY	ZZ
X+x				-Azz				-Ayy
	X+y		Azz					
		X+z				Ayy		
	Azz		Y+x					
-Azz				Y+y				-Axx
					Y+z		Axx	
		Ayy				Z+x		
					Axx		Z+y	
-Ayy				-Axx				Z+z

XBL 7012-7270

Figure 8

Hamiltonian Matrix for Triplet Plus One I = 1 Nuclear Spin

We will use for the basis states the product functions $|\mu\ \nu> = \tau_\mu\ \chi_\nu$, which form a set of eigenfunctions that diagonalize H_{SS} and H_Q. τ_μ and χ_ν are the electron and nuclear spin function while μ and ν correspond to x, y and z.

The complete Hamiltonian is a 9 x 9 matrix as shown in Figure 8, where we have also included the in-plane hyperfine elements for completeness. Since we are only considering the A_{xx} element of the hyperfine interaction, we can solve the energies exactly by diagonalizing only two 2 x 2 matrices. However, a satisfactory solution is obtained by second order perturbation theroy. As is shown in Figure 9, the energy of the states $|Zz>$ and $|Zy>$ are shifted by an amount β, where

$$\beta = \frac{A_{xx}^{\ 2}}{E_y - E_z} \tag{58}$$

while the states $|Yz>$ and $|Yy>$ are shifted by an amount $-\beta$.

In our axis system the triplet state energy levels would be ordered $Z > Y > X$ and the nuclear quadrupole energy levels ordered $x > z > y$. The eigenvectors of the states which are coupled by A_{xx} are

$$\begin{aligned}
|Zz>' &= (1 - \beta)\ |\ Zz> - \beta|\ Yy> \\
|Zy>' &= (1 - \beta)\ |\ Zy> - \beta|\ Yz> \\
|Yz>' &= (1 - \beta)\ |\ Yz> + \beta|\ Zy> \\
|Yy>' &= (1 - \beta)\ |\ Yy> + \beta|\ Zz> \quad .
\end{aligned} \tag{59}$$

The probability for microwave transitions between the triplet state magnetic sublevels is given by

$$I \approx |\ <\mu_1\nu_1|H_{RF(t)}|\mu_2\nu_2>|^2 \tag{60}$$

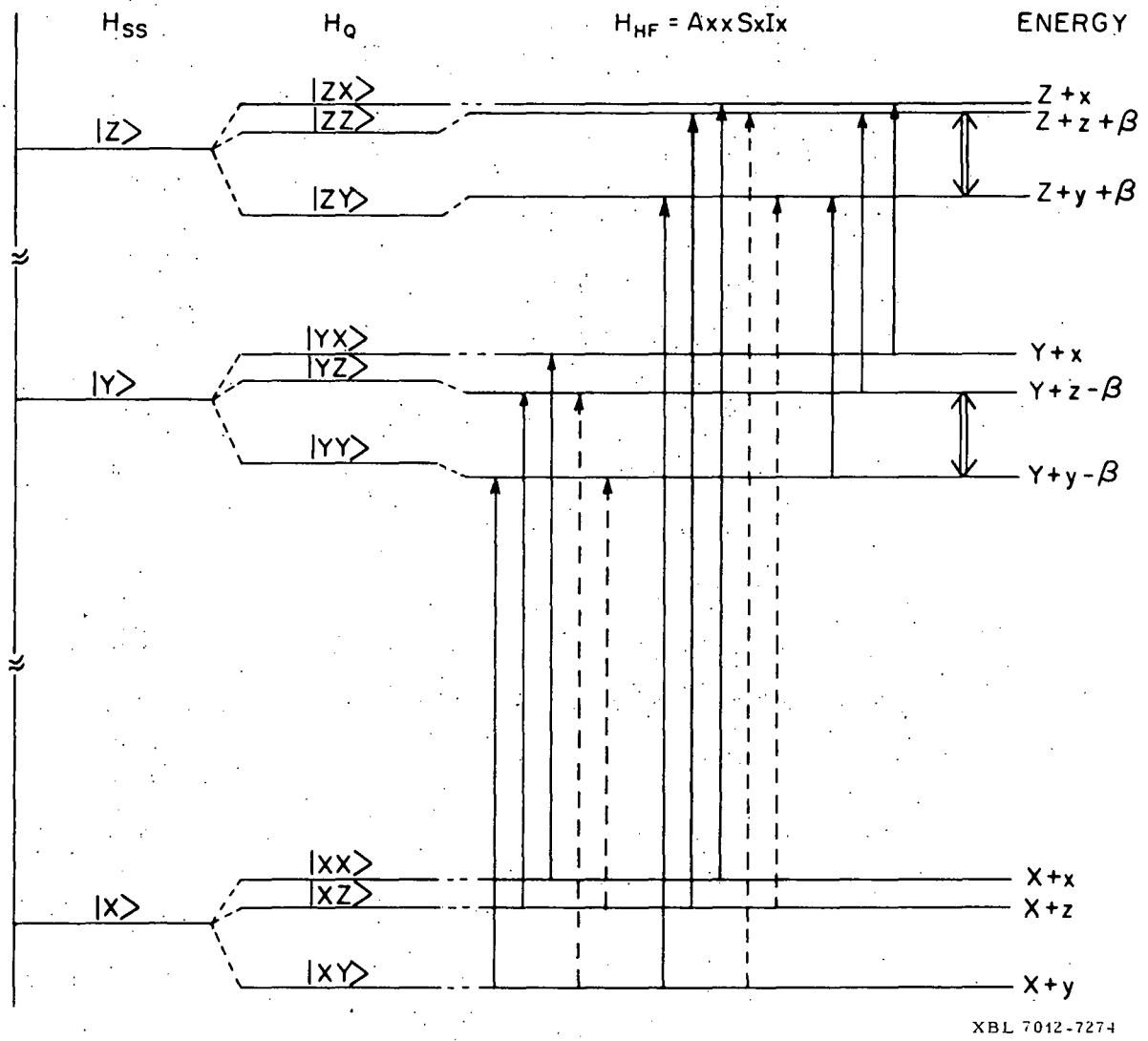

Figure 9

Energy Level Diagram for the Triplet and One I = 1 Nuclear Spin

Considering only the A_{xx} Hyperfine Component

where $H_{RF(t)}$ is the magnetic dipole transition operator defined by;

$$H_{RF(t)} = H_1(t)\,\hbar\,(\gamma_n \cdot I + \gamma_e \cdot S) \tag{61}$$

and $H_1(t)$ is the magnitude of the time dependent magnetic field, γ_n is the nuclear gyromagnetic ratio $\left(\frac{g_n\beta_n}{\hbar}\right)$ and γ_e is the electron gyromagnetic ratio $\left(\frac{g_e\beta_e}{\hbar}\right)$.

The electron spin magnetic dipole transition operator will connect states with $\mu_1 \neq \mu_2$ and $\nu_1 = \nu_2$, while the nuclear spin operator will connect states with $\mu_1 = \mu_2$ and $\nu_1 \neq \nu_2$. However, the mixing of the basis function by A_{xx} will allow the observation of "forbidden" simultaneous electron and nuclear transitions. This is clearly shown by considering the transition from $|Xz>'$ to $|Yy>'$. The intensity of the transition is given by

$$I \approx | < Xz \mid \gamma_e H_1(t) \mid [(1 - \beta)|\, Yy > + \beta|Zz>]|^2 \tag{62}$$

$$I \approx \beta^2\, \gamma_e{}^2\, H_1(t)^2 \tag{63}$$

It should be noted that it is necessary to have a hyperfine interaction in order to observe the nuclear quadrupole satellites since the hyperfine term is the only method of coupling the electron and nuclear Hamiltonians.

In Figure 10, the spectra expected for the three zero field transitions are shown in terms of the components of the total Hamiltonian. It is clear that the separation of the quadrupole satellites for both the $\tau_x \rightarrow \tau_z$ and $\tau_x \rightarrow \tau_y$ transitions are separated by $2(z - y)$ and therefore only one of the three possible nuclear quadrupole transitions equal

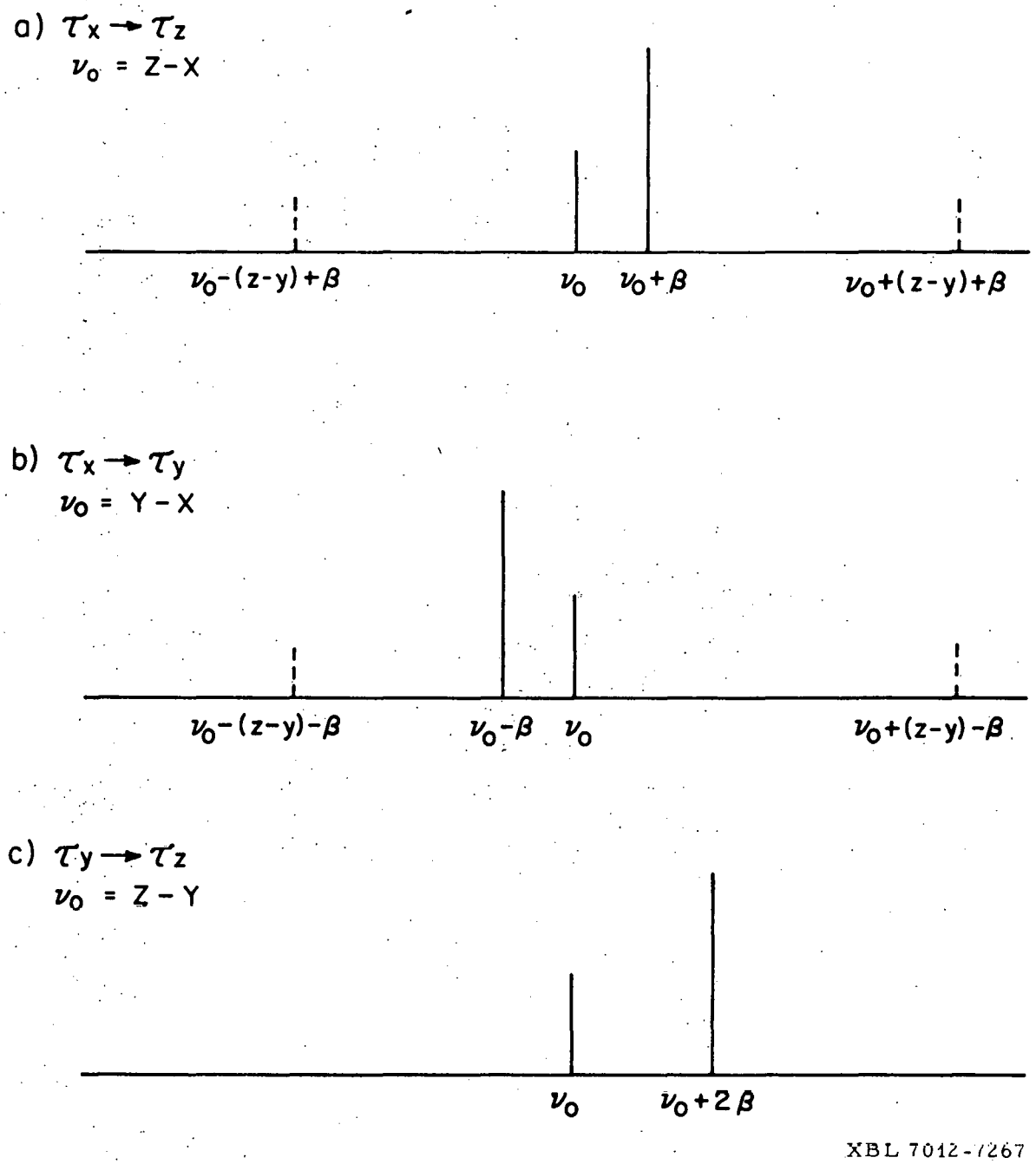

Figure 10

ODMR Spectra Predicted for the Energy Level Diagram Shown in Figure 9

to $(3/4)\ e^2qQ\ (1 - \eta/3)$ is observed.[24] The value of the hyperfine coupling constant A_{xx} is easily obtained from the separation of the two allowed components of each of the three transitions. If we had chosen to use A_{yy} or A_{zz} as the only hyperfine interaction instead of A_{xx}, the spectra would be the same as that shown in Figure 10 if a cyclic perturbation is applied to our labeling.

Although in this simple example all the parameters in the Hamiltonian can be determined from the three zero field transitions, in practice this is usually not the case. This can be due to such problems as poor resolution of the spectra or the failure to include enough terms in the Hamiltonian to adequately describe the interactions. Therefore, it is usually advantageous to also perform an electron nuclear double resonance (ENDOR) experiment to improve the resolution and confirm the assignment of the spectra. The ENDOR transitions are shown in Figure 9 by the double arrows. However, spectra have been assigned incorrectly because of a failure to consider the proper form of the magnetic dipole transition operator.[26] Therefore, let us consider, as an example, the intensity of the ENDOR transition from $|\ Yy >'$ to $|Yz >'$;

$$I \approx \left|\left[(1 - \beta) < Yy\ | + \beta < Zy\ |\right]\right|\ H_{RF(t)}\ \left|\left[(1 - \beta)|\ Yz > + \beta|\ Zy >\right]\right|^2 \quad (64)$$

$$I \approx \left[(1 - \beta)^2\ \gamma_n\ H_1 + 2\beta\,(1 - \beta)\ \gamma_e\ H_1 + \beta^2\ \gamma_n\ H_1\right]^2 \quad . \quad (65)$$

Since H_1 is a constant, we will drop it and may now write

$$I \approx 4\gamma_e^2\left[\beta^2(1-\beta)\right] + 4\ \gamma_e\ \gamma_n\left[\beta(1 - \beta)^3 + \beta^3\ (1 - \beta)\right]$$

$$+ \gamma_n^2\left[(1 - \beta)^4 + \beta^4 + 2\beta^2\ (1 - \beta)^2\right] \quad (66)$$

Since β is usually on the order of $1X10^{-2}$ for $\pi\pi^*$ triplets, we can reasonably approximate Eq. 11 by

$$I \approx 4\beta^2 \gamma_e^2 + 4\beta \gamma_e \gamma_n + \gamma_n^2 \qquad (67)$$

In contrast, if there were no hyperfine coupling as in the τ_x manifold in our example, the intensity would be given by

$$I \approx \gamma_n^2 \quad . \qquad (68)$$

Therefore, the ratio of the intensity of the ENDOR transitions due to the electron magnetic dipole operator to those due to the nuclear magnetic dipole operator is approximately $4\beta^2 \gamma_e^2/\gamma_n^2$ and therefore, unless $4\beta^2/\gamma_n^2$ is greater than $1/\gamma_e^2$, the electron dipole moment transition operator will be the major source of the intensity in ENDOR transitions.

An example, for ^{14}N the ratio of $\gamma_e/\gamma_n = 8.6X10^6$ and therefore, β must be less than $1.57X10^{-3}$ for the nuclear magnetic dipole transition operator to be comparable to the electron magnetic dipole transition operator in producing intensity in the ENDOR transitions. For a typical separation of τ_z-τ_y of 1000 MHz this would correspond to an extremely small hyperfine element, A_{xx} of only 1.5 HMz, which is much smaller than any out-of-plane hyperfine elements reported for aza-aromatics

Example #2, I=3/2

An example of a molecule characterized by the interaction of the unpaired electrons with one I=3/2 nuclear spin is the $\pi\pi^*$ state of chlorobenzene. The ESR spectrum in this case is somewhat more difficult to calculate due to the lack of a basis set that diagonalizes both H_{SS} and H_Q for an arbitrary value of the assymetry parameter. This problem may be avoided by making the reasonable assumption that the chlorine assymetry

parameter equals zero. In this case both H_{SS} and H_Q are diagonal with the basis set $| \mu \nu > = \tau_\mu \chi_\nu$ where τ and χ represent the electron and nuclear spin functions respectively, while μ corresponds to X, Y, and Z and ν to 3/2, 1/2, -1/2 and -3/2.

For this example, again only the out-of-plane component of the hyperfine tensor (A_{xx}) will be considered and therefore the spin Hamiltonian may be written

$$H = H_{SS} + H_Q + H_{HF}$$

Since only the A_{xx} component of the hyperfine tensor is being considered, H_{HF} may be written as:

$$H_{HF} = 1/2 \ [A_{xx} S_x (I_+ + I_-)]. \qquad (69)$$

Therefore, the basis states in the τ_z manifold are coupled to those in the τ_y manifold that differ in their nuclear spin quantum number (I_z) by ± 1.

In order to make the Hamiltonian real it is convenient to redefine the electron spin basis states as,

$$\begin{aligned} |\tau_x> &= (1/\sqrt{2})(|-1> - |+1>) \\ |\tau_y> &= (1/\sqrt{2})(|-1> + |+1>) \qquad (70) \\ |\tau_z> &= |0> \end{aligned}$$

The complete spin Hamiltonian including both the A_{xx} and A_{zz} hyperfine elements is shown in Fig. 11. The hyperfine Hamiltonian may be treated as a perturbation of the eigenstates of H_{SS} and H_Q by non-degenerate perturbation theory since the degenerate nuclear levels are not coupled by the same hyperfine element.

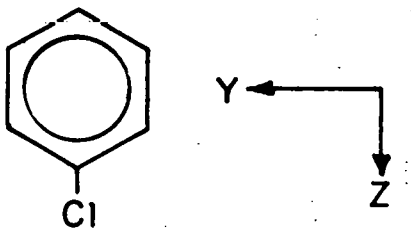

X 3/2	X -1/2	X -3/2	X +1/2	Y 3/2	Y -1/2	Y -3/2	Y +1/2	Z 1/2	Z -3/2	Z -1/2	Z 3/2
X+A				-3/2 Azz							
	X-A				+1/2 Azz						
		X+A				+3/2 Azz					
			X-A				-1/2 Azz				
-3/2 Azz				Y+A				$\sqrt{3}/2$ Axx			
	+1/2 Azz				Y-A			Axx	$\sqrt{3}/2$ Axx		
		+3/2 Azz				Y+A				$\sqrt{3}/2$ Axx	
			-1/2 Azz				Y-A			Axx	$\sqrt{3}/2$ Axx
				$\sqrt{3}/2$ Axx	Axx			Z-A			
					$\sqrt{3}/2$ Axx				Z+A		
						$\sqrt{3}/2$ Axx	Axx			Z-A	
							$\sqrt{3}/2$ Axx				Z+A

XBL 7012-7269

Figure 11

Hamiltonian Matrix for the Triplet Plus One I = 3/2 Nuclear Spin

Considering only the A_{xx} and A_{zz} Hyperfine Components

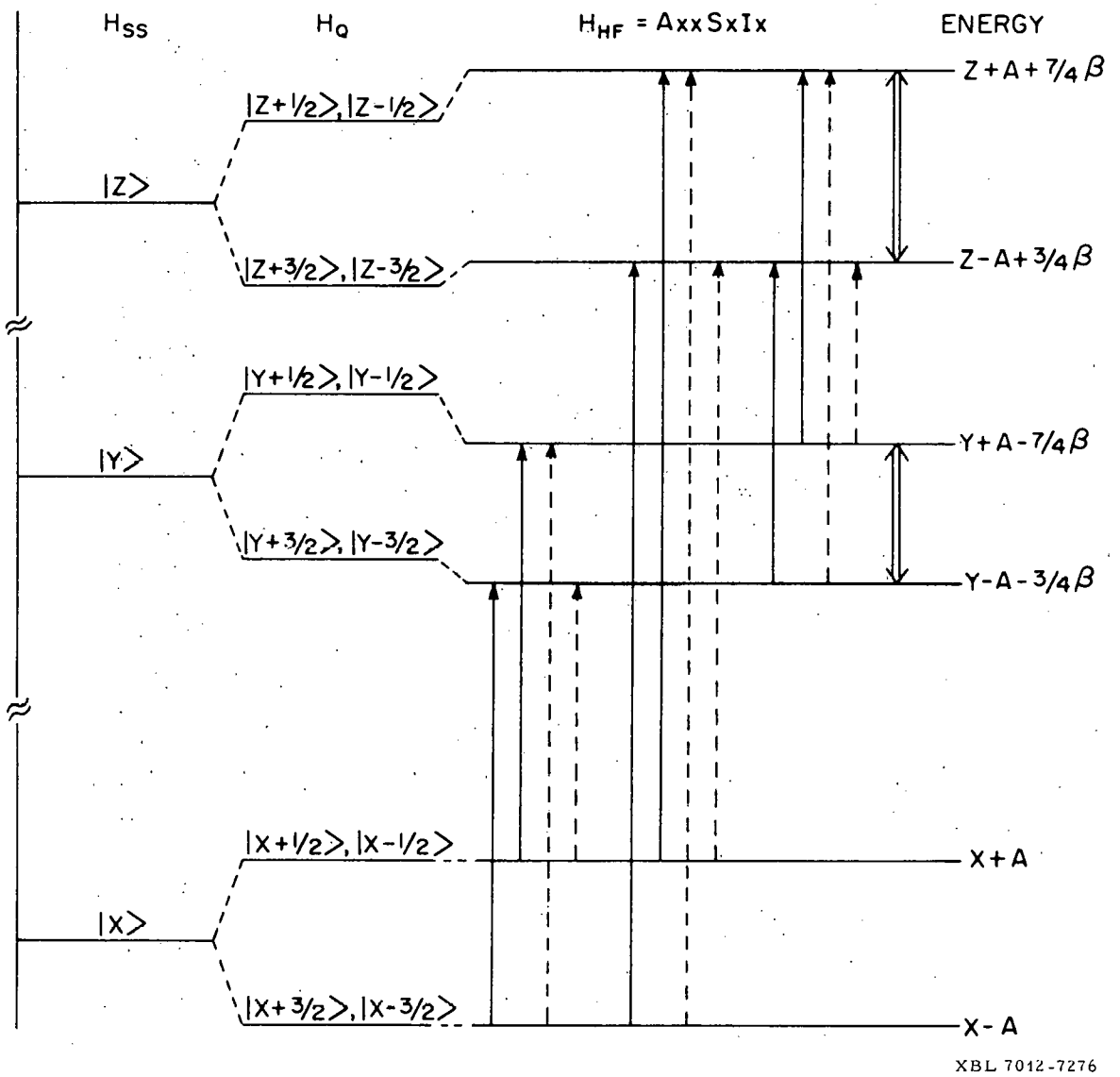

Figure 12

Energy Level Diagram for the Triplet and One I = 3/2 Nuclear Spin Considering only the A_{xx} Hyperfine Component

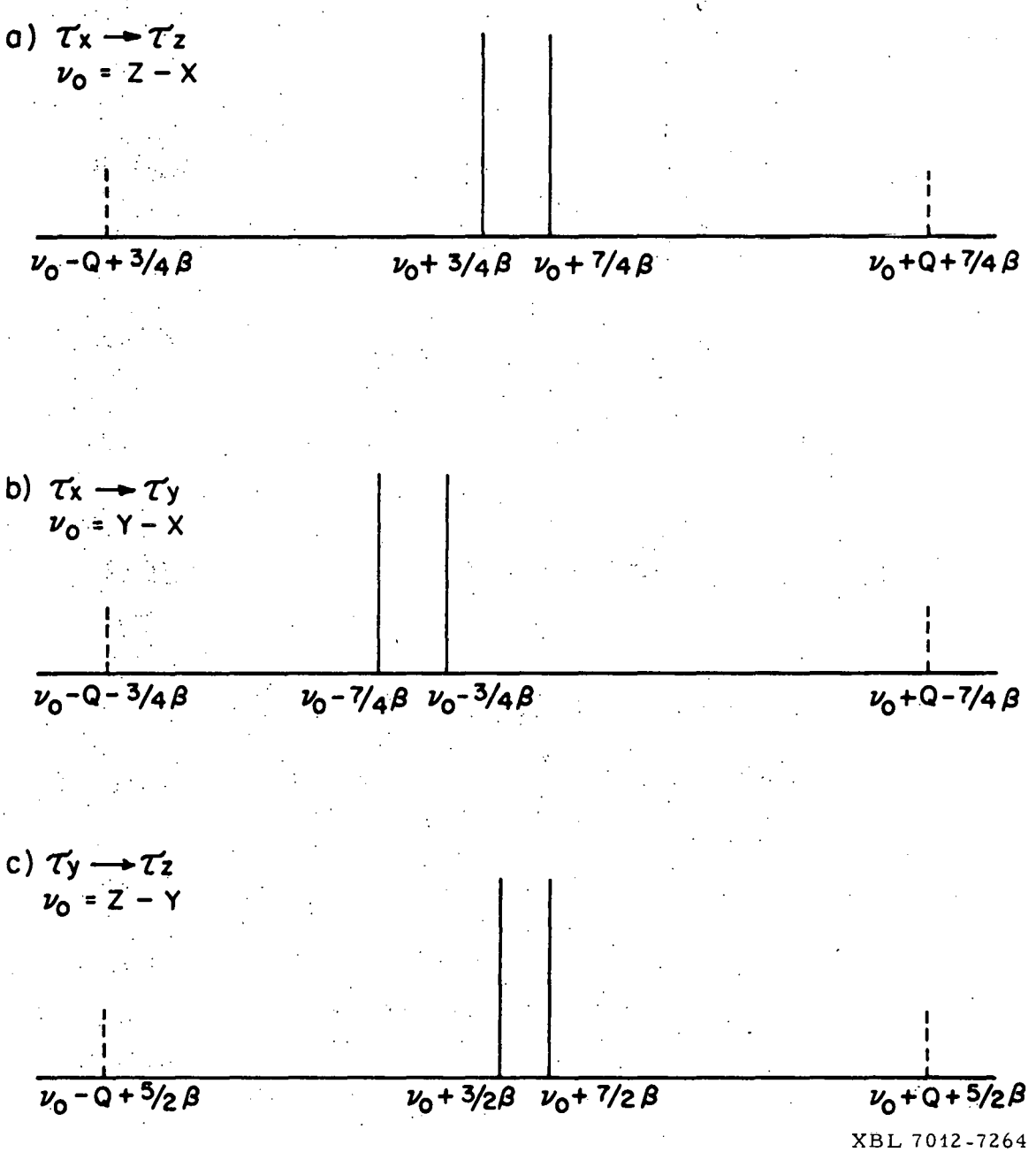

Figure 13

ODMR Spectra Predicted for the Energy Level Diagram Shown in Figure 12

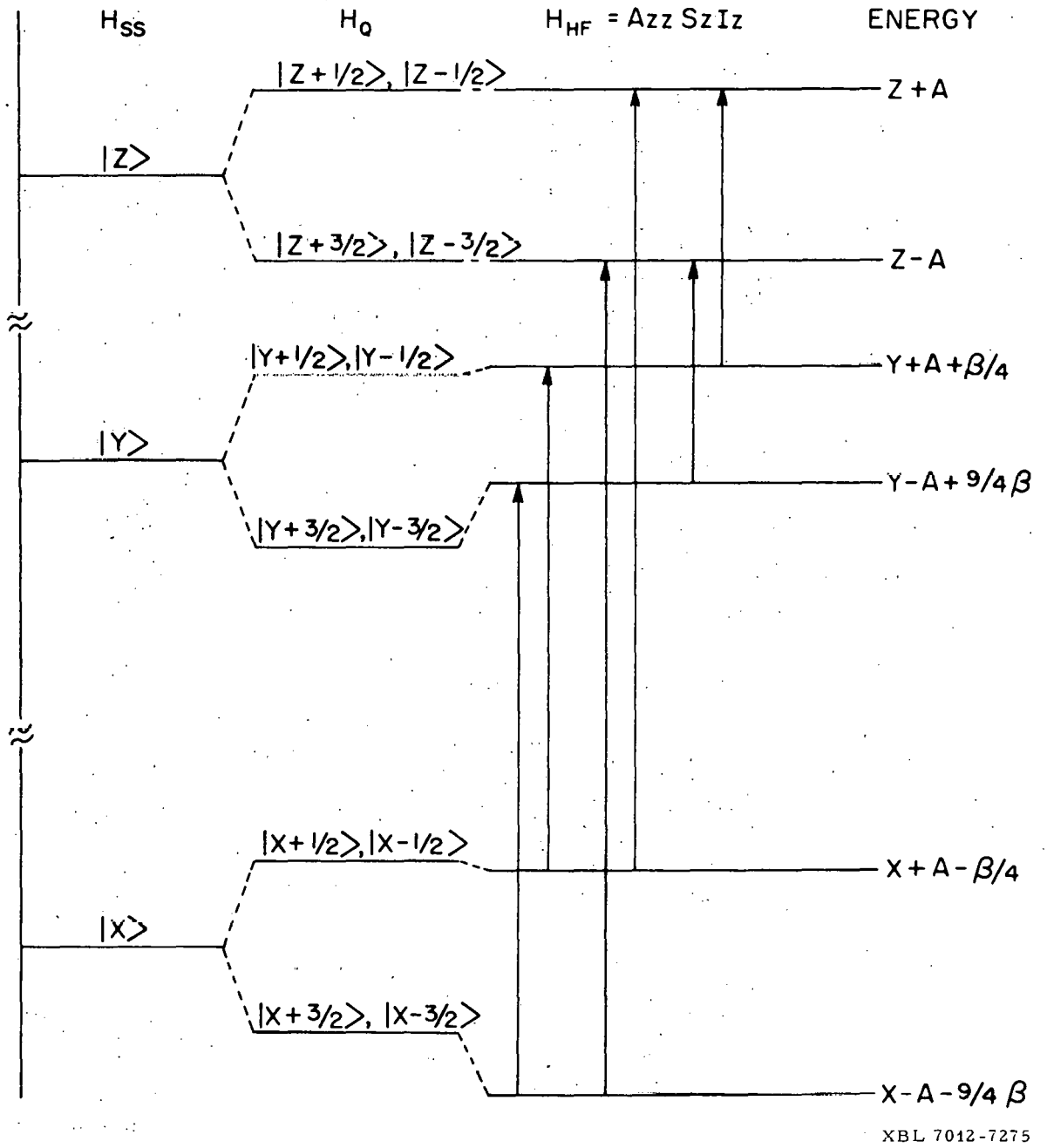

Figure 14

Energy Level Diagram for the Triplet and One I = 3/2 Nuclear Spin Considering only the A_{zz} Hyperfine Component

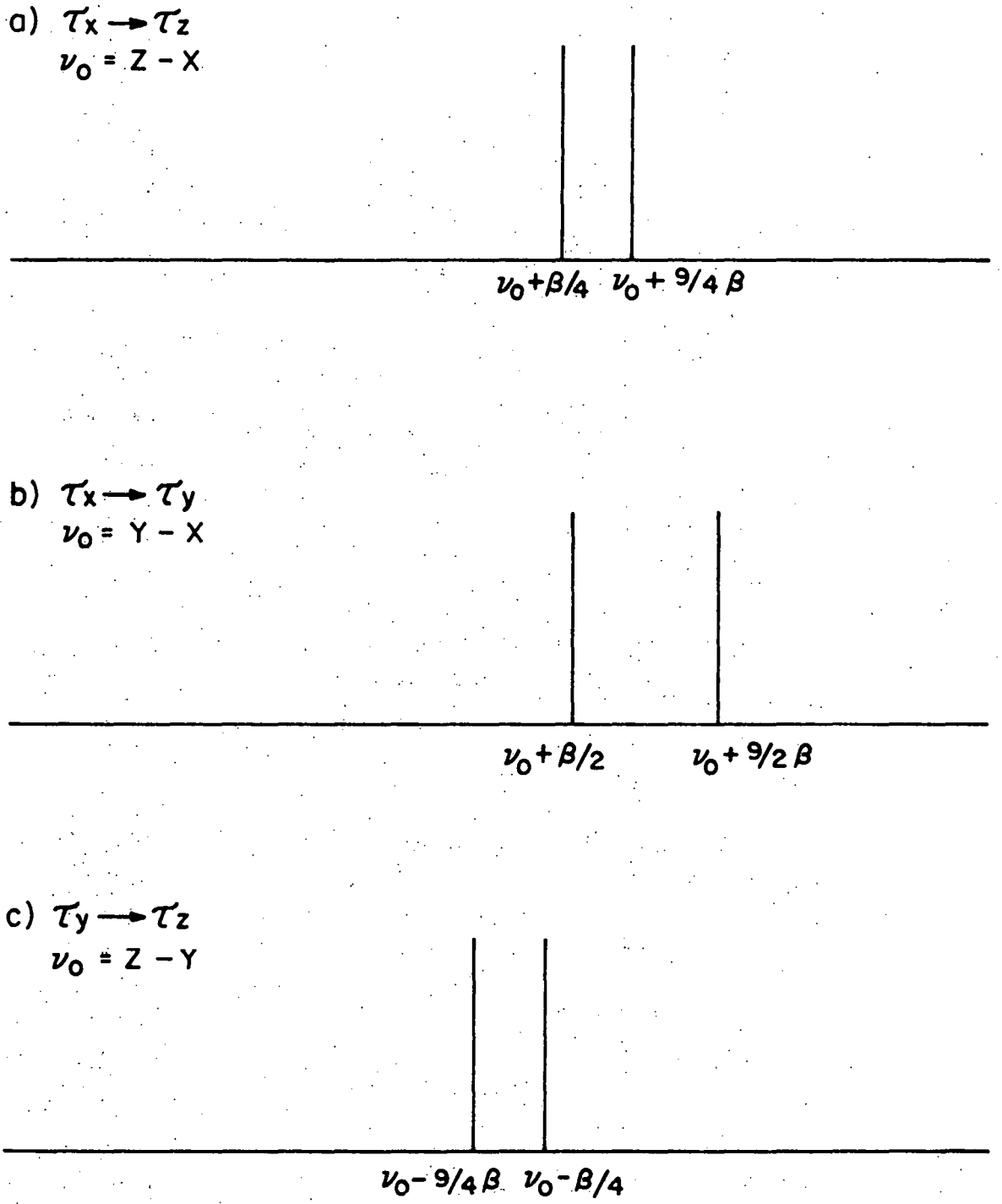

Figure 15

ODMR Spectra Predicted for the Energy Level Diagram Shown in Figure 14

The basis states that are coupled by A_{xx} may be represented graphically as

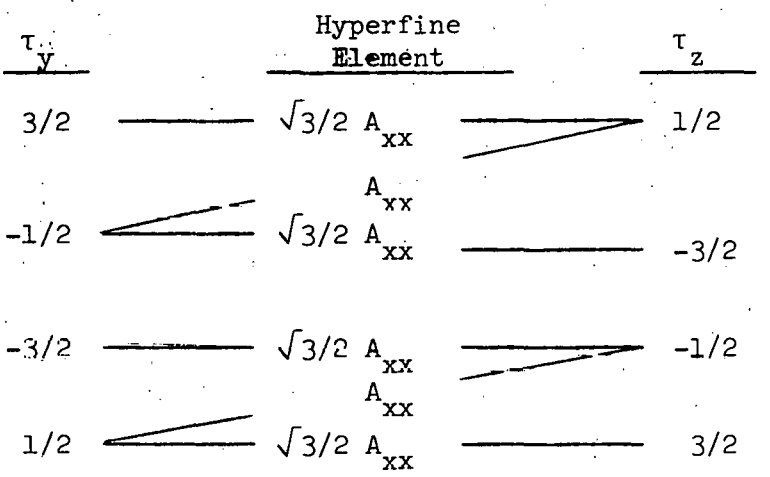

The effect of the perterbation treatment is that, to second order, the energy of the $\pm 3/2$ nuclear levels in the τ_y manifold are shifted to higher energy by an amount $3/4\ \beta$, where β is given by

$$\beta = \frac{Axx^2}{Ey - Ez}$$

and the $\pm 3/2$ level in the τ_z manifold is shifted to lower energy by an equal amount.

The $\pm 1/2$ levels of the τ_y manifold are shifted to higher energy by an amount $7/4\ \beta$ while the $\pm 1/2$ levels in the τ_z manifold are shifted an equal amount to lower energy. The resulting energy level diagram is shown in Fig. 12. Since this spin system has a total spin that is a half integer (5/2), it is a Kramers doublet, and therefore all the energy levels are twofold degenerate in the absence of an external magnetic field.

The hyperfine coupling therefore will never remove the degeneracy of the $\pm$ nuclear levels and consequently there are only six energy levels to consider.

In Fig. 13 the spectra corresponding to the three ESR transitions is shown. The "allowed" structure on each transition is split into two components separated by β for both the $\tau_x \rightarrow \tau_z$ and the $\tau_y \rightarrow \tau_z$ transitions and 2β for the $\tau_y \rightarrow \tau_z$ transitions.

The "forbidden" transitions, shown by the dotted lines in Fig. 13, correspond to simultaneous electron nuclear flips. The separation of the two forbidden satellites in each ESR transition is equal to $e^2qQ+\beta$, $e^2qQ-\beta$ and e^2qQ for the $\tau_x \rightarrow \tau_z$, $\tau_x \rightarrow \tau_y$ and $\tau_y \rightarrow \tau_z$ transitions respectively.

It is interesting to note that if only the perturbation due to the A_{yy} component of the hyperfine tensor is considered, the results may be obtained by an appropriate relabeling of Figs. 12 and 13. However, if only the A_{zz} component is considered, the nuclear sublevels in the τ_x manifold are mixed with those in the τ_y manifold having the same value of the I_z quantum number;

τ_x	Hyperfine Element	τ_y
3/2	3/2 A_{zz}	3/2
1/2	1/2 A_{zz}	1/2
-1/2	-1/2 A_{zz}	-1/2
-3/2	-3/2 A_{zz}	-3/2

therefore, no satellites due to nuclear transitions are observed. The resulting energy level diagram, considering only the A_{zz} component of the hyperfine tensor is given in Fig. 14 and the resulting spectra in Fig. 15.

The ENDOR transitions permitted by the electron dipole moment transition operator, for the case with only the A_{xx} hyperfine element, are shown by the double arrows in Figure 12. The analysis of the ENDOR spectra follows the same method as that for a spin one nucleus, with the same expression for the intensity of the transitions induced by the electron magnetic dipole moment transition operator and the nuclear magnetic dipole moment transition operator. When only the A_{zz} hyperfine element is present, the electron magnetic dipole transition operator is ineffective in producing ENDOR transitions and consequently the intensity of any observed ENDOR signal is due solely to the nuclear magnetic dipole transition operator.

Some generalizations can be made at this point concerning the appearance of "forbidden" satellites whose separation is in zeroth order the pure nuclear quadrupole transition frequency of the molecule in an excited triplet state. (a) For a nuclear spin $I = 1$ (e.g. ^{14}N) a hyperfine element associated with a direction i, A_{ii}, gives intensity into a simultaneous electron-nuclear flip in the plane normal to i. Thus, at least two nuclear hyperfine elements must be finite to obtain independently both e^2qQ and η. (b) For a nuclear spin $I = 3/2$ (e.g. ^{35}Cl), a nuclear hyperfine element parallel to the principal axis of the field gradient (i.e., A_{zz}) does not introduce mixing between electron-nuclear states that admit intensity into forbidden satellites. (c) For a nuclear spin $I = 3/2$, a nuclear hyperfine element perpendicular to the principal axis of the field gradient introduces intensity into forbidden satellites whose separation in zeroth order is the pure

nuclear quadrupole transition frequency; however, e^2qQ and η can never be obtained independently in the absence of an external magnetic field.

Although we have not treated explicitly the case where two nuclei are present on the same molecule, both having nuclear spin $I \geq 1$, the generalizations (a)-(c) hold with one additional feature being manifested, that is the possibility of simultaneous multiple nuclear-electron spin flips. In addition, simultaneous multiple nuclear ENDOR transitions are expected and, indeed, observed.

IV. EXPERIMENTAL EQUIPMENT AND PROCEDURE

In this section the procedures and equipment used in performing both the ESR and ENDOR experiments are given. In addition, some variations of the basic experiments are listed and their advantages discussed.

A. The ESR Experiment

The basic experimental arrangement is shown in Figure 16. The sample is mounted inside a helical slow wave structure[72] which is attached to a rigid stainless steel coaxial line suspended in a liquid helium dewar. The exciting light is supplied by a PEK 100-watt mercury short arc lamp mounted in a PEK M912 lamp housing. The output of the lamp is filtered by either an interference filter centered at 2500 Å, 2800 Å or 3100 Å; or a combination of Corning glass and solution filters.[73]

The phosphorescence is collected at a 90 degree angle to the exciting light and focused through an appropriate Corning filter (to remove scattered light) and onto the entrance slit of a Jarrel-Ash model 48-490, 3/4 meter spectrometer. The spectrometer has an f number of 6.5 and is equipped with adjustable curved slits. The resolving power of the spectrometer is greater than 30,000 with a dispersion of 8.2 Å/mm in first order. The spectral range in air is from 1900 to 16,000 Å.

The light at the exit slit is detected with an EMI 6256S photomultiplier mounted in an EMI dry-ice cooled housing. A Fluke 415B power supply is used to maintain the cathode of the photomultiplier at -1800 V. The output of the photomultiplier is connected to a Keithly model 610 CR

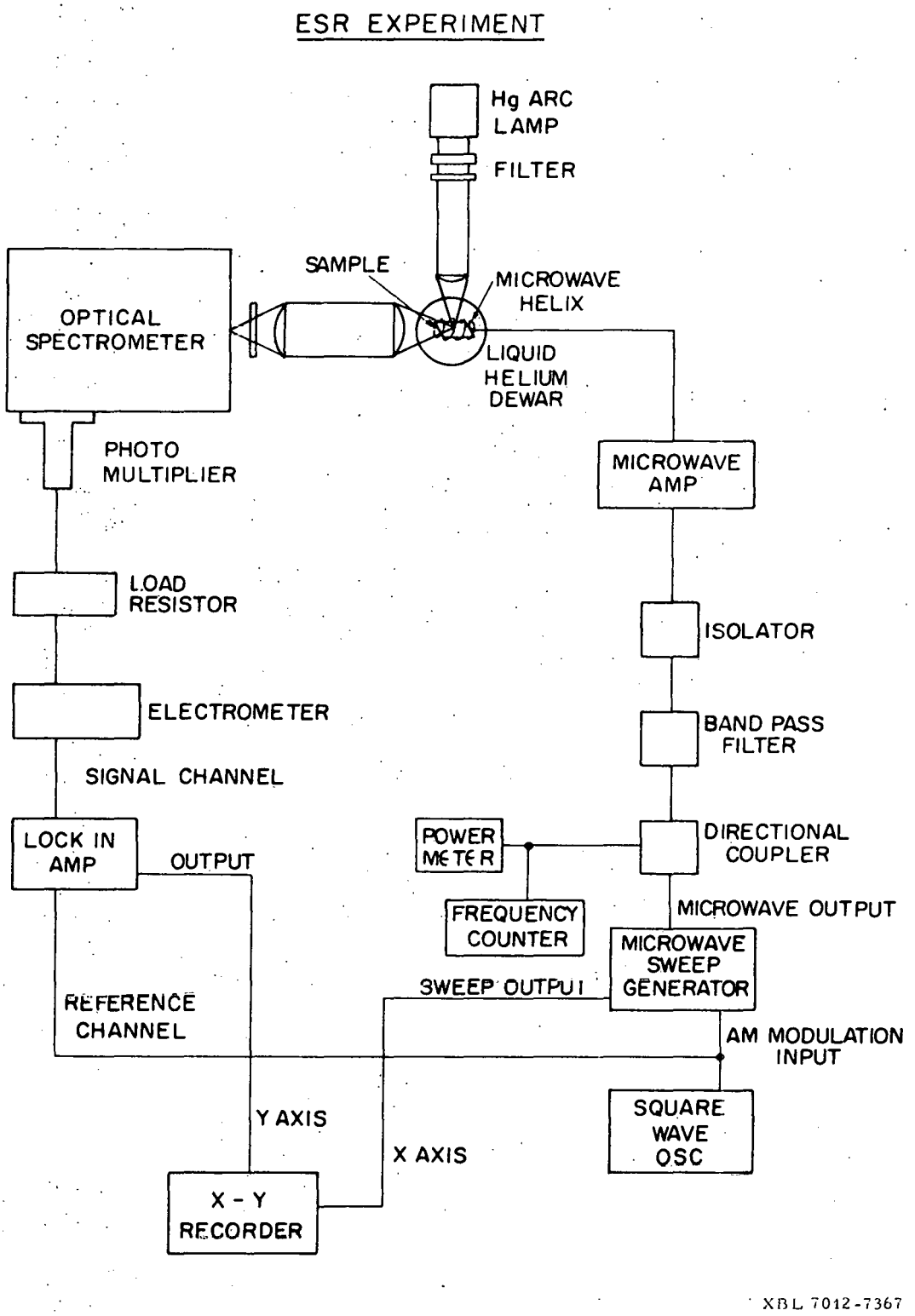

Figure 16

Experimental Arrangement for Optically Detected Electron Spin Resonance in Zero Magnetic Field

B. The ENDOR Experiment

The experimental arrangement usually employed is shown in Figure 17. An enlarged view of the sample, helix, and ENDOR coils is shown in Figure 18. The optical and microwave equipment is the same as that used in the ESR experiment with the exception that the microwave field (H_1) is not modulated. The radiofrequency field (H_2) is supplied by a Hewlett Packard model 8601A sweep oscillator that covers the region from 0.1 to 110 MHz. The output is modulated by an E G & G model LG101/N linear gate. The gate is driven by the square wave generator which also drives the reference channel of the lock-in amplifier.

The RF is then amplified by two broad-band distributed amplifiers,[74] a four watt unit (see Figure 19) and a 20 watt unit (Figure 20), and connected to the ENDOR coils. These amplifiers have the advantage that they operate over the range of 1 to 50 MHz without the need of adjustment. A series of these amplifiers was designed and constructed in collaboration with Bob Smith and Bill Gagnon of Lawrence Radiation Laboratory for use in pulsed nuclear quadrupole resonance experiments. Since these amplifiers are a significant advancement in high power broad-band amplifiers, the schematics are shown in Figures 21-26. The largest unit will produce 10,000 watt pulses of RF with a 20 percent duty cycle.

The ENDOR coil consists of a "bridge T" constant resistance network[75] in a Helmholtz arrangement as shown in Figure 18.

The x axis of the recorder is driven by the ramp voltage from the RF sweep oscillator and the y axis from the output of the lock-in amplifier.

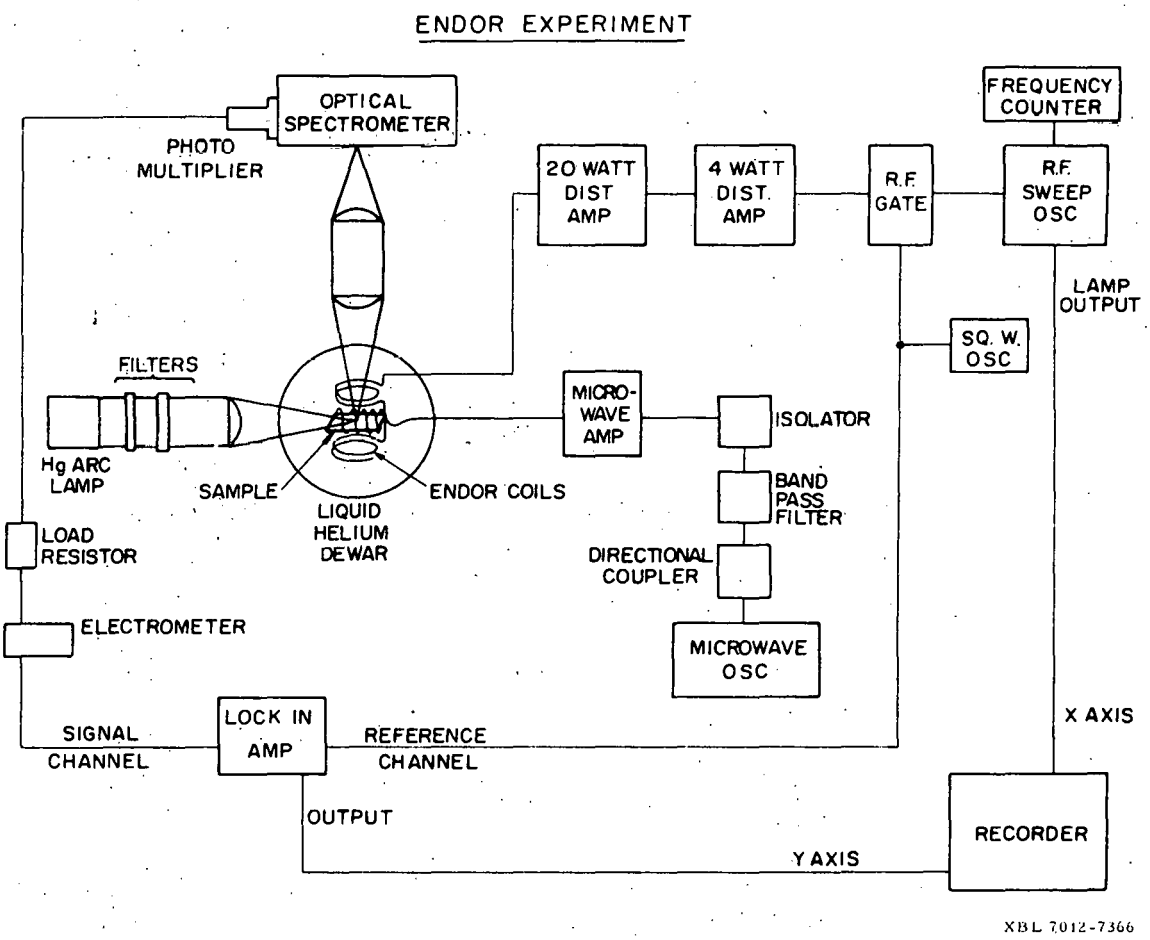

Figure 17

Experimental Arrangement for Optically Detected ENDOR in Zero Magnetic Field

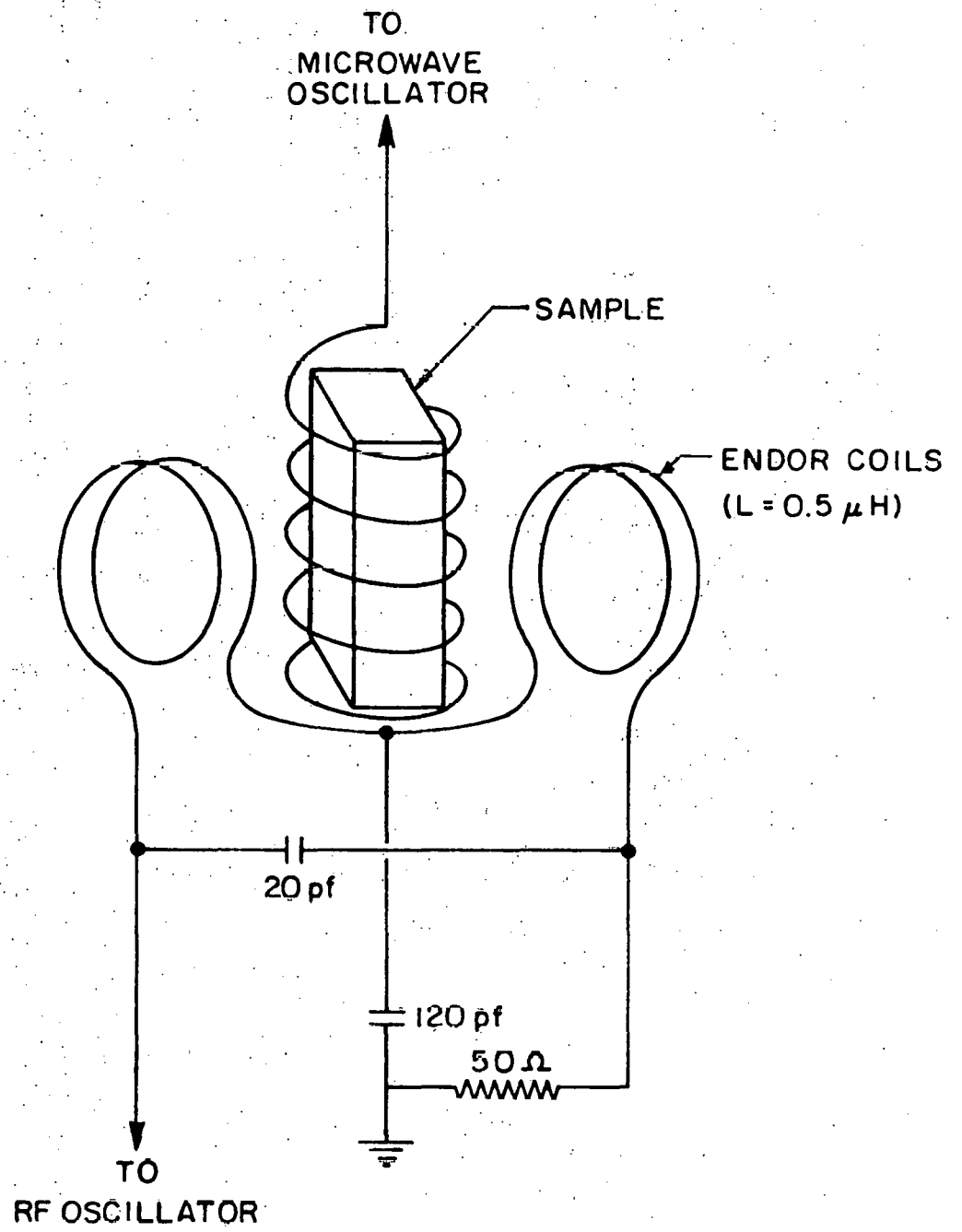

XBL 7012-7365

Figure 18

Sample Arrangement and ENDOR Coil Schematic

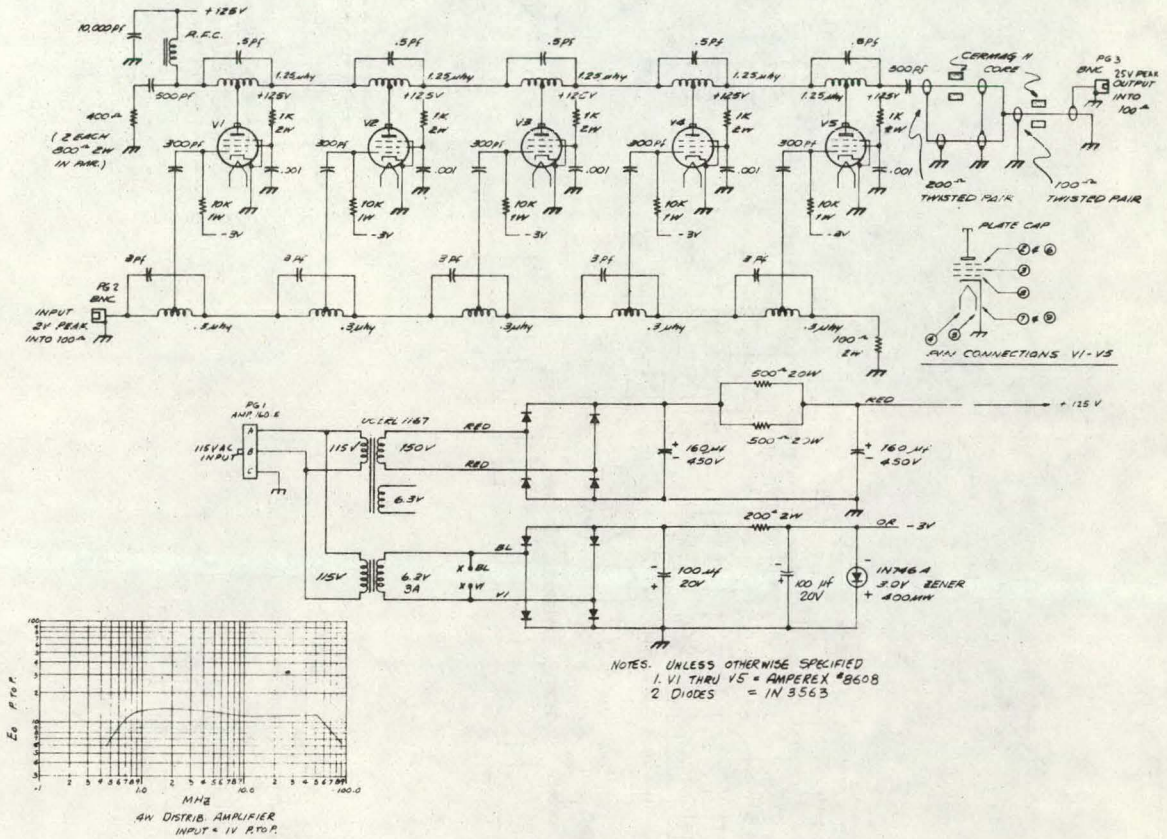

XBL 7012-7278

Figure 19

½ Watt Distributive Amplifier Schematic

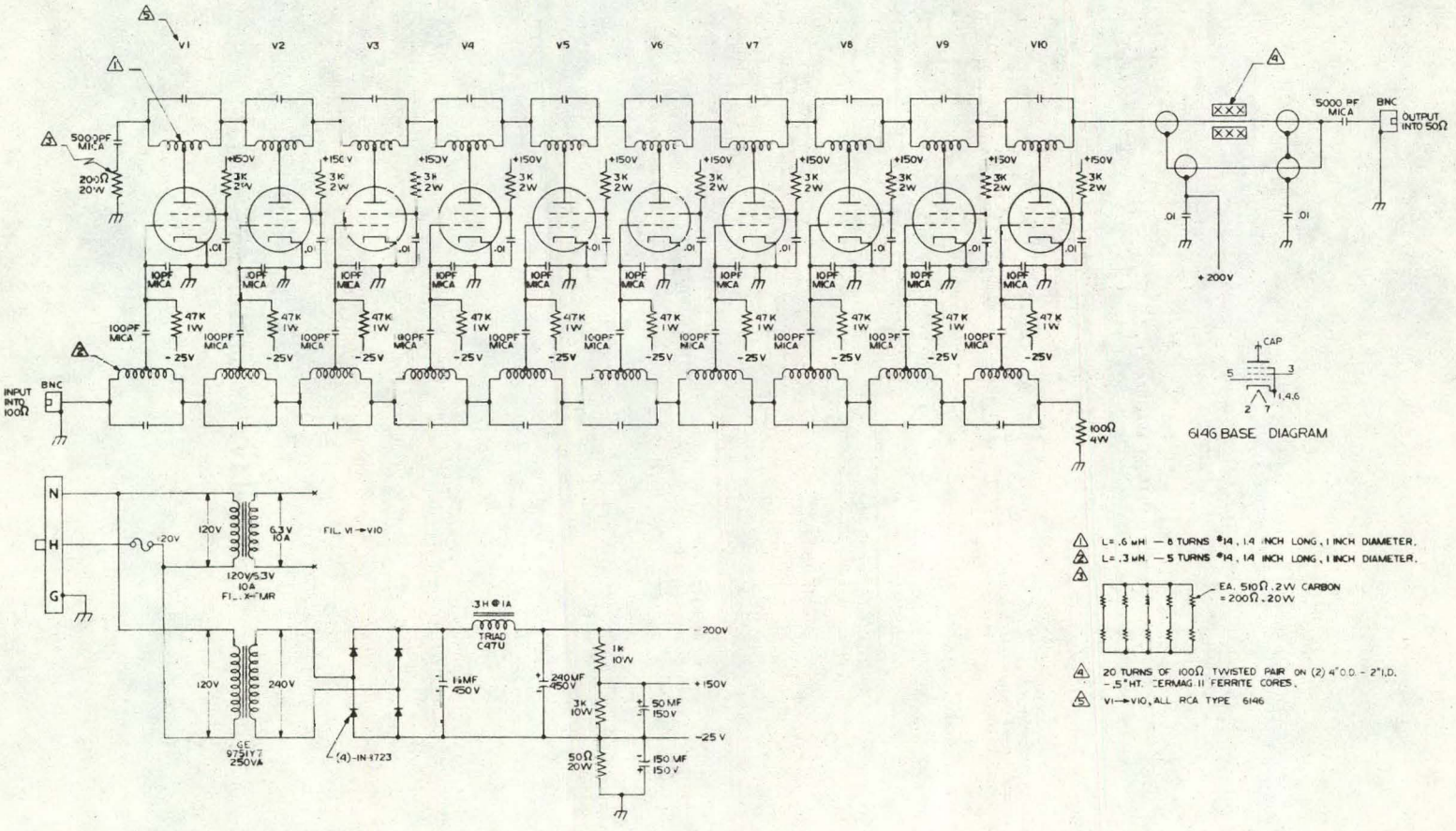

Figure 20

20 Watt Distributive Amplifier Schematic

1. L=.6 MH. — 8 TURNS #14, 1.4 INCH LONG, 1 INCH DIAMETER.
2. L=.3 MH. — 5 TURNS #14, 1.4 INCH LONG, 1 INCH DIAMETER.
3. EA. 510Ω, 2W CARBON = 200Ω, 20W
4. 20 TURNS OF 100Ω TWISTED PAIR ON (2) 4" O.D. - 2" I.D. - .5" HT. FERMAG II FERRITE CORES.
5. V1→V10, ALL RCA TYPE 6146

XBL 7012-7257

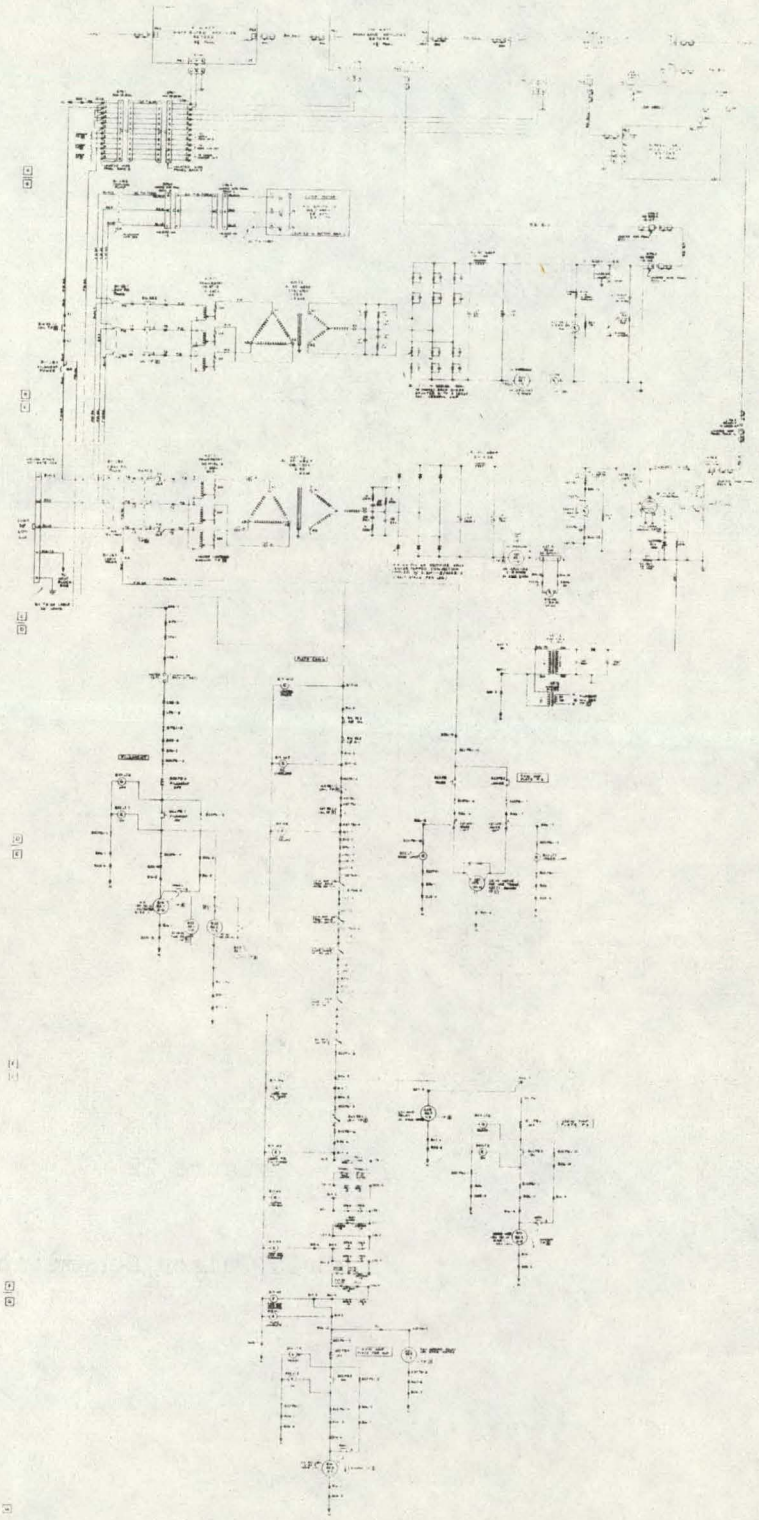

XBL 7012-7353

Figure 21

Broad Band Distributive Amplifier System Master Schematic

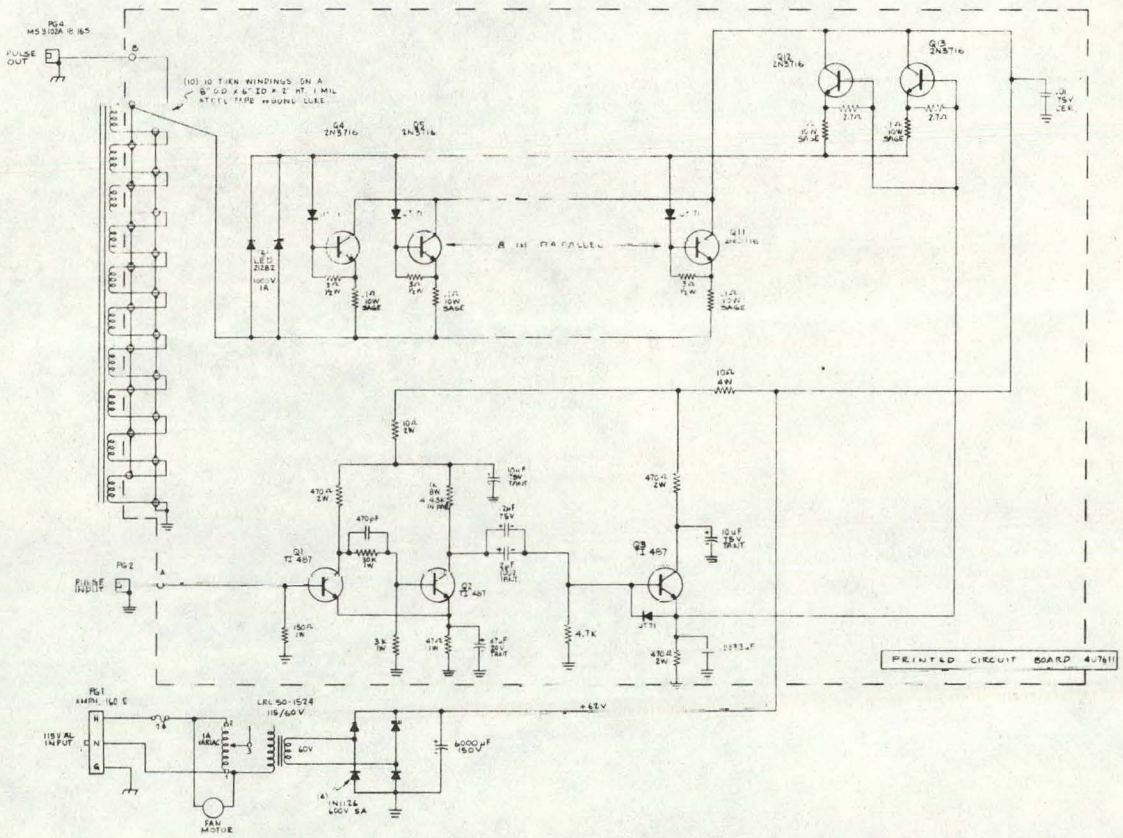

XBL 7012-7351

Figure 22

Grid Pulser Schematic

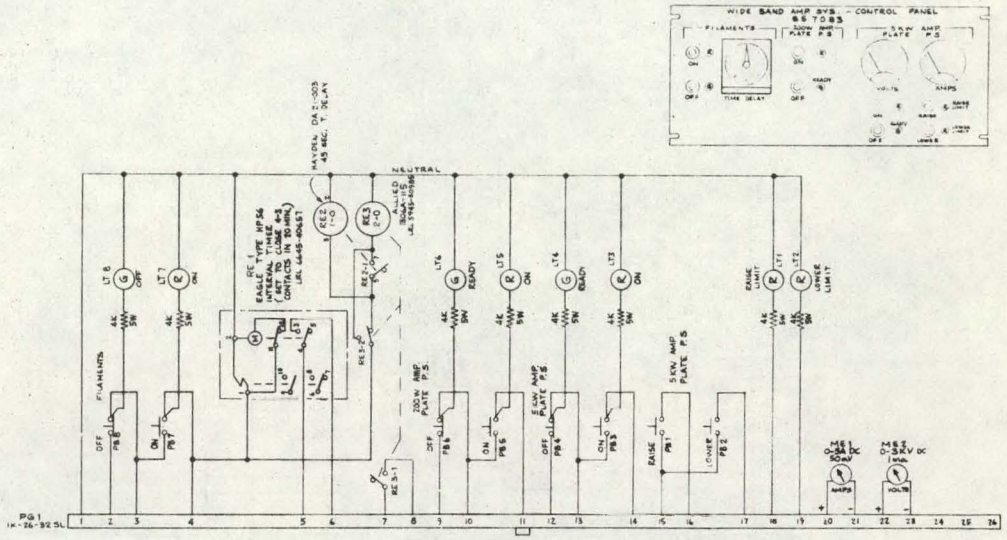

PARTS

PB 4,6,8	- ACRO 4DC5-5P N.C. PUSHBUTTON
PB 1,2,3,5,7	- " 4DO5-5P N.O. "
LT 1-8	- SOCKETS DIALCO 162-8430
	- RED LENS " 162-971
	- GRN " " " -972
	- LAMPS GE 327 28V

6¾" PANEL

XBL 7012-7352

Figure 23

Control Panel Schematic

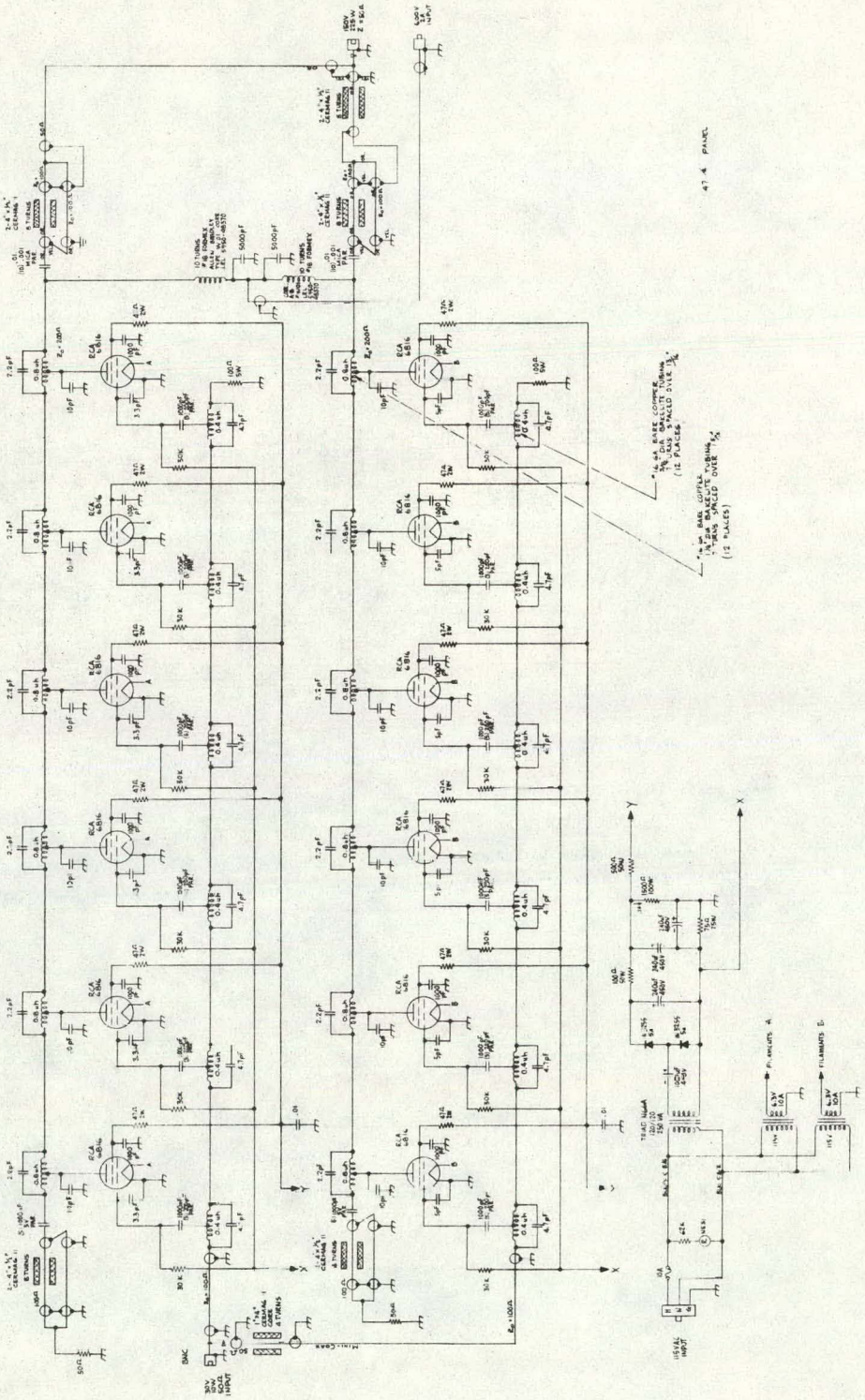

XBL 7012-7355

Figure 24

200 Watt Push-Pull Distributive Amplifier Schematic

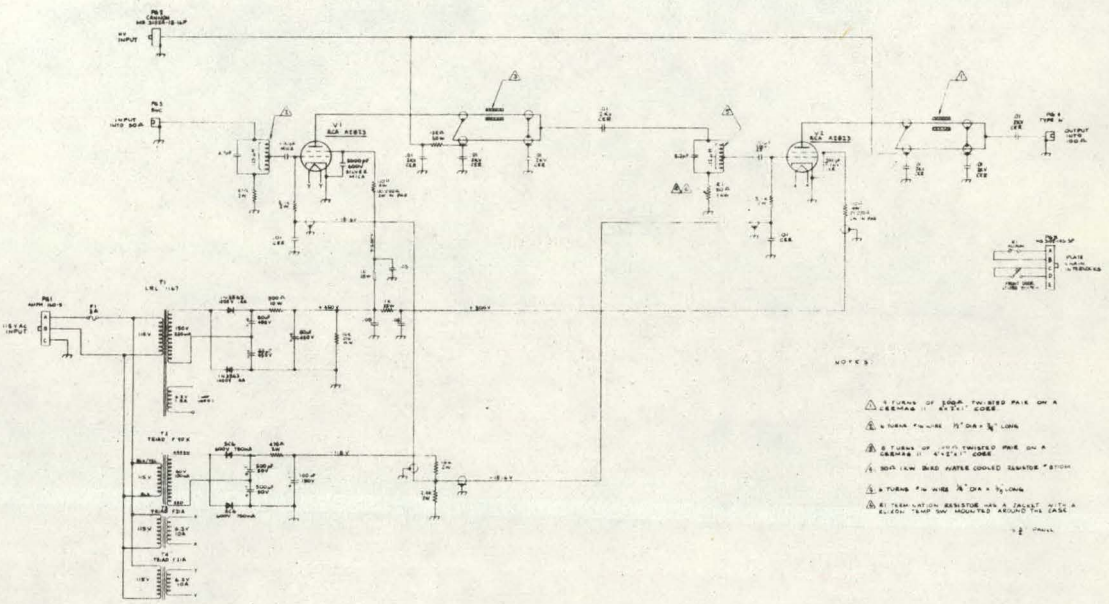

XBL 7012-7277

Figure 25

200 Watt Distributive Amplifier Schematic

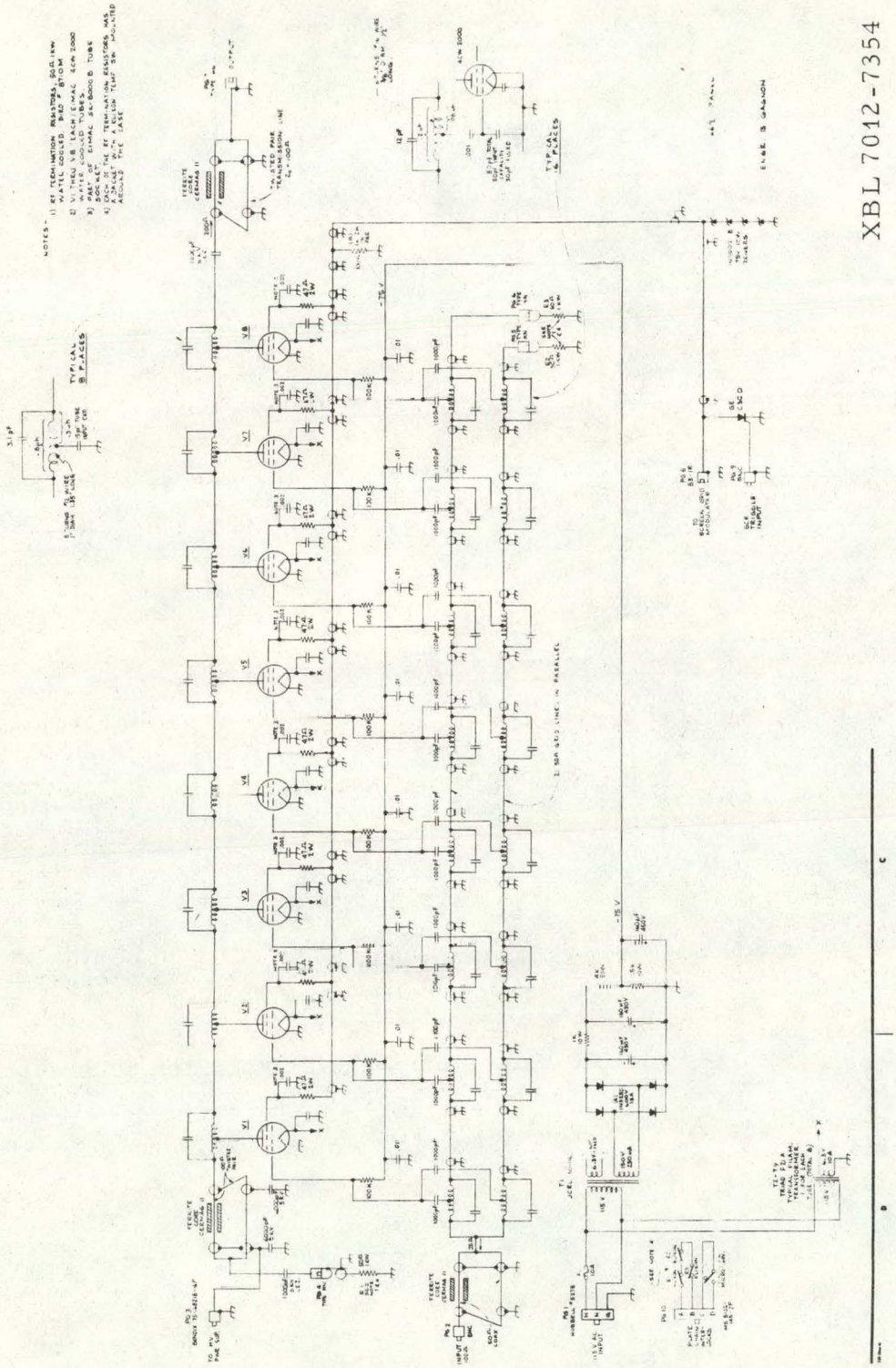

XBL 7012-7354

Figure 26

10,000 Watt Distributive Amplifier Schematic

C. Variations of the Basic Experiments

The optical detection of magnetic resonance permits several additional parameters to be experimentally adjusted. These include the energy and bandwidth of the phosphorescence that is monitored as well as the energy, bandwidth and intensity of the exciting light. In addition, the power of the microwave field H_1 may be adjusted over a wider range than in experiments in which the absorption of microwave power is monitored. This is due to the fact that saturation gives the maximum signal strength using optical detection techniques, while with absorption experiments the signal strength will decrease as the power is increased above that needed for saturation. The advantage of this is that the signal strength of weak "forbidden" transitions may be improved by the application of large H_1 fields without a decrease in the signal strength of the allowed transitions.

Some of the most useful variations of the basic experiment are listed in Table IV. If a high resolution spectrometer is employed to isolate the phosphorescence emission, the optically detected ESR may be used to simplify the phosphorescence spectrum by amplitude modulation of the H_1 field while saturating an ESR transition. The modulation of the phosphorescence is detected with a phase sensitive amplifier while sweeping the optical spectrum. Since only two of the three triplet levels are coupled by the H_1 field, only the emission from these two levels will be detected. Therefore, by repeating the experiment while saturating the remaining two ESR transitions, three spectra are obtained, each including only the emission from two of the three zero field levels.

electrometer through an adjustable load resistor. The output of the electrometer is connected to the signal channel input of a PAR model HR-8 lock-in amplifier.

The microwave field is supplied by a Hewlett Packard sweep oscillator model 8690B equipped with plug-in units to cover the range from 0.1 to 18 GHz. The output is connected to a Servo Corp. traveling wave tube amplifier (1 to 12 GHz at 1 watt, #3003; 1 to 2 GHz at 20 watts, #2210; and 2 to 4 GHz at 20 watts, #2220). The output of the amplifier is then fed consecutively through a directional coupler, a band-pass filter, and an isolator to the rigid coaxial line on which the helix is mounted.

The microwave sweep oscillator is amplitude modulated with a Hewlett-Packard model 211 AR square wave generator which is also connected to the reference channel of the lock-in amplifier. The output of the lock-in amplifier drives the y axis of a Hewlett Packard model 7004B recorder while the ramp voltage from the microwave sweep oscillator drives the x axis.

The temperature of the sample is usually lowered to approximately 1.3° K by pumping on the liquid helium with three Kinney model KTC-21 vacuum pumps operated in parallel.

The ESR experiment is performed by monitoring the change in emission of the sample while varying the frequency of the modulated microwave field. As explained in section II, the signal may either increase or decrease. With a lock-in amplifier a decrease in emission intensity corresponds to a phase shift of 180 degrees relative to the signal obtained for an increase in emission intensity.

The information obtained from the analysis of phosphorescence spectra is extremely useful by itself in characterizing the triplet state, and complementary to the information obtained from the analysis of the ESR spectrum.

In ENDOR experiments the radiofrequency field H_2 may also be adjusted. These experiments are usually performed by saturating an ESR transition while varying the frequency of the H_2 field. Either the H_1 or H_2 fields may be modulated; however, it is usually preferable to modulate the H_2 field since, in this case, only the change in intensity of the phosphorescence due to the ENDOR resonance is detected with a lock-in amplifier. On the other hand, if the H_1 field is modulated, there is a constant signal due to the ESR transition which changes in intensity when the H_2 field is swept through resonance. A useful modification of this technique is achieved by modulation of the H_2 field while simultaneously saturating an ENDOR transition and sweeping the H_1 field. In this case, only the ESR transitions that connect energy levels simultaneously coupled by the H_1 and the H_2 fields are detected. This method is useful in analyzing the structure of the ESR transition since the contribution to the spectrum due to different isotopes and/or nuclei may be isolated.

If both an ESR and an ENDOR transition are saturated while modulating the H_2 field and scanning the phosphorescence spectrum, it is possible to isolate the contribution to the phosphorescence spectrum from molecules containing different nuclear isotopes. As an example, if the phosphorescence from a molecule such as chlorobenzene is monitored and a Cl^{35} ENDOR transition saturated while modulating the H_2 field, only the

contribution to the phosphorescence spectrum from molecules containing the Cl^{35} isotope will be detected. The same experiment may then be repeated detecting only the contribution from the molecules containing the Cl^{37} isotope. The difficulty in this experiment is that only small, if any, variations in the phosphorescence spectrum would be expected and consequently, the maximum resolution of the optical spectrometer must be employed. This severely limits the signal to noise ratio of the ENDOR signal.

TABLE IV

Techniques of Optical Detection of ESR

	Excitation Light	Optical Spectrometer	Microwave Modulation	Advantages
1)	C.W.	No	No	measure absolute change in total emission
2)	C.W.	Yes	No	Measure absolute change in emission of particular vibronic bands
3)	Chopped	Optional	No	Improvement in S/N over Methods 1 and 2 by narrow band phase sensitive detection of the phosphorescence
4)	C.W.	Optional	A.M.	detect only the change in emission from either the total emission or a particular vibronic band
5)	C.W.	Optional	F.M.	detect the derivative of the spectrum, helpful in resolving spectra
6)	C.W.	Sweep	A.M.	detect only the emission from 2 of the 3 sublevels while sweeping the optical spectrum
7)	Sweep	Yes	A.M.	useful in studying the pathways of intersystem crossing

V. RESULTS AND DISCUSSION

A. The $\pi\pi^*$ state of 8 - Chloroquinoline

One of the primary objectives of our research is the measurement of nuclear quadrupole coupling constants of nuclei in molecules in their excited triplet state. In particular we are interested in measuring the nuclear quadrupole coupling constants of chlorine since this is probably the most thoroughly investigated of all nuclei for molecules in their ground state. The zero field detection of the electron spin resonance and chlorine ENDOR of 8-chloroquinoline in its $\pi\pi^*$ state has been observed and the spectrum interpreted in terms of a spin Hamiltonian which includes the ^{14}N, ^{35}Cl, and ^{37}Cl hyperfine and nuclear quadrupole interactions. In addition, chlorine satellites have been observed in the ESR and chlorine ENDOR observed for the $\pi\pi^*$ state of 2-3 dichloroquinoxaline.

The sample consisted of a single crystal of durene doped with approximately 0.1 mole percent 8-chloroquinoline grown from the melt. The sample was mounted inside a helical slow-wave structure with a 2 mm inside diameter. The helix is matched to a rigid coaxial line which is supported vertically inside a liquid helium dewar which was maintained at 1.7° K by pumping on the liquid helium. The 3100 Å region of the mercury short arc lamp was used as the exciting source, the sample being irradiated with light through the open helix windings. The 0 - 0 band of the phosphorescence of 8-chloroquinoline was detected at a 90° angle to the exciting source and isolated with the Jarrell-Ash optical spectrometer. All ESR experiments were performed by using continuous

microwave power. The resonance was detected by monitoring the change in intensity of the phosphorescence as a function of microwave power. The apparatus used for both the ESR and ENDOR experiments is essentially the same as that shown in Figures 16 and 17 except that the output of the electrometer was plotted directly since no modulation was used. The ENDOR experiments used the arrangement shown in Figure 18 which allowed both the nitrogen and chlorine resonances to be observed without having to change coils.

Two of the three electron transitions, those associated with the $\tau_y \rightarrow \tau_z$ and $\tau_x \rightarrow \tau_z$ electron spin manifolds, were observed with satisfactory resolution. The $\tau_y \rightarrow \tau_z$ multiplet is centered at 860 MHz while the $\tau_x \rightarrow \tau_z$ multiplet is centered at 3483 MHz. In both cases, under steady state exciting light conditions, the 0-0 band phosphorescence emission increased when the microwave field coupled the respective spin manifolds. At low microwave power (10 μ watts) the strong "allowed" electron transitions were found. As the microwave power was increased (100 μ watts), "forbidden" satellites split off the major transitions by ~3 MHz were observed. At higher powers (100-1000 μ watts) "forbidden" satellites saturated and an additional multiplet of satellites were observed split ~25-40 MHz from the center section. Figure 27 illustrates a microwave power study of the $\tau_x \rightarrow \tau_z$ transition. The same basic pattern was observed for the $\tau_y \rightarrow \tau_z$ transitions. ^{35}Cl and ^{37}Cl ENDOR were observed by monitoring the change in the phosphorescence intensity of the 0-0 band while saturating one of the $\tau_y \rightarrow \tau_z$ microwave transitions in the outer satellite multiplet and simultaneously sweeping

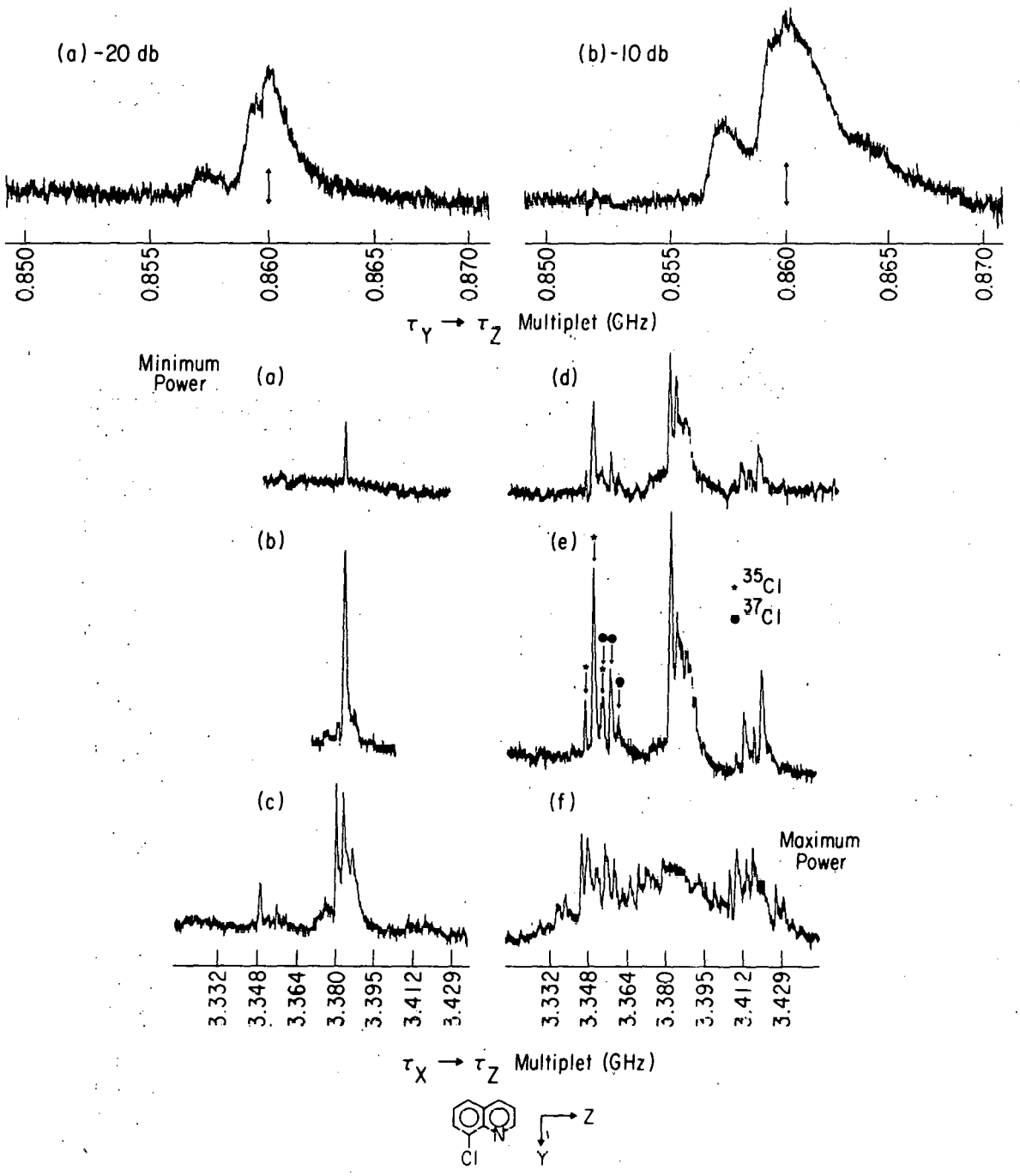

XBL 7012-7258

Figure 27

ODMR Transitions Observed in 8-Chloroquinoline

the rf frequency. An example of an optically detected ^{35}Cl ENDOR in zero field is shown in Figure 28. All observed frequencies and relative intensities are given in Tables 5, 8, and 9. Measurement of the transition frequencies with an accuracy better than ~0.4 MHz was generally not possible due to the line widths associated with the individual lines (~ 1.0 MHz) and their overlap with other transitions.

The structure of the zero field transition $\tau_y \rightarrow \tau_z$ and $\tau_x \rightarrow \tau_z$ and the accompanying ENDOR observed in 8-chloroquinoline can be understood in terms of the spin Hamiltonian already developed,

$$H = H_{SS} + H_Q^N + H_Q^{Cl} + H_{HF}^N + H_{HF}^{Cl} \qquad (1)$$

where H_{SS} is the zero field splitting Hamiltonian

$$H_{SS} = -(XS_x^2 + YS_y^2 + ZS_z^2) \qquad (2)$$

and H_Q^N, H_Q^{Cl}, and H_{HF}^N, H_{HF}^{Cl} are the nuclear quadrupole interaction and electron-nuclear hyperfine interaction for nitrogen and chlorine. Equation 1 may be simplified by the following assumptions.

First, we assume that the y and z components of H_{HF}^N and H_{HF}^{Cl} may be neglected. This is justified insofar as the EPR measurements of Maki et al.[42,43] on quinoline have shown that $A_{xx} > A_{yy}$, A_{zz} for the ^{14}N hyperfine interaction. Moreover, since the perturbations due to reasonable in-plane components for either ^{14}N or $^{35,37}Cl$ would be much smaller than those due to A_{xx}, they can, to a first approximation, be ignored. We shall also assume that the principal axes of the tensor

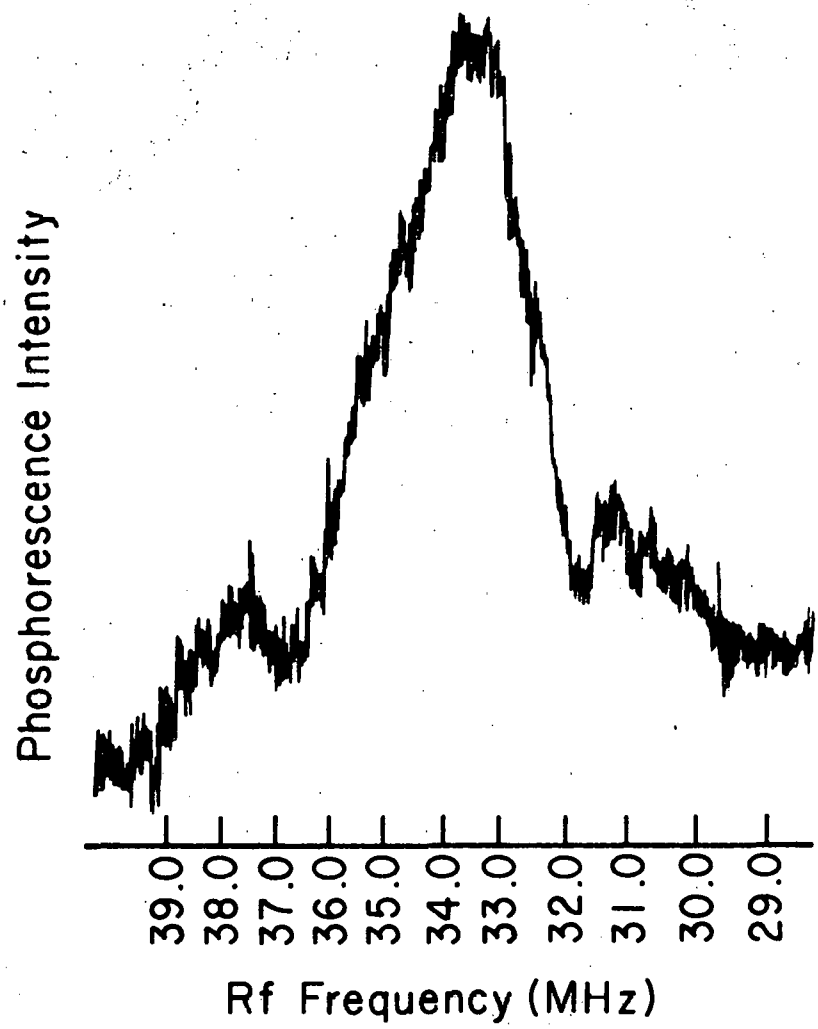

XBL 7012-7272

Figue 28

Optically Detected ^{35}Cl ENDOR Observed While Saturating the Microwave Transition at 826.2 MHz in the $\tau_y \rightarrow \tau_z$ Multiplet

interactions H_{SS}, H_Q^N, and H_Q^{Cl}, coincide. It is reasonable to assume that the principal axis of H_Q^N and H_Q^{Cl} would be close to the direction of the nitrogen lone pair orbital and along the C-Cl bond respectively (approximately along the Y molecular axis). Furthermore, in quinoline the nitrogen lone pair direction and the Y axis of H_{SS} are within a few degrees of each other.[42,43] We assume that 8-chloroquinoline does not deviate appreciably in this respect. With these approximations we can write*

$$H_Q^N = - xI_x^2 - yI_y^2 - zI_z^2 \qquad (3)$$

$$H_Q^{Cl} = H_Q^{Cl} = e^2qQ(Cl)[3I_z^2 - 15/4]/12 + H_Q^{Cl}(\eta) \qquad (4a)$$

$$H_Q^{Cl}(\eta) = e^2qQ(Cl)\eta[I_+^2 + I_-^2]/24 \qquad (4b)$$

$$H_{HF}^N = A_{xx}(N)I_xS_x \qquad (5)$$

$$H_{HF}^{Cl} = A_{xx}(Cl)(1/2i)[I_+S_x - I_-S_x] \qquad (6)$$

With this coordinate system the nitrogen and molecular axis are coincident, the chlorine x axis is along the molecular x axis, the chlorine y axis along the molecular z axis and the chlorine z

* We have defined I_x as $(1/2i)\,[I_+ - I_-]$ rather than the conventional $(1/2)\,[I_+ + I_-]$. In our definition the Hamiltonian matrix is thus real so long as $A_{yz}(Cl)$ and $A_{zy}(Cl) = 0$. We could have reversed the molecular x and y axes and used the standard convention but we chose to have the axis system for quinoline[25,26] and 8-chloroquinoline the same.

axis is along the molecular y axis. Therefore we will designate the out of plane chlorine hyperfine component as A_{xx}, the component along the molecular y axis as A_{zy} and the component along the molecular z axis as A_{yz}. In order to simplify the following discussion we will initially consider only the ^{35}Cl isotope.

The product functions $< u\ f\ v\ |^{\pm} = \tau_u \chi_f^{\pm} \chi_v$ form a set of eigenfunctions which diagonalize H_{SS}, H_Q^N and H_Q^{Cl} (excluding $H_Q^{Cl}(\eta)$), τ_u, $\chi_f^{\pm}$ and χ_v are the electron, chlorine nuclear and nitrogen spin functions respectively. u and v correspond to x, y and z while $\chi_f^{\pm}$ take on values +3/2, -3/2, +1/2, and -1/2. With this choice of basis functions, only H_{HF}^N, H_{HF}^{Cl} and the parameter containing the Cl field gradient asymmetry, $H_Q^{Cl}(\eta)$, are off-diagonal in the Hamiltonian matrix. An energy level diagram appropriate to the $\tau_y \rightarrow \tau_z$ transition in 8-chloroquinoline is given in Figure 29 with the zero field energies arranged in the order $E_z > E_y > E_x$. The result of $H_Q^{Cl}(\eta)$ is to mix the states $< u\ f\ v\ |^{\pm}$ differing in f by ±2; thus, η cannot give intensity to "forbidden" transitions between the different spin manifolds. However, since $H_Q^{Cl}(\eta)$ couples states that are also coupled to states in a different electron spin manifold by H_{HF}^{Cl}, η may give rise to small frequency (~10 kHz) shifts and intensity variations via the interaction with H_{HF}^{Cl}. Since these variations are very small, η cannot be obtained reliably from our data. Therefore, the ^{35}Cl first order nuclear quadrupole splitting between $< Z\ 3/2|^{\pm}$ and $< Z\ 1/2|^{\pm}$, or $< Y\ 3/2|^{\pm}$ and $< Y\ 1/2|^{\pm}$ will be written in terms of one parameter $^{35}Q'$, by defining

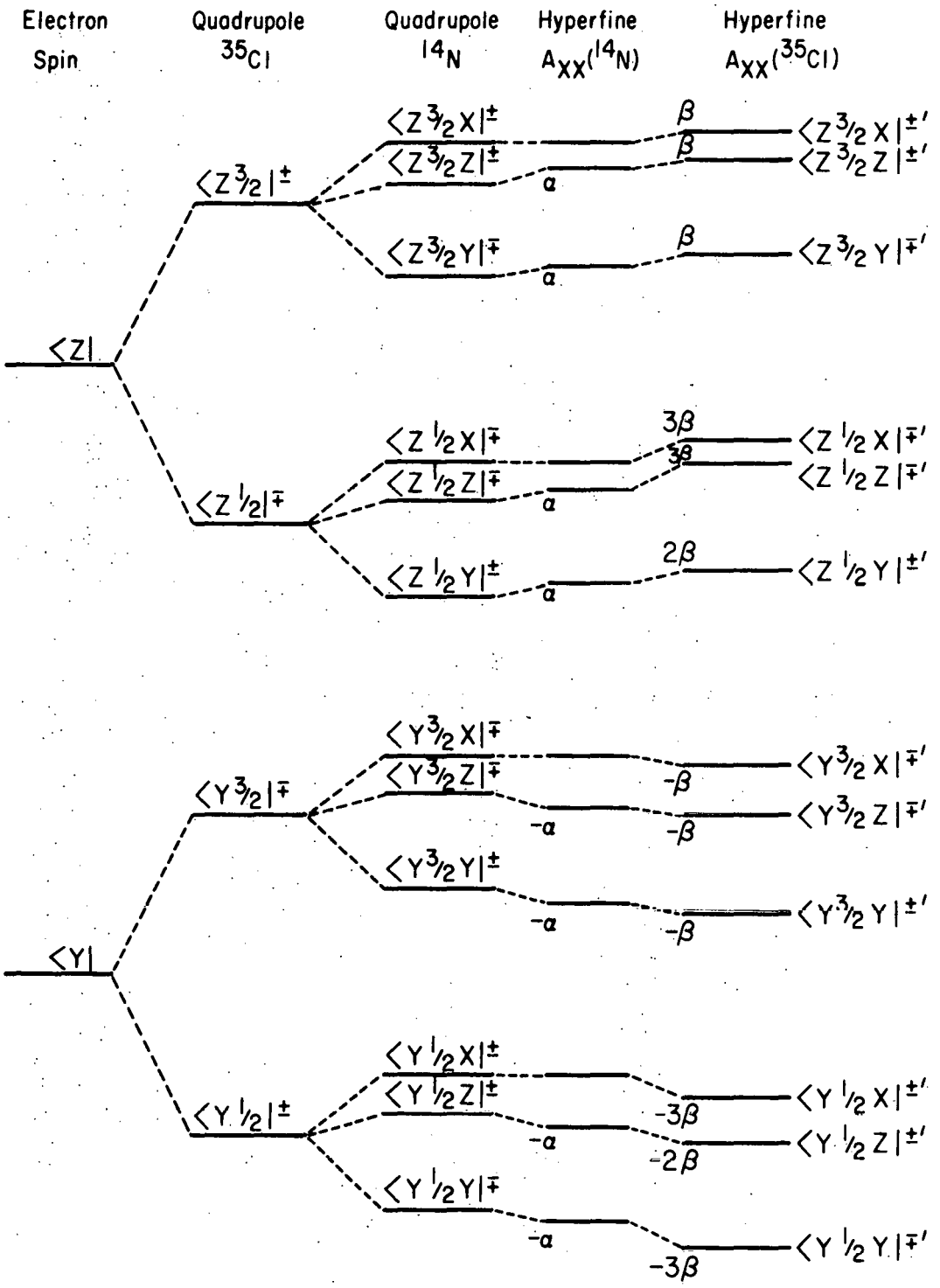

XBL 7012-7273

Figue 29

Energy Level Diagram for the τ_z and τ_y Triplet Manifolds

$$^{35}Q' = e^2qQ(^{35}Cl)(1 + {}^2/3)^{1/2} \quad . \qquad (7)$$

In the case of the nitrogen quadrupole interaction it has been shown[26] that in the approximation $A_{yy}(N)$, $A_{zz}(N) = 0$, $e^2qQ(^{14}N)$ and η cannot be obtained separately therefore, we shall use the measured parameter ν_- with the assumption that both the nitrogen asymmetry parameter, η, and the nitrogen quadrupole coupling constant, $e^2qQ(^{14}N)$, are positive.

The principal result of H_{HF}^{N} acting as a perturbation is that the levels $< Z\ 3/2\ Z|^{\pm}$, $< Z\ 3/2\ Y|^{\pm}$, $< Z\ 1/2\ Z|^{\pm}$, and $< Z\ 1/2\ Y|^{\pm}$ shift to a higher energy by an amount $\alpha = A_{xx}{}^2(N)/(Z\text{-}Y)$ and the levels $< Y\ 3/2\ Z|^{\pm}$, $< Y\ 3/2\ Y|^{\pm}$, $< Y\ 1/2\ Z|^{\pm}$, and $< Y\ 1/2\ Y|^{\pm}$ shift to lower energies by an equal amount (cf. Figure 29). Similarly, the result of H_{HF}^{Cl} is the mix the states in the τ_y and τ_z manifolds. The order of the plus and minus sign, $< |^{\pm}$ corresponds to the components of Kramers pair which are not split in zero field. Table 6 lists the states mixed under these perturbations. Because H_{HF}^{Cl} mixes states involving two or more basis states in the same electron spin manifold, H_{HF}^{Cl} cannot be adequately treated by first order perturbation theory. Therefore computer diagonalization of the Hamiltonian matrix was employed. It was found that under the perturbation H_{HF}^{Cl}, the states shifted to a first approximation by energies related to multiples of $\beta = A_{xx}{}^2(Cl)\rho(Z\text{-}Y)$. An analysis of the problem revealed that this approximation was good to within 0.3 MHz over a reasonable range of $A_{xx}(Cl)$ values. We should

emphasize that this is only an approximation but is empirically* verified. Since we resolve no splittings in the spectra directly attributable of H_{HF}^{Cl}, the β's are employed to treat H_{HF}^{Cl} as a "pseudo" first order perturbation.

From an inspection of the states mixed by H_{HF}^{N} and H_{HF}^{Cl} (See table 6) four types of transition between the electron spin manifolds can be classified using the electron magnetic dipole moment transition operator. These can be described as: (a) electron spin transitions only, (b) simultaneous electron and nitrogen spin transitions, (c) simultaneous electron and chlorine spin transitions, and (d) simultaneous electron, nitrogen and chlorine spin transitions. The approximate transition energies are given in Table 5 in terms of the spin Hamiltonian parameters. It should be noted that with the approximation that both the chlorine and nitrogen in-plane hyperfine elements can be neglected, the τ_x manifold is not mixed with τ_y or τ_z; thus, the basis functions $|u\ f\ v>^{\pm}$ are not perturbed. The primed states in the tables and figures correspond to the perturbed basis functions. With the above approximation it is immediately apparent from table 5 that all parameters except $A_{xx}(Cl)$ can be obtained easily with reasonable accuracy. For example, $A_{xx}(N)$ can be estimated from the energy difference between the transitions $<Y\ 3/2\ X|' \rightarrow <Z\ 3/2\ X|'$ and the degenerate pair $<Y\ 3/2\ Z|' : <Y\ 3/2\ Y|' \rightarrow <Z\ 3/2\ Z|' : <Z\ 3/2\ Y|'$ while $\nu_-\ (^{14}N)$ can be obtained to a first approximation from

* The use of empirical connotes the observation of the shifts resulting in the computer diagonalization of the Hamiltonian matrix over a range of $A_{xx}(Cl)$ values.

the difference in the transition energies $<Y\ 3/2\ Z|' \rightarrow <Z\ 3/2\ Y|'$ and $<Y\ 3/2\ Y|' \rightarrow <Z\ 3/2\ Z|'$. This region of the electron spin transitions $\tau_y \rightarrow \tau_z$ is shown in Figure 27. In a similar fashion the ^{35}Cl field gradient parameter $^{35}Q'$ can be estimated from transitions associated with either the $\tau_x \rightarrow \tau_z$ or $\tau_y \rightarrow \tau_z$ manifolds. For instance, the transitions $<X\ 1/2\ X| \rightarrow <Z\ 3/2\ X|'$ and $<X\ 3/2\ X| \rightarrow <Z\ 1/2\ X|'$ or $<Y\ 1/2\ X|' \rightarrow <Z\ 3/2\ X|'$ and $<Y\ 3/2\ X|' \rightarrow <Z\ 1/2\ X|'$ may be used. In fact all parameters except $A_{xx}(Cl)$ can be obtained from many different combinations of transitions as shown in Table 5. Table 7 lists the values and standard deviations obtained by averaging many of the different combinations possible in Table 5. The difficulty in obtaining an accurate measurement of $A_{xx}(Cl)$ is reflected in the large error assigned to its value.

As in the cases of quinoline,[25,26] quinoxaline[25] and 2,3-dichloroquinoxaline[24] optically detected ENDOR is predicted in 8-chloroquinoline. The intensity of the ENDOR transitions can be accounted for solely in terms of the electron magnetic dipole transition operator. Thus, ENDOR is expected between nuclear levels in only the τ_y and τ_z manifolds since within our approximations, the τ_x manifold is not mixed with other electron spin states. Three different types of ENDOR are predicted and can be described as: (a) nitrogen spin transitions only, (b) chlorine spin transitions only, and (c) simultaneous chlorine and nitrogen spin transitions. In addition the ENDOR transitions should be associated with specific microwave transitions between the $\tau_y \rightarrow \tau_z$ or $\tau_x \rightarrow \tau_z$ manifolds. Table 8 lists the observed ENDOR transitions and

assigns each of them to one of the above classifications in addition to the microwave transitions with which they are associated. Indeed all three types are observed and excellent agreement between the transition energies and associated microwave transitions is obtained. These data provide a sensitive test of the uniqueness of the assignments made in Table 5 and the parameters used to obtain the transition energies.

Although we have dealt specifically with ^{35}Cl, we can explain and assign transitions associated with ^{37}Cl nuclear quadrupole and nuclear electron hyperfine interactions. The observed microwave transitions and assignments are listed in Table 9 along with the ENDOR transitions for the low frequency $\tau_y \rightarrow \tau_z$ microwave transitions. Naturally the intensity of these transitions are a factor of three lower than the corresponding ^{35}Cl transition because of their relative isotopic abundance. Although the difference between the ^{35}Cl and ^{37}Cl nuclear quadrupole moment is clearly observed, the difference in the nuclear magnetic moment cannot be observed since the splittings arising from the chlorine hyperfine interaction is not sufficiently resolved.

The value of the chlorine coupling constant $e^2qQ(^{35}Cl)(1 - \eta^2/3)^{1/2} =$ 68.4 MHz is approximately the same as that reported for the ground state of 6-chloroquinoline (69.256 MHz) and 7-chloroquinoline (69.362 MHz),[79,80] indicating that in the $\pi\pi^*$ triplet state the electron environment of the chlorine nucleus is not changed significantly from that of the ground state.

Although our analysis of the observed spectra accounts for the major features of the data, there are several minor discrepancies which

cannot be understood within our approximations.* First, it appears that we must consider finite $A_{yy}(N)$, $A_{zz}(N)$, $A_{yz}(Cl)$ and $A_{zy}(Cl)$ values to fit all transition energies more accurately and to account for the line widths. Secondly, at maximum power (cf. Figure 1(f)), six pairs of satellites appear in the $\tau_x \rightarrow \tau_z$ multiplet centered at ~3.339, 3.367, 3.373, 3.398, 3.404 and 3.431 GHz. These satellites may be due to ^{13}C or ^{1}H interactions or alternatively guest-host interactions. The possibilities should be distinguishable by isotope substitution and/or small Zeeman perturbations.

In order to find out if the observation of the interaction of the chlorine nuclei is generally observable, we repeated the experiments of Tinti[23] et al. on 2-3 dichloroquinoxaline. The power dependence of the $\tau_y \rightarrow \tau_z$ transition is shown in Figure 30. As can be seen, at minimum power (Figure 30a) the resonance shows only the structure due to the nitrogen hyperfine and quadrupole interactions. As the power is increased (Figures 30b and 30c), the chlorine satellites split approximately 35 MHz from the center section are observable and increase in intensity, until with maximum power (~100 mWatts) the chlorine satellites are almost as strong as the center or "allowed" section and transitions split approximately 70 MHz from the center section due to simultaneous electron and two chlorine spin transitions are observed. In addition ^{35}Cl and ^{37}Cl ENDOR resonances were observed while saturating the $\tau_y \rightarrow \tau_z$ multiplet.

* Since the completion of this experiment the weak emission from a second site of 8-chloroquinoline in durene has been identified.[36] The zero field splitting for the two sites are different (ΔD = 2.4 MHz and ΔE = 150 MHz) which may increase the experimental line width and perhaps partially explain the anomalous power dependence of the ESR transitions.

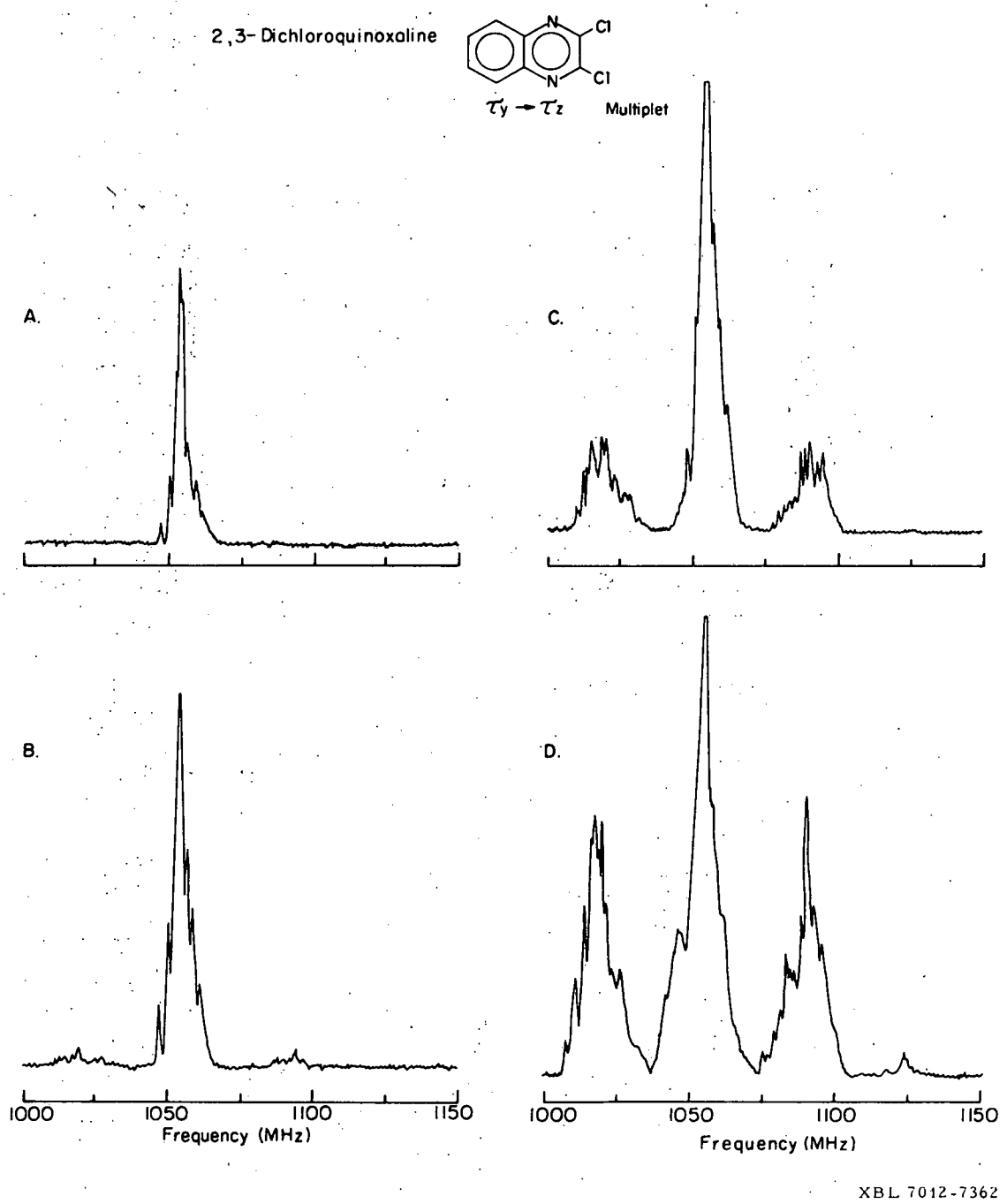

Figure 30

ODMR Spectra of $\tau_y \rightarrow \tau_z$ Multiplet of 2-3 Dichloroquinoxaline

No attempt was made to make a quantitative analysis of the spectra since there are two chlorine nuclei and two nitrogen nuclei in addition to the triplet electrons. Since this system has a total spin of 6, it is not a Kromers doublet and therefore, a 432 x 432 matrix would have to be diagonalized in order to fit the spectra. However, the two lines in the center section of the spectra that could not be assigned and the small splitting observed in the ^{14}N ENDOR (see Reference 24) are most likely due to the hyperfine interaction of the chlorine nuclei.

Table 5

Energies and assignments of observed frequencies involving electron, ^{14}N, and ^{35}Cl transitions

Transition	Energy *	Observed frequency (MHz)	Relative ‡ intensity	Classification
$\langle Y3/2X\vert' \rightarrow \langle Z3/2X\vert'$	$Z-Y+2\beta$	859.3	1.9	a
$\langle Y1/2X\vert' \rightarrow \langle Z1/2X\vert'$	$Z-Y+6\beta$			a
$\langle Y3/2Z\vert' \rightarrow \langle Z3/2Z\vert'$	$Z-Y+2\alpha+2\beta$	860.1	2.7	a
$\langle Y3/2Y\vert' \rightarrow \langle Z3/2Y\vert'$	$Z-Y+2\alpha+2\beta$			a
$\langle Y1/2Z\vert' \rightarrow \langle Z1/2Z\vert'$	$Z-Y+2\alpha+5\beta$			a
$\langle Y1/2Y\vert' \rightarrow \langle Z1/2Y\vert'$	$Z-Y+2\alpha+5\beta$			a
$\langle Y3/2Z\vert' \rightarrow \langle Z3/2Y\vert'$	$Z-Y-\nu_-+2\alpha+2\beta$	857.3	1.6	b
$\langle Y1/2Z\vert' \rightarrow \langle Z1/2Y\vert'$	$Z-Y-\nu_-+2\alpha+4\beta$			b
$\langle Y3/2Y\vert' \rightarrow \langle Z3/2Z\vert'$	$Z-Y+\nu_-+2\alpha+2\beta$	863.8	1.3	b
$\langle Y1/2Y\vert' \rightarrow \langle Z1/2Z\vert'$	$Z-Y+\nu_-+2\alpha+6\beta$			b
$\langle Y3/2X\vert' \rightarrow \langle Z1/2X\vert'$	$Z-Y-(Q'/2)+4\beta$	826.2	2	c
$\langle Y3/2Y\vert' \rightarrow \langle Z1/2Y\vert'$	$Z-Y-(Q'/2)+2\alpha+3\beta$			c
$\langle Y3/2Z\vert' \rightarrow \langle Z1/2Z\vert'$	$Z-Y-(Q'/2)+2\alpha+4\beta$			c
$\langle Y1/2X\vert' \rightarrow \langle Z3/2X\vert'$	$Z-Y+(Q'/2)+4\beta$	895.0	1.8	c
$\langle Y1/2Z\vert' \rightarrow \langle Z3/2Z\vert'$	$Z-Y+(Q'/2)+2\alpha+3\beta$			c
$\langle Y1/2Y\vert' \rightarrow \langle Z3/2Y\vert'$	$Z-Y+(Q'/2)+2\alpha+4\beta$			c
$\langle Y3/2Z\vert' \rightarrow \langle Z1/2Y\vert'$	$Z-Y-(Q'/2)-\nu_-+2\alpha+3\beta$	822.8	1.9	d
$\langle Y3/2Y\vert' \rightarrow \langle Z1/2Z\vert'$	$Z-Y-(Q'/2)+\nu_-+2\alpha+4\beta$	829.2	1.7	d
$\langle Y1/2Z\vert' \rightarrow \langle Z3/2Y\vert'$	$Z-Y+(Q'/2)-\nu_-+2\alpha+3\beta$	891.6	1.8	d
$\langle Y1/2Y\vert' \rightarrow \langle Z3/2Z\vert'$	$Z-Y+(Q'/2)+\nu_-+2\alpha+4\beta$	898.1	1.5	d
$\langle X3/2X\vert \rightarrow \langle Z3/2X\vert'$	$Z-X+\beta$	3384.7	2.8	a
$\langle X3/2Z\vert \rightarrow \langle Z3/2Z\vert'$	$Z-X+\alpha+\beta$			a
$\langle X3/2Y\vert \rightarrow \langle Z3/2Y\vert'$	$Z-X+\alpha+\beta$			a
$\langle X1/2X\vert \rightarrow \langle Z1/2X\vert'$	$Z-X+3\beta$			a
$\langle X1/2Z\vert \rightarrow \langle Z1/2Z\vert'$	$Z-X+\alpha+3\beta$			a
$\langle X1/2Y\vert \rightarrow \langle Z1/2Y\vert'$	$Z-X+\alpha+2\beta$			a
$\langle X3/2Z\vert \rightarrow \langle Z3/2Y\vert'$	$Z-X-\nu_-+\alpha+\beta$	3381.9	2	b
$\langle X1/2Z\vert \rightarrow \langle Z1/2Y\vert'$	$Z-X-\nu_-+\alpha+2\beta$			b
$\langle X3/2Y\vert \rightarrow \langle Z3/2Z\vert'$	$Z-X+\nu_-+\alpha+\beta$	3388.7	1.0	b
$\langle X1/2Y\vert \rightarrow \langle Z1/2Z\vert'$	$Z-X+\nu_-+\alpha+3\beta$			b
$\langle X1/2X\vert \rightarrow \langle Z3/2X\vert'$	$Z-X+(Q'/2)+\beta$	3419.5	2.1	c
$\langle X1/2Z\vert \rightarrow \langle Z3/2Z\vert'$	$Z-X+(Q'/2)+\alpha+\beta$			c
$\langle X1/2Y\vert \rightarrow \langle Z3/2Y\vert'$	$Z-X+(Q'/2)+\alpha+\beta$			c
$\langle X3/2X\vert \rightarrow \langle Z1/2X\vert'$	$Z-X-(Q'/2)+3\beta$	3350.8	2.8	c
$\langle X3/2Z\vert \rightarrow \langle Z1/2Z\vert'$	$Z-X-(Q'/2)+\alpha+3\beta$			c
$\langle X3/2Y\vert \rightarrow \langle Z1/2Y\vert'$	$Z-X-(Q'/2)+\alpha+2\beta$			c
$\langle X1/2Y\vert \rightarrow \langle Z3/2Z\vert'$	$Z-X+(Q'/2)+\nu_-+\alpha+\beta$	3422.7	0.8	d
$\langle X1/2Z\vert \rightarrow \langle Z3/2Y\vert'$	$Z-X+(Q'/2)-\nu_-+\alpha+\beta$	3416.5	1.6	d
$\langle X3/2Y\vert \rightarrow \langle Z1/2Z\vert'$	$Z-X-(Q'/2)+\nu_-+\alpha+3\beta$	3354.3	1.2	d
$\langle X3/2Z\vert \rightarrow \langle Z1/2Y\vert'$	$Z-X-(Q'/2)-\nu_-+\alpha+2\beta$	3348.1	2.1	d

* $\nu_- = 3e^2qQ(^{14}N)(1-\eta/3)/4$; $Q' = e^2qQ(^{35}Cl)(1-\eta^2/3)^{1/2}$.

‡ Relative within the same classification only.

a Electron spin transition.

b Simultaneous electron and nitrogen spin transition.

c Simultaneous electron and chlorine spin transition.

d Simultaneous electron, nitrogen, and chlorine spin transition.

Table 6

Basis states mixed by A_{xx}(N) and A_{xx}(Cl)

A_{xx}(N)			
$\{\langle Z\,3/2\,Z\|^{\pm}$,	$\langle Y\,3/2\,Y\|^{\pm}\}$		
$\{\langle Z\,3/2\,Y\|^{\pm}$,	$\langle Y\,3/2\,Z\|^{\pm}\}$		
$\{\langle Z\,1/2\,Z\|^{\pm}$,	$\langle Y\,1/2\,Y\|^{\pm}\}$		
$\{\langle Z\,1/2\,Y\|^{\perp}$,	$\langle Y\,1/2\,Z\|^{\pm}\}$		
A_{xx}(N) and A_{xx}(Cl)			
$\{\langle Z\,3/2\,X\|^{\pm}$,	$\langle Z\,1/2\,X\|^{\mp}$,	$\langle Y\,1/2\,X\|^{\pm}$,	$\langle Y\,3/2\,X\|^{\mp}\}$
$\langle Z\,3/2\,Z\|^{\pm}$,	$\langle Z\,1/2\,Y\|^{\pm}$,	$\langle Z\,3/2\,Y\|^{\mp}$,	$\langle Z\,1/2\,Z\|^{\mp}\}$
$\langle Y\,3/2\,Y\|^{\pm}$,	$\langle Y\,1/2\,Z\|^{\pm}$,	$\langle Y\,1/2\,Y\|^{\mp}$,	$\langle Y\,3/2\,Z\|^{\mp}\}$

$\langle\ \ |^{\pm}$ indicate Kramers pairs.

Table 7

Spin-hamiltonian values for 8-chloroquinoline

Parameter	Value (MHz)	Standard deviation (MHz)	Number of combinations used from tables 1;4
X	-1970.0[a]	± 0.5	7
Y	555.5[a]	± 0.5	7
Z	1414.5[a]	± 0.5	7
$\lvert A_{xx}(\mathrm{N})\rvert$	19.5	± 1.0	3
$\lvert A_{yy}(\mathrm{N})\rvert$	b	-	-
$\lvert A_{zz}(\mathrm{N})\rvert$	b	-	-
$\lvert A_{xx}(\mathrm{Cl})\rvert$	15	- 10.+ 15	12
$\lvert A_{yz}(\mathrm{Cl})\rvert$	b	-	-
$\lvert A_{zy}(\mathrm{Cl})\rvert$	b	-	-
$\lvert \nu_{-}(\mathrm{N})\rvert$	3.2	± 0.2	20
$\lvert Q'(^{35}\mathrm{Cl})\rvert$	68.4	± 0.6	17

a) Obtained from the convention $x+y+z=0$. and assuming the same order of the zero field levels as in quinoline.
b) Date does not provide reliable values.

Table 8

Energies and assignments of ^{14}N and ^{35}Cl ENDOR

ENDOR * Transition	Microwave transition saturated (MHz)	ENDOR‡ energy	Observed ENDOR frequency (MHz)	Relative intensity	Classification
$\langle Z\,3/2\,Y\vert' \rightarrow \langle Z\,3/2\,Z\vert'$		ν_-			a
$\langle Z\,1/2\,Y\vert' \rightarrow \langle Z\,1/2\,Z\vert'$		$\nu_- + \beta$			a
$\langle Y\,3/2\,Y\vert' \rightarrow \langle Y\,3/2\,Z\vert'$	857.3	ν_-	3.2	10	a
$\langle Y\,1/2\,Y\vert' \rightarrow \langle Y\,1/2\,Z\vert'$		$\nu_- + \beta$			a
$\langle Z\,1/2\,X\vert' \rightarrow \langle Z\,3/2\,X\vert'$		$(Q'/2) - 2\beta$			b
$\langle Z\,1/2\,Z\vert' \rightarrow \langle Z\,3/2\,Z\vert'$		$(Q'/2) - 2\beta$			b
$\langle Z\,1/2\,Y\vert' \rightarrow \langle Z\,3/2\,Y\vert'$		$(Q'/2) - \beta$			b
$\langle Y\,1/2\,X\vert' \rightarrow \langle Y\,3/2\,X\vert'$	826.2	$(Q'/2) + 2\beta$	33.5	11	b
$\langle Y\,1/2\,Z\vert' \rightarrow \langle Y\,3/2\,Z\vert'$	822.8	$(Q'/2) + \beta$	33.9	2	b
$\langle Y\,1/2\,Y\vert' \rightarrow \langle Y\,3/2\,Y\vert'$	829.2;826.2	$(Q'/2) + 2\beta$	33.5	2;11	b
$\langle Z\,1/2\,Z\vert' \rightarrow \langle Z\,3/2\,Y\vert'$		$(Q'/2) - \nu_- - 2\beta$			c
$\langle Z\,1/2\,Y\vert' \rightarrow \langle Z\,3/2\,Z\vert'$		$(Q'/2) - \nu_- - \beta$			c
$\langle Y\,1/2\,Z\vert' \rightarrow \langle Y\,3/2\,Y\vert'$	829.2;826.2	$(Q'/2) - \nu_- + \beta$	31.5	2;2	c
$\langle Y\,1/2\,Y\vert' \rightarrow \langle Y\,3/2\,Z\vert'$	822.8;826.2	$(Q'/2) + \nu_- - 2\beta$	37.5	7;2	c

* We do not see ENDOR while saturating microwave transition in the $\tau_x \rightarrow \tau_z$ multiplet. Since ENDOR is not predicted in the τ_x manifold and presumably some relaxation mechanism interferes in the τ_z manifold, the observed ENDOR is assigned to the τ_y manifold.

‡ $\nu_- = 3e^2qQ(^{14}N)(1-\eta/3)/4$; $Q' = e^2qQ(^{35}Cl)(1-\eta^2/3)^{1/2}$.

a ^{14}N nuclear spin transition.

b ^{35}Cl nuclear spin transition.

c Simultaneous ^{14}N and ^{35}Cl nuclear spin transition.

Table 9a

Energies and assignments of observed frequencies involving electron, ^{14}N, and ^{37}Cl transitions

Transition	Energy *	Observed frequency (MHz)	Relative‡ intensity	Classification
$\langle Y\,3/2\,X\|' \rightarrow \langle Z\,1/2\,X\|'$	$Z - Y - (Q'/2) + 4\beta$			a
$\langle Y\,3/2\,Y\|' \rightarrow \langle Z\,1/2\,Y\|'$	$Z - Y - (Q'/2) + 2\alpha + 3\beta$	833.0	1.5	a
$\langle Y\,3/2\,Z\|' \rightarrow \langle Z\,1/2\,Z\|'$	$Z - Y - (Q'/2) + 2\alpha + 4\beta$			a
$\langle Y\,1/2\,X\|' \rightarrow \langle Z\,3/2\,X\|'$	$Z - Y + (Q'/2) + 4\beta$			a
$\langle Y\,1/2\,Z\|' \rightarrow \langle Z\,3/2\,Z\|'$	$Z - Y + (Q'/2) + 2\alpha + 3\beta$	887.9	1.3	a
$\langle Y\,1/2\,Y\|' \rightarrow \langle Z\,3/2\,Y\|'$	$Z - Y + (Q'/2) + 2\alpha + 4\beta$			a
$\langle Y\,3/2\,Z\|' \rightarrow \langle Z\,1/2\,Y\|'$	$Z - Y - (Q'/2) - \nu_- + 2\alpha + 3\beta$	829.2	1.7	b
$\langle Y\,3/2\,Y\|' \rightarrow \langle Z\,1/2\,Z\|'$	$Z - Y - (Q'/2) + \nu_- + 2\alpha + 4\beta$	835.9	1.1	b
$\langle Y\,1/2\,Z\|' \rightarrow \langle Z\,3/2\,Y\|'$	$Z - Y + (Q'/2) - \nu_- + 2\alpha + 3\beta$	884.1	1.9	b
$\langle Y\,1/2\,Y\|' \rightarrow \langle Z\,3/2\,Z\|'$	$Z - Y + (Q'/2) + \nu_- + 2\alpha + 4\beta$	891.6	1.5	b
$\langle X\,1/2\,X\| \rightarrow \langle Z\,3/2\,X\|'$	$Z - X + (Q'/2) + \beta$			a
$\langle X\,1/2\,Z\| \rightarrow \langle Z\,3/2\,Z\|'$	$Z - X + (Q'/2) + \alpha + \beta$	3412.0	1.9	a
$\langle X\,1/2\,Y\| \rightarrow \langle Z\,3/2\,Y\|'$	$Z - X + (Q'/2) + \alpha + \beta$			a
$\langle X\,3/2\,X\| \rightarrow \langle Z\,1/2\,X\|'$	$Z - X - (Q'/2) + 3\beta$			a
$\langle X\,3/2\,Z\| \rightarrow \langle Z\,1/2\,Z\|'$	$Z - X - (Q'/2) + \alpha + 3\beta$	3358.0	2.1	a
$\langle X\,3/2\,Y\| \rightarrow \langle Z\,1/2\,Y\|'$	$Z - X - (Q'/2) + \alpha + 2\beta$			a
$\langle X\,1/2\,Y\| \rightarrow \langle Z\,3/2\,Z\|'$	$Z - X + (Q'/2) + \nu_- + \alpha + \beta$	3416.5	1.2	b
$\langle X\,1/2\,Z\| \rightarrow \langle Z\,3/2\,Y\|'$	$Z - X + (Q'/2) - \nu_- + \alpha + \beta$	3409.2	0.8	b
$\langle X\,3/2\,Y\| \rightarrow \langle Z\,1/2\,Z\|'$	$Z - X - (Q'/2) + \nu_- + \alpha + 3\beta$	3361.5	0.8	b
$\langle X\,3/2\,Z\| \rightarrow \langle Z\,1/2\,Y\|'$	$Z - X - (Q'/2) - \nu_- + \alpha + 2\beta$	3354.3	1.2	b

Table 9b

Energies and assignments of observed frequencies involving electron, ^{14}N, and ^{37}Cl transitions

ENDOR Transition	Microwave transition saturated (MHz)	ENDOR energy *	Observed ENDOR frequency (MHz)	Relative† intensity	Classification
$\langle Y\,1/2\,X\|' \rightarrow \langle Y\,3/2\,X\|'$	833.0	$(Q'/2) + 2\beta$	26.8	1	c
$\langle Y\,1/2\,Z\|' \rightarrow \langle Y\,3/2\,Y\|'$	835.9	$(Q'/2) - \nu_- + \beta$	24.0	1	d
$\langle Y\,1/2\,Y\|' \rightarrow \langle Y\,3/2\,Z\|'$	829.2	$(Q'/2) + \nu_- - 2\beta$	31.5	1	d

* $Q' = e^2qQ(^{37}Cl)(1 - \eta^2/3)^{1/2}$; $\nu_- = 3e^2qQ(^{14}N)(1 - \eta/3)$

‡ Relative within the same classification only.

a Simultaneous electron spin and ^{37}Cl nuclear spin transition.

b Simultaneous electron spin, ^{14}N, and ^{37}Cl nuclear spin transitions.

c ^{37}Cl nuclear spin transition.

d Simultaneous ^{37}Cl and ^{14}N nuclear spin transition.

B. The $^3n\pi^*$ State of Pyrazine

Since pyrazine is an example of the class of molecules in which an electron is excited from a non-bonding (n) orbital to an anti-bonding (π^*) orbital, it has been the subject of considerable interest for many years.[81-84] The purpose of our investigation is to gain a measure of the electron distribution in the excited $n\pi^*$ state of pyrazine by measuring the electron spin-spin, nitrogen hyperfine and nitrogen nuclear quadrupole interactions.

In contrast to $\pi\pi^*$ triplets, where because of the Pauli Principle the unpaired electrons may not be on the same atomic centers, in $n\pi^*$ triplets the unpaired electrons are in orthogonal orbitals and therefore may reside on the same atomic center. The $n\pi^*$ triplet therefore has large one-center contributions to both the spin-orbit and zero field Hamiltonians. Experimentally, this results in both a short lifetime for the excited $n\pi^*$ state due to the larger spin-orbit coupling contribution and higher frequency ESR transitions due to the larger electron spin-spin interaction.

Both of these effects have contributed to the failure to detect triplets using conventional absorption techniques. Since the sensitivity of experiments in which the absorption of energy is monitored is directly dependent on the concentration of spins, the short lifetime results in a reduction in sensitivity directly proportional to the shorter lifetime of the excited state. With ODMR on the other hand, the sensitivity is dependent on the number of photons detected per unit time which is approximately equal to the steady state population divided by

the lifetime. Since, to a first approximation, the steady state population is proportional to the lifetime, the sensitivity using optical detection techniques is independent of the lifetime of the excited state.

The sample consisted of a single crystal of paradichlorobenzene (pDB) doped with 1% pyrazine h-4 or d-4 grown from the melt. The starting material was recrystallized, vacuum sublimed and zone refined. The experimental arrangement was essentially the same as that shown in Figure 16. The sample was maintained at 2.0° K while being irradiated with the 3100 Å region of the mercury arc lamp. The 0-0 band of the pyrazine phosphorescence was detected at a 90° angle to the exciting light. The microwave sweep oscillator was amplitude modulated at 40 Hz for the $D + |E|$ and $D - |E|$ transitions while a Hewlett-Packard model 3200B Rf oscillator was used without modulation for the 2E transition.

The $D + |E|$ and $D - |E|$ transitions for pyrazine-h4 and -d4 are shown in Figures 31 and 32, and the power dependence of the 2E transition in Figure 33. The large linewidth of the three zero field transitions is primarily due to the large hyperfine interaction. As discussed in Section III, the main features of the spectra can be explained by a second order perturbation treatment. The high frequency or $D + |E|$ transition (see Figures 31B and 32B) should be shifted to a higher energy by an amount $\alpha = A_{zz}^2/(E_x - E_y)$ while the $D - |E|$ transition (see Figures 31A and 32A) should be shifted to lower energy by an equal amount and the 2E transition (see Figure 33) shifted to higher energy by an amount 2α. The measured values of D and E

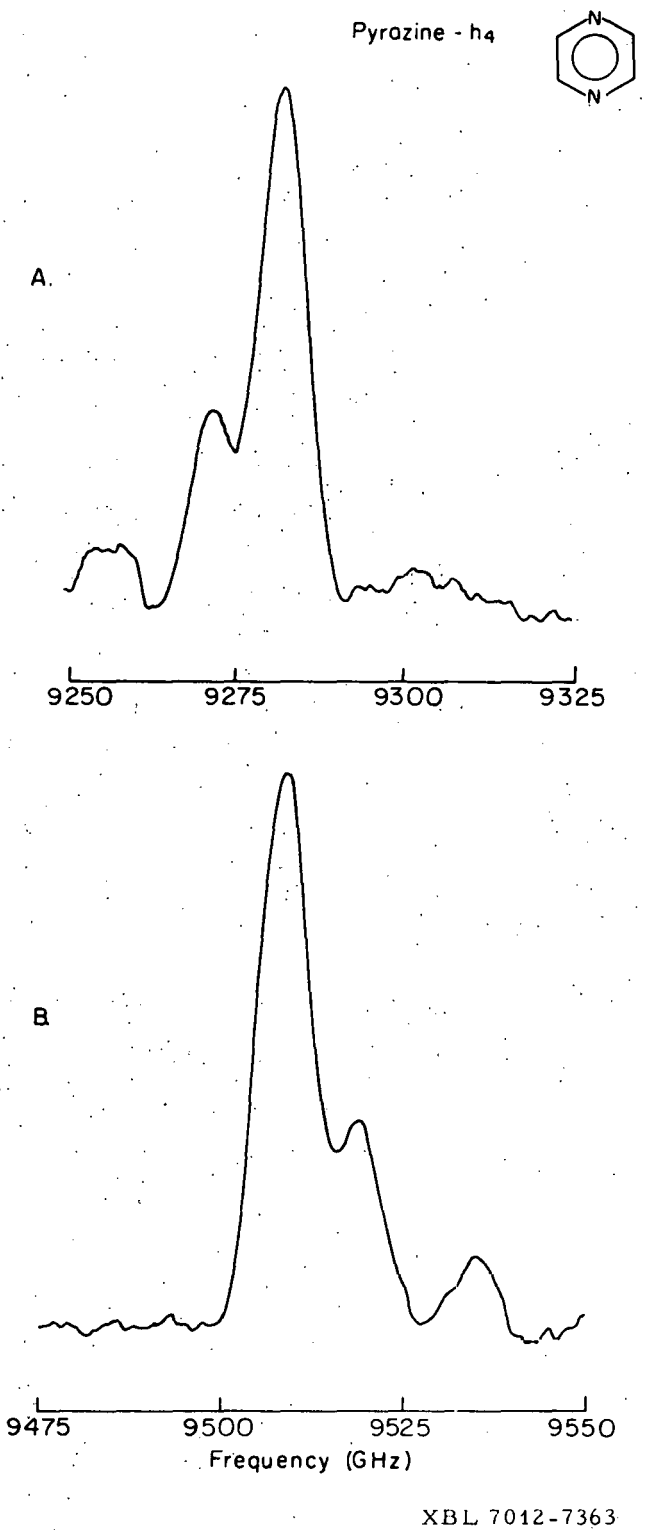

Figure 31

Pyrazine-h4 ODMR of the D + E (a) and D - E (b) Zero Field Transitions

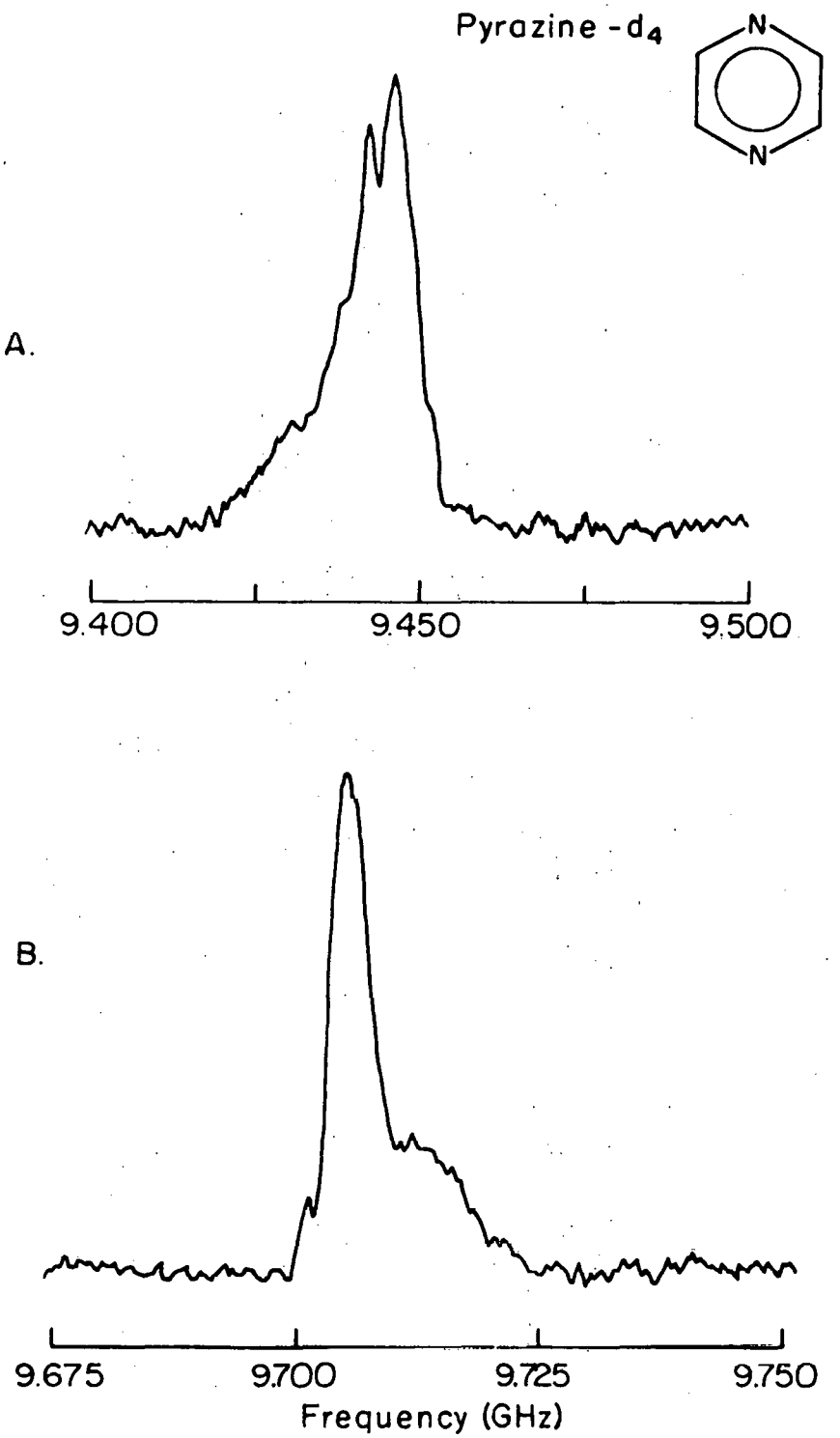

XBL 7012-7364

Figure 32

Pyrazine-d4 ODMR of the D + E (a) and D - E (b) Zero Field Transitions

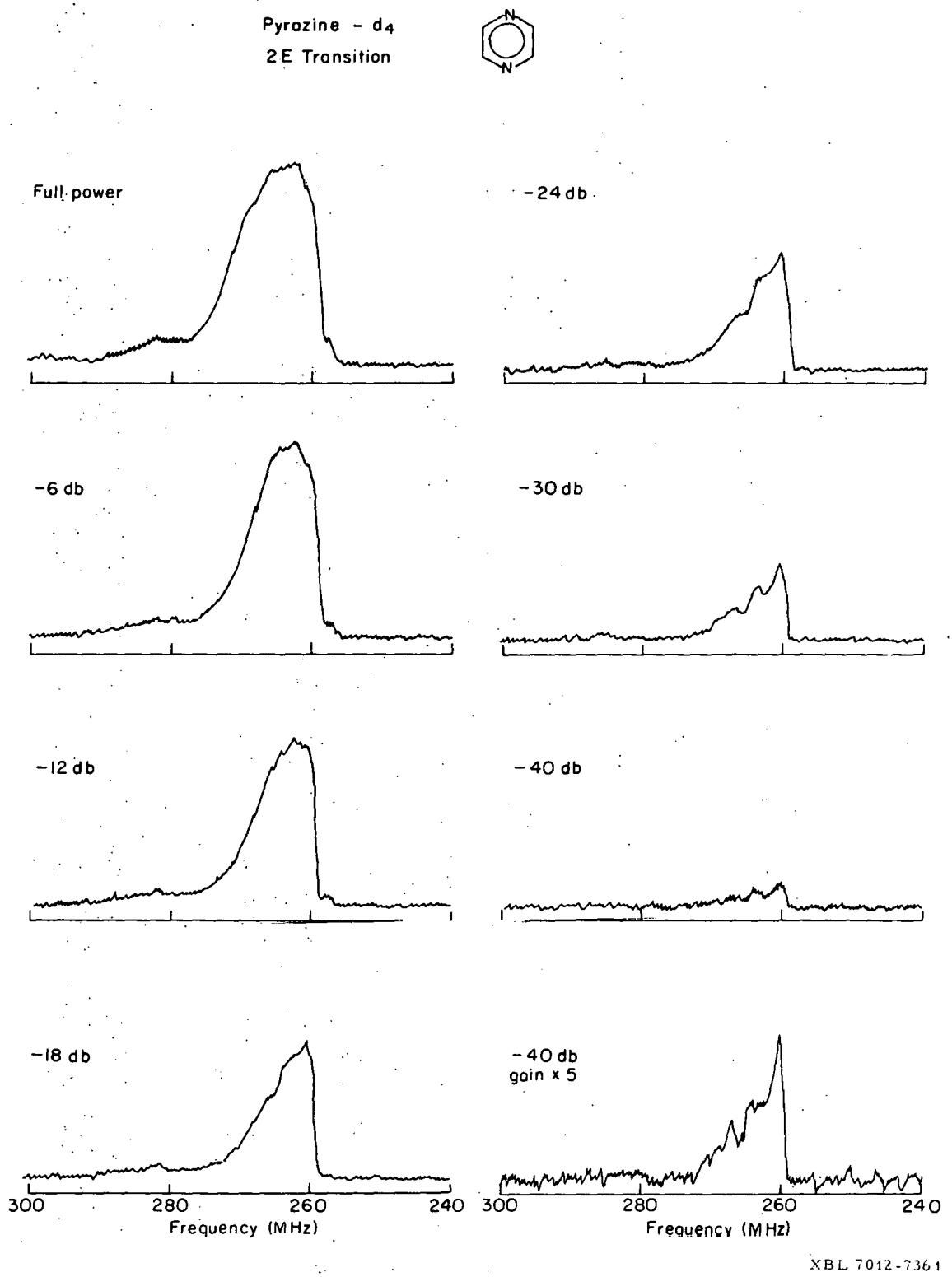

Figure 33

Power Dependence of the 2E Transition of Pyrazine-d4

for pyrazine-h4 are $|D| = 9.3959$ GHz, $|E| = 0.1126$ GHz and for pyrazine-d4 $|D| = 9.5782$ GHz and $|E| = 0.1286$ GHz.

The high field optical detection of the pyrazine-h4 ESR has been reported by Sharnoff[37] with the values $D = +9.264$ GHz and $E = -0.180$ GHz, while Cheng and Kwiram[38] have reported the low field and zero field optical detection of the $D + |E|$ and $D - |E|$ transitions. The values they report are, for pyrazine-h4, $D = \pm 10.1698$ GHz, $E = \mp 0.2155$ GHz; and for pyrazine-d4, $D = +10.2043$ GHz and $E = \mp 0.2057$ GHz. In addition, Hochstrasser and Lin[85] have observed the zero field splitting of pyrazine in the optical spectra by use of a large Zeeman field. They report the value $D = +0.3$ cm^{-1} (9 GHz) which is consistent with the ESR studies.

The discrepancy between our results and Sharnoff's are most likely due to the lower accuracy inherent in his high field experiments, while the difference between our results and those of Cheng and Kwiram are believed to be due to differences in sample preparation. Chenge and Kwiram performed their experiments shortly after the crystal was grown from the melt, while our experiments were performed approximately one year after growing the crystal. The sensitivity of pDB to its recent thermal history will be discussed in more detail in the section on the ESR of that molecule, but most likely the sample used by Cheng and Kwiram contained an appreciable concentration of the triclinic (or high temperature) form of pDB. The environmental difference between the monoclinic and triclinic forms of pDB are believed to account for the approximately 10% variation in the values of D.

On the basis of the optical spectra, the spacial symmetry of the $^3n\pi^*$ state of pyrazine has been assigned as B_{3u}[86] in D_{2h} using an axis system with the N-N axis as the $y(B_{1u})$ axis, the other in-plane axis as $z(B_{1u})$ and the out-of-plane axis as $x(B_{3u})$. The three triplet levels transform as the product of the space and spin representations and therefore the total symmetry of the triplet levels may be expressed as,

$$\begin{aligned} \tau_x &= B_{3u} \times B_{3g} = A_u \\ \tau_y &= B_{3u} \times B_{2g} = B_{1u} \\ \tau_z &= B_{3u} \times B_{1g} = B_{2u} \quad . \end{aligned} \tag{8}$$

In contrast to ESR experiments using a magnetic field, experiments at zero magnetic field do not give any information as to the sign of D and E. The experiments of Cheng and Kwiram using a magnetic field have established that D and E must be of opposite signs. This requires that the energy levels be ordered $E_z < E_y < E_x$ or vice versa. A simple analysis of the electron spin-spin interaction centered on the nitrogen predicts that E_x and E_y are positive and E_z negative which requires that D be >0 and $E<0$. In addition, the excited nitrogen atom fragments are isoelectronic with the $>C:$ fragment in diphenylmethylene and fluorenylidene[47] in which D is >0 and $E<0$ using our axis system. This assignment of the order of the energy levels is further supported by Sharnoff, except that he gives the opposite signs for D and E with the same ordering of the energy levels. The energies of the triplet levels for pyrazine-h4 are therefore:

$$X = 3.2446 \qquad Y = 3.0194 \qquad Z = -6.2640 \text{ GHz}$$

and for pyrazine-d4,

$$X = 3.1213 \qquad Y = 3.0641 \qquad Z = -6.3854 \text{ GHz}$$

An accurate interpretation of the zero field values is of course dependent on an ab initio calculation of the excited $n\pi^*$ state of pyrazine. However, several conclusions can be drawn from a simple analysis of the spacial dependence of the zero field interaction for two unpaired electrons in orthagonal p orbitals located on the same atomic center.

The approximate equivalence of the X and Y triplet levels requires with this model that the electron density in the lone pair and π^* orbitals on the nitrogen atoms be approximately equivalent. This would imply that the electron in the π^* orbital does not spend much time on the carbon atoms.

Considering only the nitrogen one-center contributions to the zero field splitting, the small ratio of E/D indicates a small amount of s character in the nitrogen lone pair orbital. Sternlicht,[87] on the basis of sp^2 hybridization calculated a ratio of E/D of -0.5 while the measured values are for pyrazine-h4, E/D =-0.0120 and for pyrazine-d4, E/D =-0.0134. Without any s character in the lone pair orbital the value of E would of course be zero.

The nitrogen hyperfine interaction has been obtained by fitting the spectra to a Hamiltonian incorporating the zero field, nitrogen hyperfine and nitrogen nuclear quadrupole terms. Due to the large line

widths it was not possible to obtain an accurate measure of the nitrogen quadrupole coupling constant and therefore the ground state values[88] were used in fitting the spectra. The values obtained for the nitrogen hyperfine interaction are

$$A_{xx}' \approx 70 \text{ MHz}$$

$$A_{yy}' \approx 80 \text{ MHz}$$

$$A_{zz}' \approx 30 \text{ MHz}$$

It must be emphasized that these are only approximate values and subject to an error on the order of ± 20%, but are essentially the same as those reported by Cheng and Kwiram. These values give for the isotropic component of the hyperfine interaction $a_c = 60$ MHz and for the anisotropic components

$$A_{xx} = 10$$

$$A_{yy} = 20$$

$$A_{zz} = -30$$

The anisotropic hyperfine coupling may be interpreted with the aid of the tables given by Asycough.[89] One electron in a p orbital will contribute an amount 2A (A = 47.8 MHz for ^{14}N)[89] in the direction of the orbital and an amount -A in the other two orthagonal directions to the anisotropic hyperfine interaction. The triplet electrons are in the π^* and lone pair orbital on the nitrogens with electron densities ρ_π and ρ_L respectively. In our axis system we may express the contribution of each of the triplet electrons to the anisotropic hyperfine components as,

$$
\begin{aligned}
A_{xx} &= (2A\rho_{\pi} - A\rho_{L}) \\
A_{yy} &= (2A\rho_{L} - A\rho_{\pi}) \\
A_{zz} &= (-A\rho_{\pi} - A\rho_{L})
\end{aligned}
\tag{9}
$$

The spin densities ρ_{π} and ρ_{L} may be obtained by solving Equation 9, which gives us,

$$
\begin{aligned}
\rho_{\pi} &= \frac{1}{3A}(A_{xx} - A_{zz}) \\
\rho_{L} &= \frac{1}{3A}(A_{yy} - A_{zz})
\end{aligned}
\tag{10}
$$

Substituting the measured values of the anisotropic hyperfine tensor we find that $\rho_{\pi} = 0.28$ and $\rho_{L} = 0.35$ for both nitrogen atoms.

Hirota, Hutchison and Palmer[94] have shown that the experimental results for naphthalene bear out McLachlan's[95] theoretical prediction that the spin density of the lowest triplet state is approximately the same as the negative ion.

Our results for the $^{3}n\pi^{*}$ state of pyrazine are consistent with this since our value for the spin density of the electron in the π^{*} orbital on the nitrogen atoms (0.28) is almost identical with the experimental value for the pyrazine anion of 0.278.[96]

The theoretical isotropic hyperfine interaction due to one electron in a nitrogen 2s orbital is 1540 MHz.[89] Since this contribution should dominate over the induced polarization of the s electrons by the triplet electrons in p orbitals, we will assume that only the direct contribution need be considered in interpreting the observed isotropic hyperfine

interaction. Therefore, the triplet spin density in the nitrogen 2s orbital ρ_s is given by

$$\rho_s = (60/1540) = 0.04 \qquad (11)$$

The coefficient of the nitrogen 2s atomic orbital in the nitrogen lone pair molecular orbital is therefore equal to $(0.04)^{\frac{1}{2}} = 0.20$. This gives us for the wave function of the nitrogen lone pair orbital

$$\psi_L = 0.20\, \phi_{2s} + 0.98\, \phi_{2p_y} \qquad (12)$$

This small amount of s character in the lone pair orbital is consistent with the zero field values and indicates a bent bond with an angle > 120°.

A quantitative estimate of the angle may be obtained by using the equation given by Higuchi[91] for the bond angle

$$\psi_L = \left[\frac{(1 + \cos\theta)}{(1 - \cos\theta)}\right]^{\frac{1}{2}} \phi_{2s} + \left[\frac{-2\cos\theta}{(1 - \cos\theta)}\right]^{\frac{1}{2}} \phi_{2p_y}$$

where ψ_L is the lone pair orbital and θ is the C-N_2C angle.

Therefore, from the measured value of the isotropic hyperfine interaction we have

$$\left[\frac{(1 + \cos\theta)}{(1 - \cos\theta)}\right]^{\frac{1}{2}} = 0.20 \qquad (13)$$

which gives us an angle of 157°. It should be noted that calculations of the ground state of pyrazine by Clementi[92] indicate a small s character (≈15%) for the lone pair orbital using a fixed geometry with θ = 120°.

Cheng and Kwiram[38] raised the question of the possibility of population inversion of the triplet levels of pyrazine. This question can of course be answered if a conventional ESR experiment can be performed. Alternatively an analysis of the change in phosphorescence intensity upon saturating the three zero field transitions will supply the same information.

It is necessary to know the lifetimes of the individual triplet levels in order to answer this question, but in the case of pyrazine the assignment is reasonably straightforward.

Since the τ_x level transforms as A_u (Eq. 8) it is symmetry forbidden to directly couple via the spin-orbit Hamiltonian with an excited singlet state. Therefore if we neglect the triplet character of the ground state, the τ_x level may only gain the admixture of single singlet character necessary for electric dipole radiation to the ground state by spin-orbit coupling through an intermediate state. Consequently the τ_x level should have the smallest amount of singlet character and therefore the longest lifetime. With this assignment of the τ_x level and the experimental observation[90] that the τ_z level has the shortest lifetime, the rate constants for the three levels are

$$k_x = 2.5 \text{ sec}^{-1}$$

$$k_y = 10 \text{ sec}^{-1}$$

$$k_z = 167 \text{ sec}^{-1}$$

where the rate constants are equal to the inverse of the lifetimes.

As was shown in section II (see Eq. 39) the change in intensity of the phosphorescence upon saturating the ESR transition between any two of the three triplet levels is given by

$$\Delta I_{ij} \approx (N_i - N_j)(K_j - K_i)$$

where $i,j = x, y, z$ and N_i are the steady state populations of the three triplet levels.

Since the ODMR of all three zero field transitions gave an increase in the phosphorescence intensity, it is clear from Eq. 14 that the populations of the triplet levels must be in an order opposite to that of their rate constants (i.e., $N_x > N_y > N_z$). Therefore the populations are inverted and we have a necessary but not sufficient condition for stimulated emission. It should be noted that our assignment of the τ_x level as the level with the longest lifetime is only necessary to predict a population inversion between the τ_x and τ_y levels. The assignment of the τ_z level as the level with the shortest lifetime is sufficient to establish that $N_z < N_x, N_y$ and therefore a population inversion certainly exists for the $D + E$ and $D - E$ zero field transitions.

C. The $^3\pi\pi$ State of Paradichlorobenzene

This section is divided into two parts. In the first, the ODMR spectra of paradichlorobenzene (pDB) are presented and the results interpreted in terms of a spin Hamiltonian incorporating the electron spin-spin, chlorine nuclear quadrupole and chlorine hyperfine interactions. In the second part, the phosphorescence microwave double resonance technique is used in investigating the vibrational structure of the phosphorescence spectrum of pDB. The vibrational structure of the phosphorescence spectra is assigned by analysis of the relative change in intensity of the phosphorescence upon saturation of the three zero field transitions. Both the ESR and phosphorescence spectra are shown to be consistent with a distortion of the excited state due to a bending of the C-Cl bonds into a trans configuration.

1. The ODMR Spectra of Paradichlorobenzene

Investigations of the first excited triplet state of benzene and substituted benzenes has been the subject of considerable interest.[107-109] The absorption and phosphorescence spectra of the first excited triplet state of pDB by Castro and Hochstrasser[71] and by George and Morris[97] have raised several questions?

1) Is the spacial symmetry of the excited triplet state of pDB B_{2u} as proposed[71] or B_{1u} as is benzene?[98]

2) Do the chlorines participate significantly in the excitation?[99]

3) Is the molecule distorted in the excited state?[71]

4) Is the electric field gradient at the chlorines changed significantly upon excitation to the first triplet state?

ODMR in zero field has been shown to be a powerful tool for studying the electron distribution of organic molecules in their first excited triplet state. Analysis of the parameters used in the spin Hamiltonian that satisfactorily accounts for the ODMR spectra of pDB should supply the information necessary to answer the above questions.

Experimental

The starting material (Eastman Organic white label) was degassed and zone refined for 100 passes. Single crystals of pDB were easily grown by the Bridgeman technique. The experimental arrangement used in the ESR experiments is essentially the same as that shown in Figure 16. The sample was excited with the 2800 Å or 3100 Å region of the mercury arc lamp by use of the appropriate interference filter.

The majority of the ESR spectra were obtained by square wave amplitude modulation of the microwave oscillator with a frequency of 10 to 20 Hz and a modulation depth of ≥ 25 db. The Hewlett Packard microwave sweep oscillator was modified by replacing the timing capacitor used for the range with the fastest sweep time with an assembly which permitted switching between external capacitors. With this arrangement sweep times as long as several thousand seconds were possible, permitting the use of sweep rates as low as .025 MHz/sec.

Frequency modulation of the microwave field was also employed in the course of this work. This was achieved by combining the sine wave output of the lock-in amplifier and the ramp output of an Exact model 255 function

generator through the + and - inputs of an operational amplifier. The output of the operational amplifier consisted of a positive ramp voltage with a superimposed sine wave. The magnitudes of the ramp and sine wave voltages were independently adjusted to give the desired sweep width and modulation excursion. The modulation rate (i.e., the frequency of the sine wave) used was varied between 10 and 20 Hz. The time constant of the lock in amplifier was varied from 0.3 to 30 seconds depending on the sweep rate of the microwave oscillator.

In addition, experiments were performed without modulation of the microwave field in which case the absolute change in intensity of the phosphorescence was monitored. The effective time constant of the electrometer was varied by changing the external load resistor.

The experimental arrangement used in performing the ENDOR experiments is shown in Figure 17 and the sample arrangement in Figure 18. The Hewlett Packard RF sweep oscillator was also modified to permit sweep times as long as 2000 seconds by use of an external timing capacitor.

The measurement of the ^{35}Cl pure nuclear quadrupole resonance of the ground state of pDB at 4.2°K was achieved with the use of a marginal oscillator described by Fayer and Harris.[100] The sample coil was extended by placing the leads to the coil inside a section of stainless steel tubing bent at a right angle in order to support the coil in a liquid helium dewar. The dewar used in this experiment was constructed by inserting a narrow mouth commercial dewar inside a larger wide mouth dewar. The outer dewar was filled with liquid nitrogen and the inner dewar with liquid helium. This arrangement held helium for about 30 minutes with the sample in place.

Zeeman modulation was achieved by a selenoid wound around the outer dewar.

The ODMR spectra in zero field

The ODMR spectra of pDB in zero magnetic field have been observed while monitoring the emission from two distinct traps. However, only the ODMR spectra due to the shallow (or x) trap will be discussed. The chlorine nuclear quadrupole and hyperfine structure of the ODMR spectra observed for the deep (or y) trap were the same as those for the x trap; however, the zero field values were about 5% lower.

The observed ODMR spectra of pDB are due to the interaction of three isotopically distinct molecular species. The relative natural abundances of the ^{35}Cl and ^{37}Cl isotopes are approximately 3/4 and 1/4 respectively. Since there are two chlorine nuclei per molecule, the fractional distribution of the molecular species are

$$\begin{aligned} &\text{I} \quad {}^{35}Cl - {}^{35}Cl - 3/4 \times 3/4 - 9/16 \\ &\text{II} \quad {}^{35}Cl - {}^{37}Cl = 2(3/4 \times 1/4) = 6/16 \\ &\text{III} \quad {}^{37}Cl - {}^{37}Cl = 1/4 \times 1/4 = 1/16 \end{aligned} \qquad (1)$$

The spectra obtained will therefore be considered as the superposition of the ODMR spectra due to each of the three molecular species.

The $\tau_x \rightarrow \tau_z$ (high frequency) transitions observed using amplitude and frequency modulation are shown in Figures 34 and 35 respectively. The resonance observed for this transition without modulation of the microwave field is shown in Figure 36. The two remaining electron spin

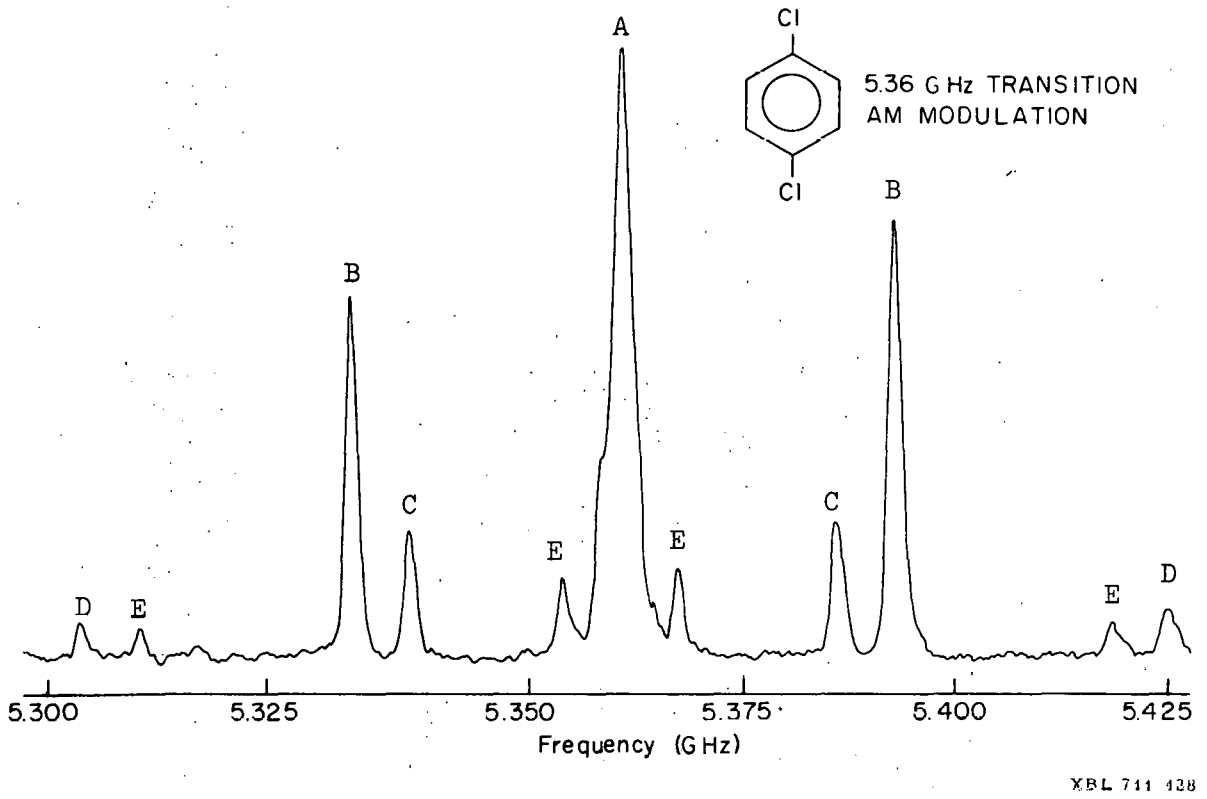

Figure 34

ODMR of the $\tau_x \rightarrow \tau_z$ multiplet of paradichlorobenzene with amplitude modulation of the microwave field

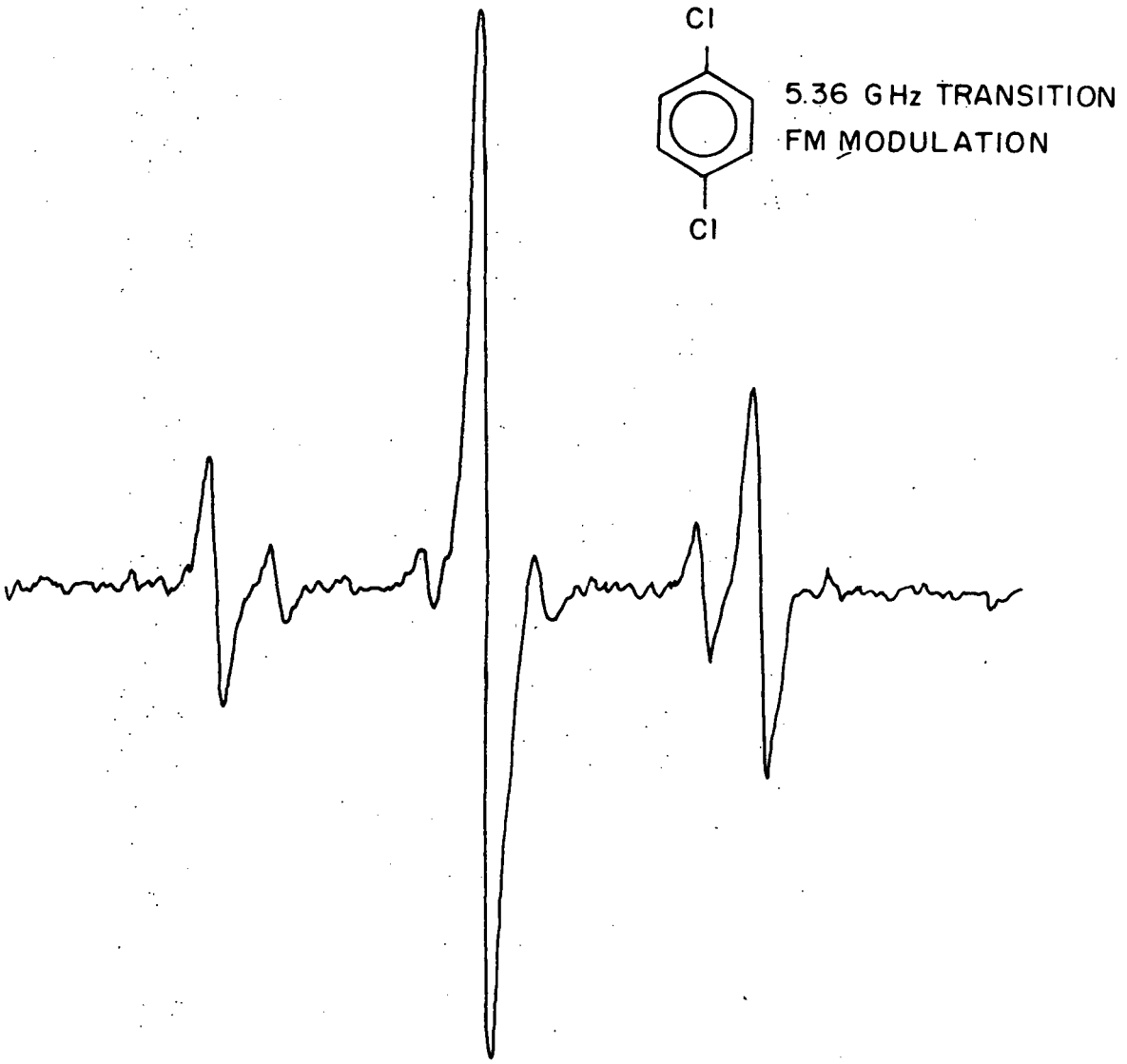

XBL 711-127

Figure 35

ODMR of the $\tau_x \rightarrow \tau_y$ multiplet of paradichlorobenzene with frequency modulation of the microwave field

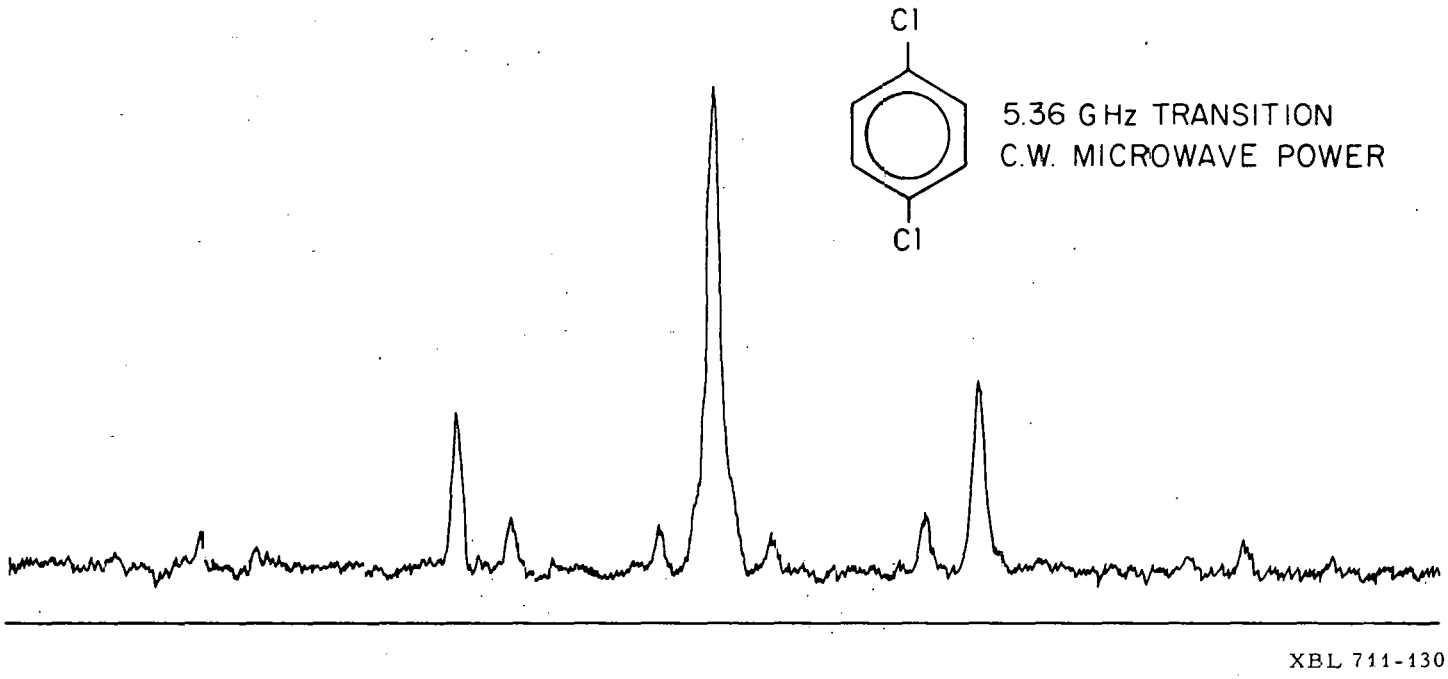

Figure 36

ODMR of the $\tau_x \rightarrow \tau_z$ multiplet of paradichlorobenzene without modulation of the microwave field

transitions observed using amplitude modulation are shown in Figures 37 ($\tau_x \rightarrow \tau_y$) and 38 ($\tau_y \rightarrow \tau_z$).

In table 10 the possible ESR transitions involving the triplet electrons and one or more chlorine nuclei are listed as to type (A, B, C, D, E, or F) and the possible molecular species (I, II, or III) which can undergo each type of transition. The intensity of the transitions involving the electron and one chlorine spin (B and C) and those involving the electron and two chlorine spins (D, E, and F) must be considered separately. The ratio of the intensities of the transitions involving a single ^{35}Cl spin to those involving a single ^{37}Cl spin is given by

$$\frac{I_B}{I_C} = \frac{2(9/16) + 6/16}{6/16 + 2(1/16)} = 3 \qquad (2)$$

Likewise the ratio of the intensities of the transitions involving two chlorine spins is:

$$I_D:I_E:I_F = 9:6:1 \qquad (3)$$

The structure of the $\tau_x \rightarrow \tau_z$ electron spin multiplet shown in Figure 34 is labeled according to the classification given in Table 10. Since the nuclear quadrupole moment of ^{35}Cl is larger than that of ^{37}Cl, the outer pair of the four strong satellites are assigned as type B (^{35}Cl) and the inner pair as type C transitions (^{37}Cl). As can be seen, the ratio of the intensity of the transitions labeled B and C is approximately 3:1 as predicted. The ratio of the outermost satellites in Figure 34 are assigned to simultaneous double chlorine transitions (labeled D and E on the spectra). The intensity of these transitions is also approximately in the predicted ratio of 9:6.

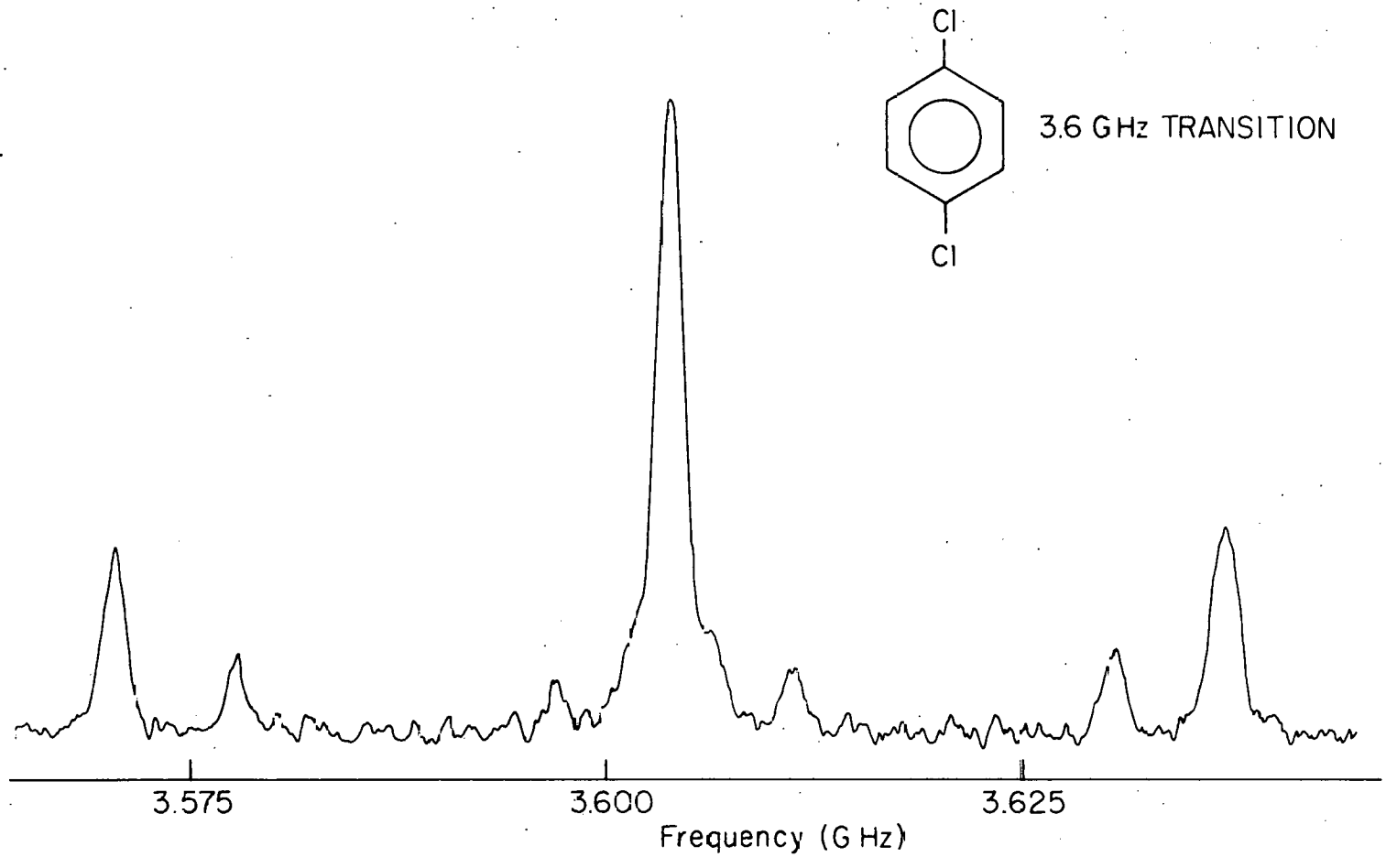

XBL 711-53

Figure 37

ODMR of the $\tau_x \rightarrow \tau_y$ multiplet of paradichlorobenzene

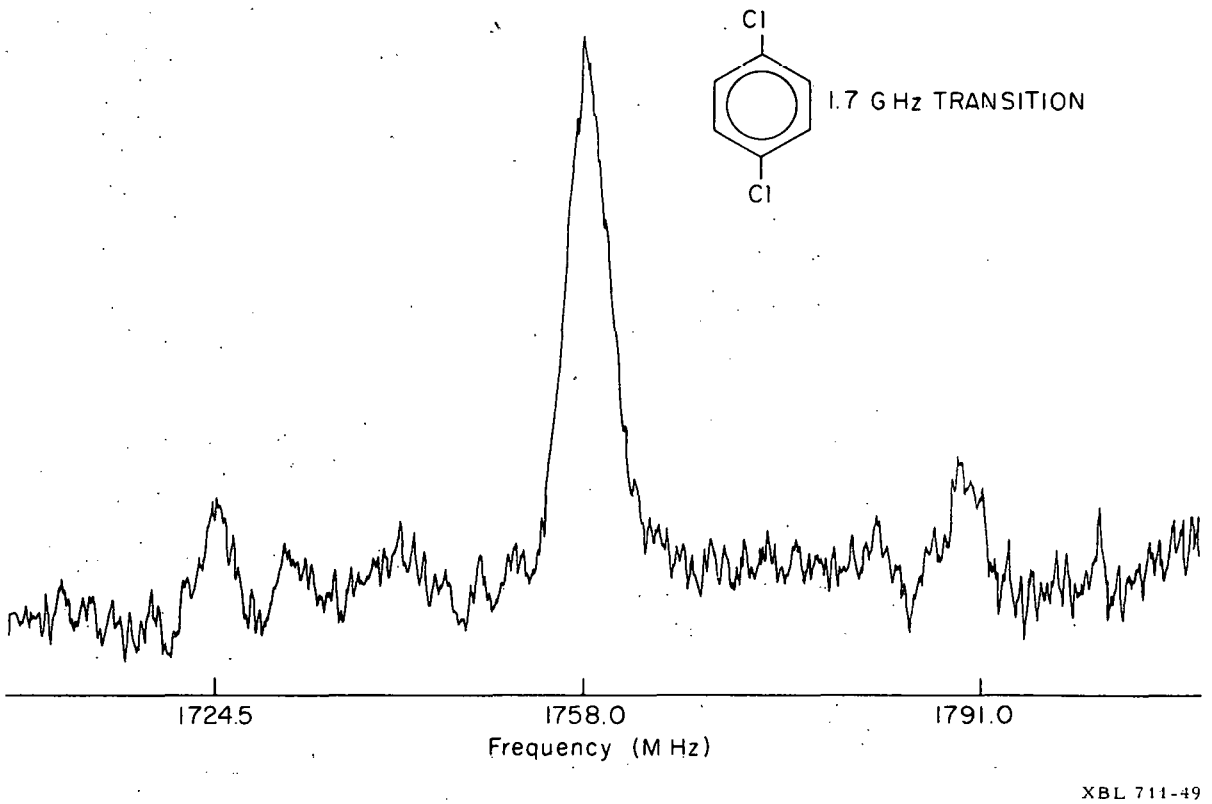

Figure 38

ODMR of the $\tau_y \rightarrow \tau_z$ multiplet of paradichlorobenzene

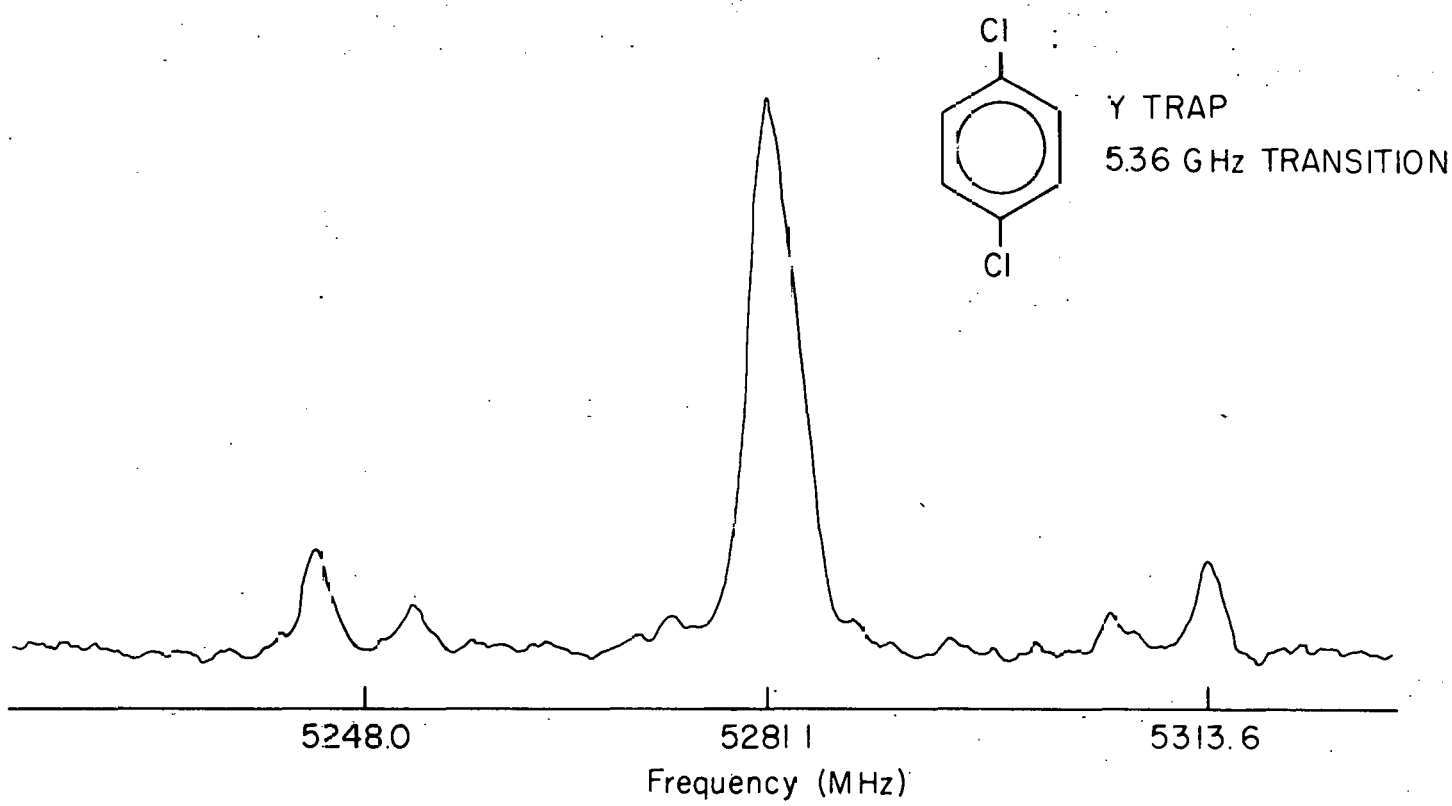

XBL 711-129

Figure 39

ODMF of the $\tau_x \rightarrow \tau_z$ multiplet of the Y trap of paradichlorobenzene

The transitions corresponding to simultaneous double ^{37}Cl transitions (type F) are not observed as would be expected from the small natural abundance of the molecular species responsible for these transitions. The inner pair of satellites (labeled E in Figure 34) may be considered as simultaneous ^{35}Cl and ^{37}Cl transitions, the higher frequency transition representing a ^{35}Cl flip up and a ^{37}Cl flip down, while the lower frequency transition represents a ^{37}Cl flip up and a ^{35}Cl flip down. Since the matrix elements for these double chlorine transitions are significantly different from those associated with the other double chlorine transitions, the intensity of the inner satellites labeled E in Figure 34 should not be compared to the intensity of the outer satellites labeled D and E.

Chlorine ENDOR transitions were also observed by saturating the ESR transitions in the D - E and D + E manifold. The ^{35}Cl and ^{37}Cl ENDOR resonances observed by saturating the D - E transition are shown in Figures 40 and 41 respectively, and the ^{35}Cl and ^{37}Cl ENDOR resonances observed by saturating the D + E transition in Figures 42 and 43 respectively.

As an extension of the Cl ENDOR experiments a ^{35}Cl ENDOR transition was saturated while sweeping the D - E microwave transition. Since only the ENDOR time dependent magnetic field was amplitude modulated and the change in phosphorescnece intensity detected with a lock in amplifier only the ESR transitions that involve a ^{35}Cl spin transition are detected. The spectrum obtained from this experiment is shown in Figure 44. As can be seen, satellites assigned as simultaneous electron and ^{37}Cl spin transitions (labeled C in Figure 34) are not observed, which confirms the assignment of the chlorine satellites.

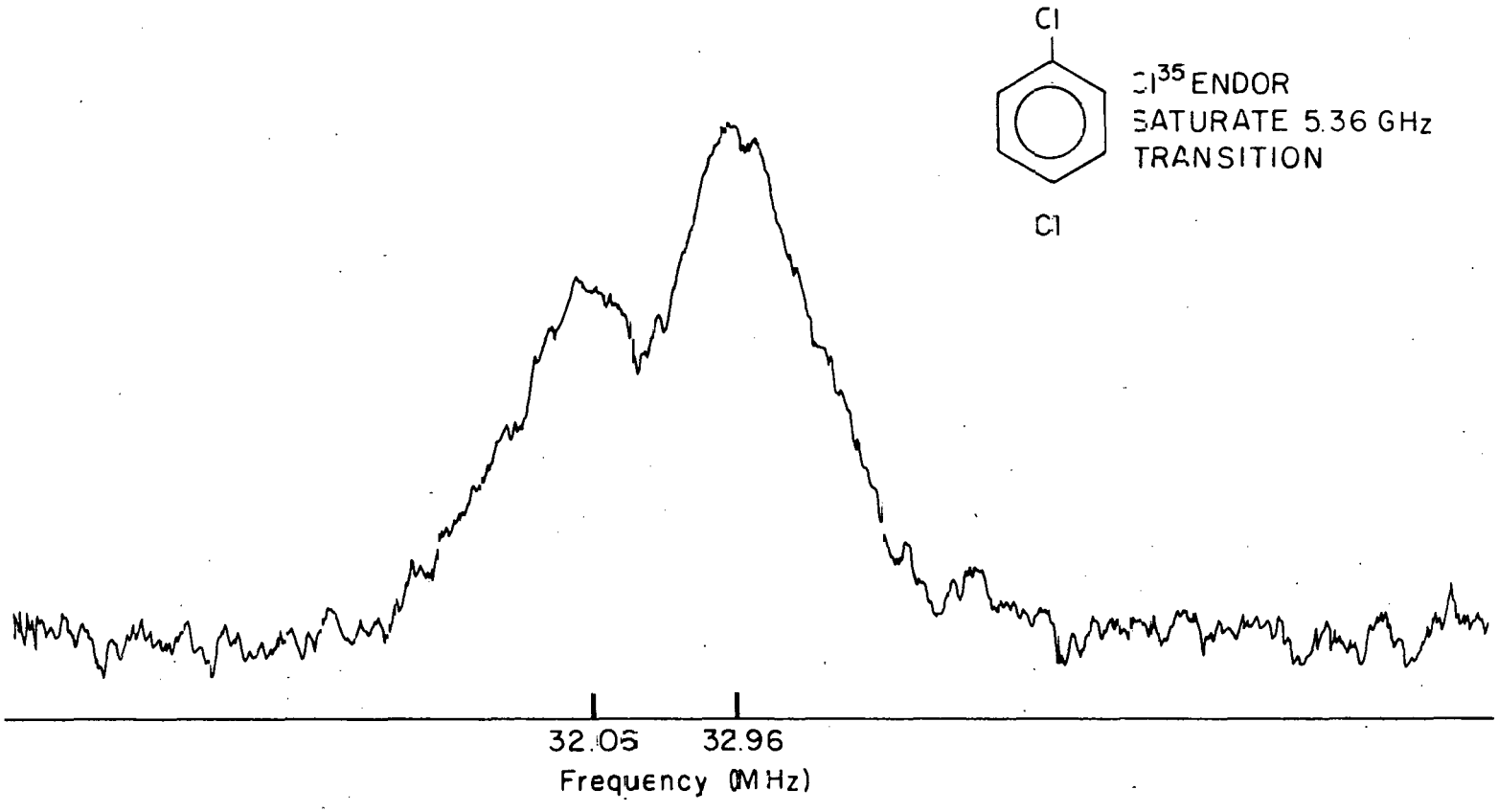

XBL 711-61

Figure 40

^{35}Cl ENDOR associated with the $\tau_x \rightarrow \tau_z$ multiplet of paradichlorobenzene

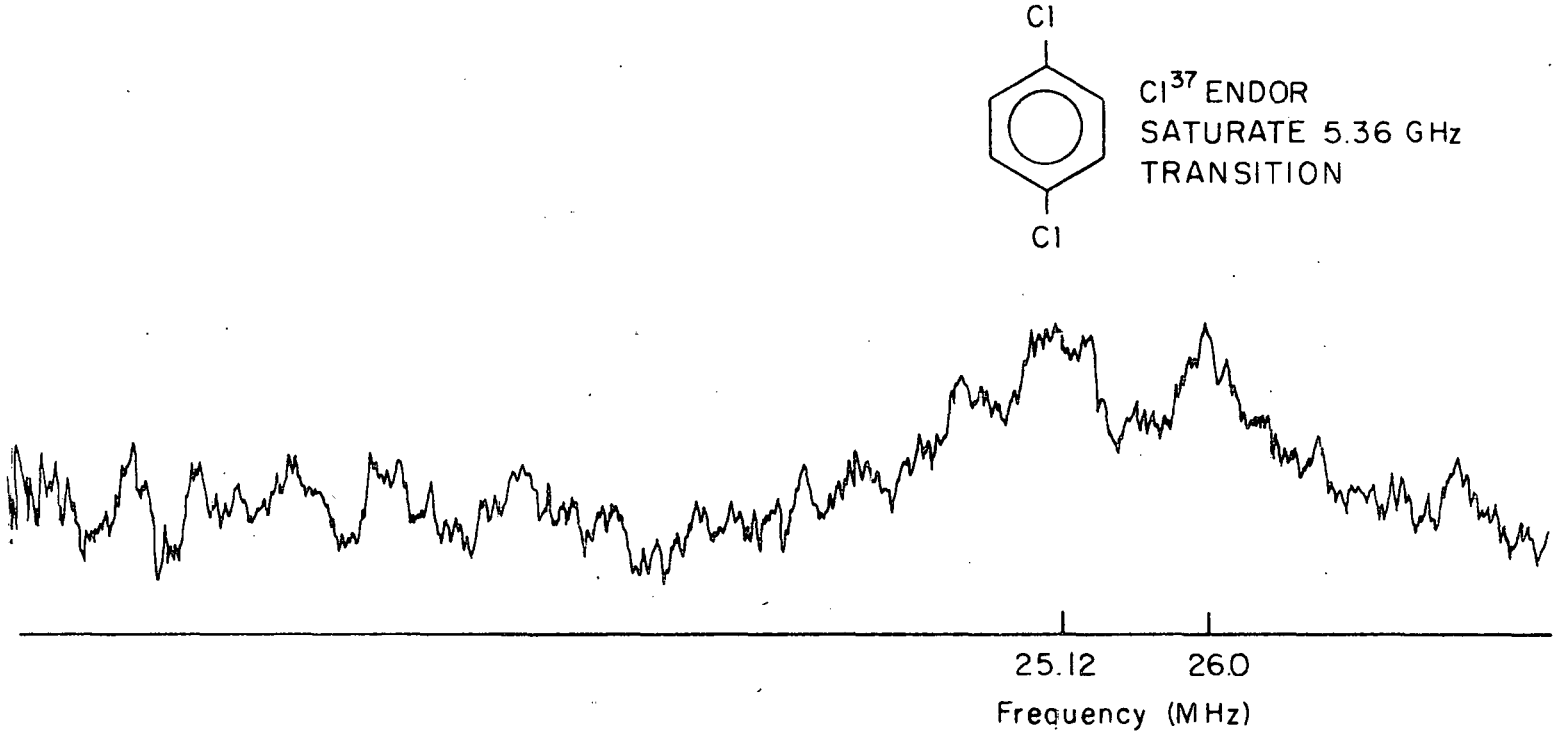

XBL 711-59

Figure 41

^{37}Cl ENDOR associated with the $\tau_x \rightarrow \tau_z$ multiplet of paradichlorobenzene

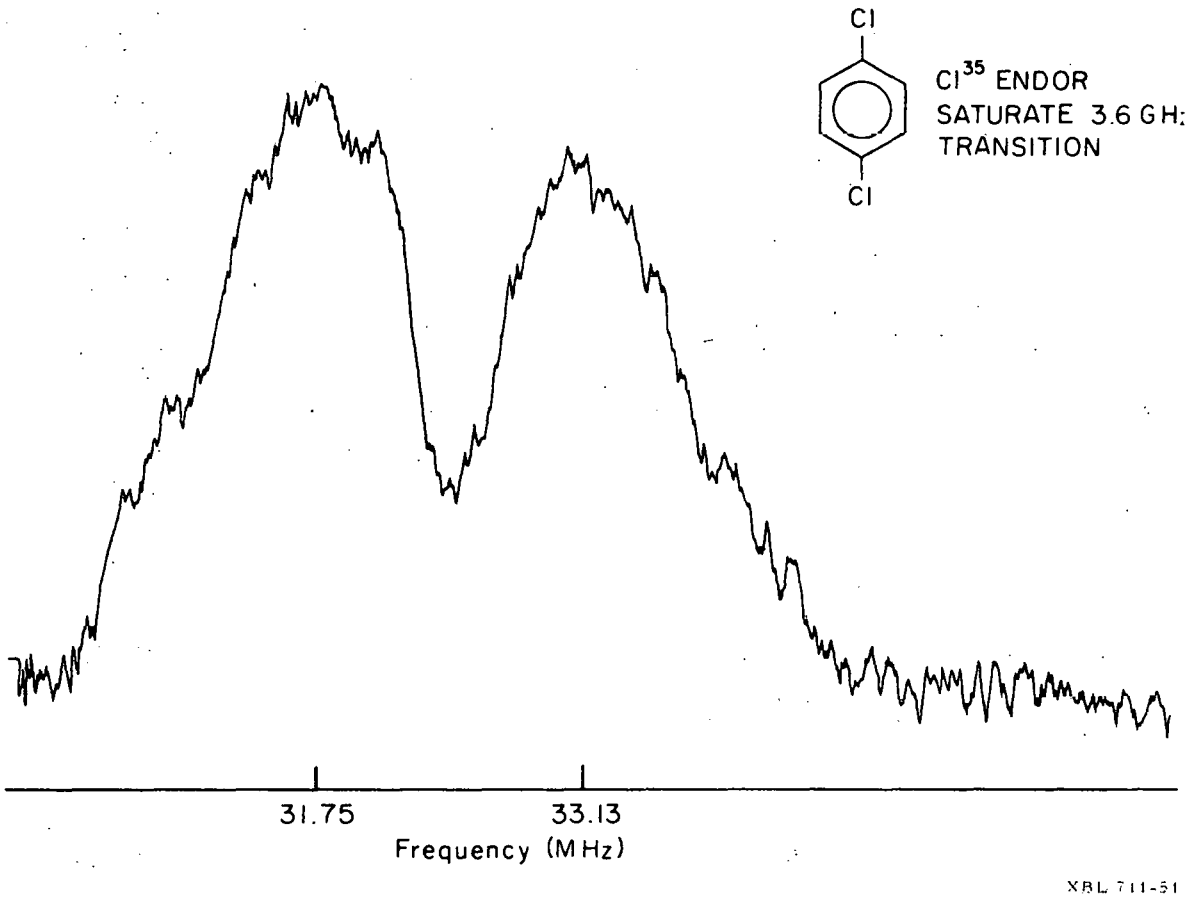

Figure 42

^{35}Cl ENDOR associated with the $\tau_x \rightarrow \tau_y$ multiplet of paradichlorobenzene

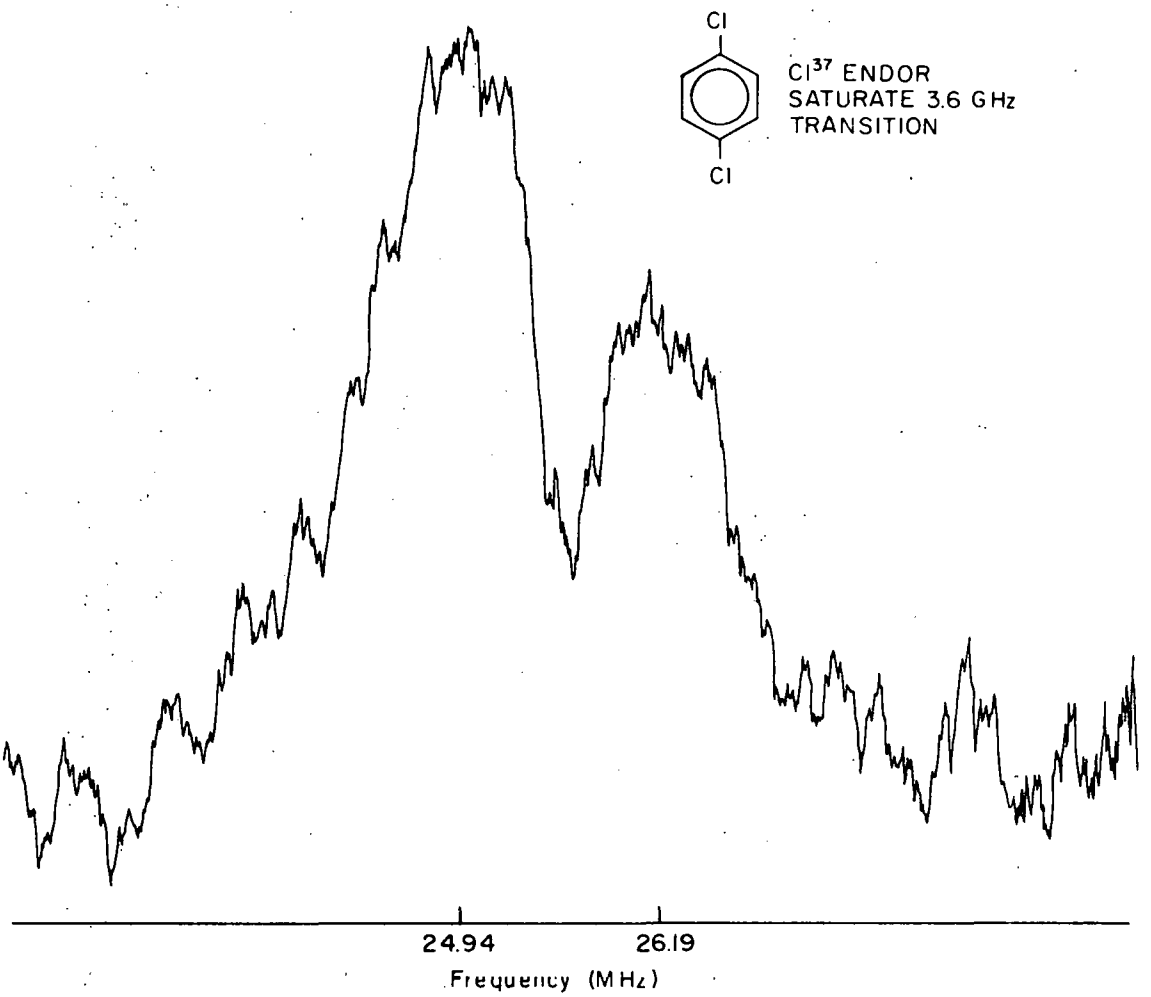

XBL 711-50

Figure 43

^{37}Cl ENDOR associated with the $\tau_x \rightarrow \tau_y$ multiplet of paradichlorobenzene

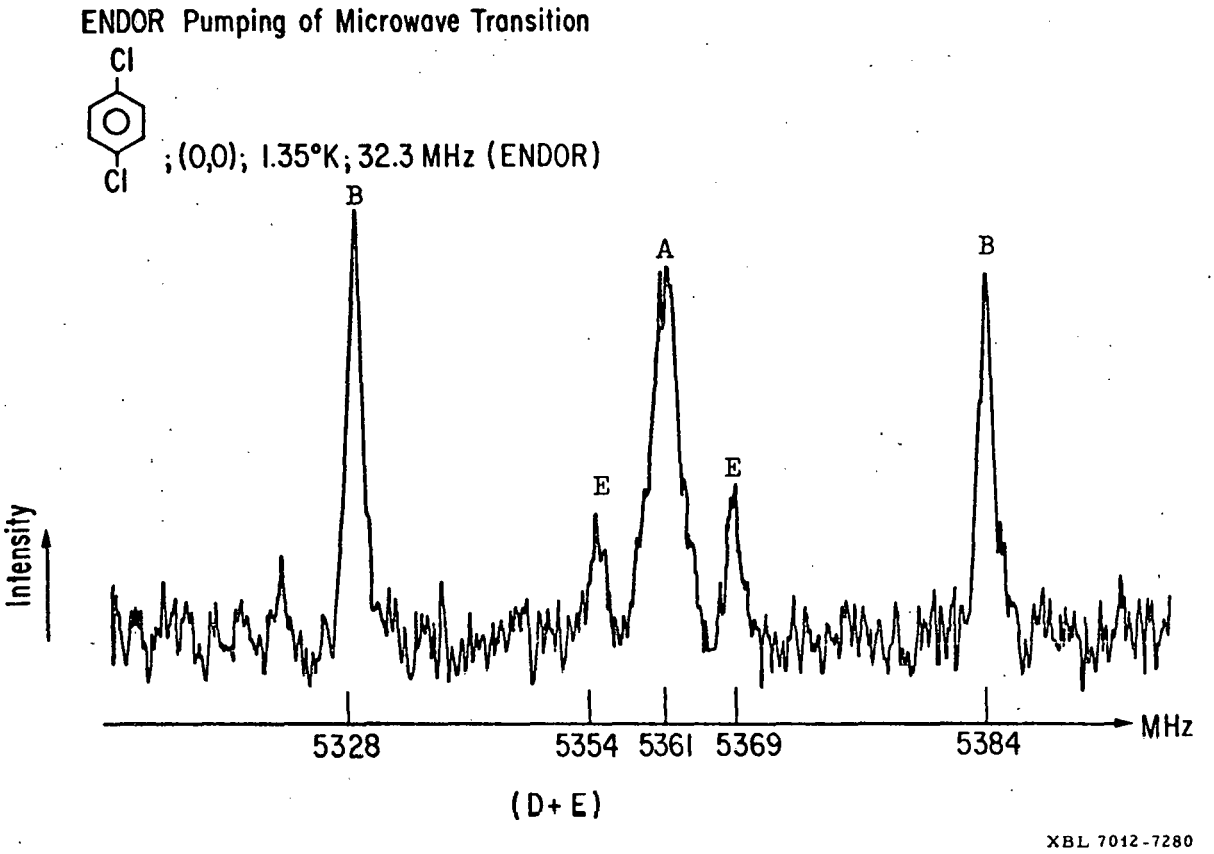

Figure 44

^{35}Cl ENDOR pumping of the $\tau_x \rightarrow \tau_z$ multiplet in paradichlorobenzene

The pure nuclear quadrupole resonance spectrum of pDB in its ground state is shown in Figure 45. Due to the long spin-lattice relaxation time it was difficult to avoid saturation and consequently the signal strength is reduced compared to that obtained at room temperature.

The Spin Hamiltonian

The observed spectra may be satisfactorily explained in terms of a Hamiltonian of the form

$$H = H_{SS} + \sum_i H_Q + \sum_i H_{HF} \qquad (4)$$

where the summation is over the chlorine nuclei. With the axis system defined as x, out-of-plane; z, along the C-Cl bond direction; and y, the other in-plane axis, we have,

$$H_{SS} = -XS_x^2 - YS_y^2 - ZS_z^2$$

$$H_Q = \frac{e^2qQ}{12}(3I_z^2 - 15/4) \qquad (5)$$

and $$H_{HF} = A_{xx}S_xI_x \ .$$

The chlorine nuclear quadrupole asymmetry parameter has been assumed to be zero since it is only a small off-diagonal term in the spin Hamiltonian and could therefore not be determined within the experimental accuracy of our measurements. In addition the chlorine hyperfine interaction was found to be characterized satisfactorily by considering only the out-of-plane hyperfine interaction. Since these experiments were performed in the absence of an external magnetic field, no information is obtained

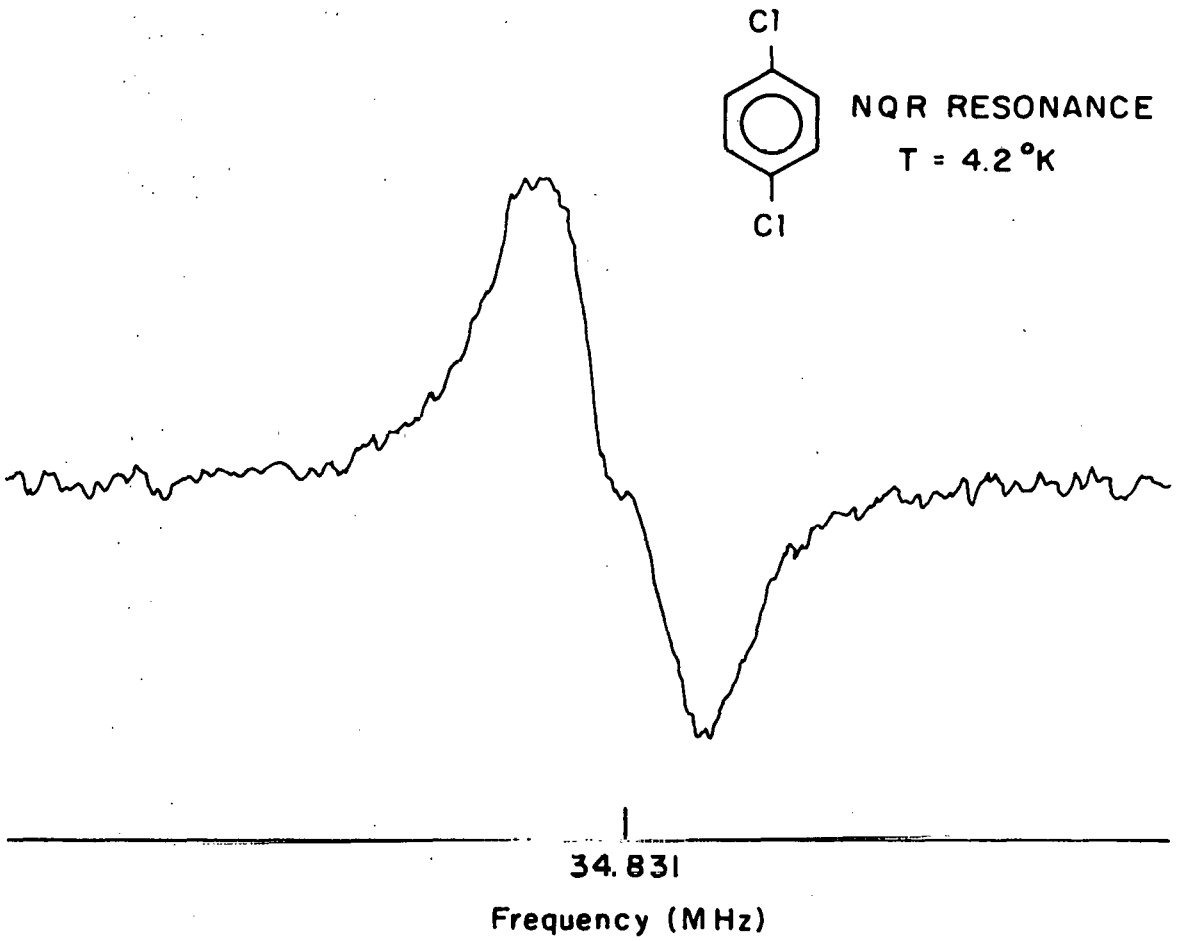

XBL 711-126

Figure 45

Pure NQR resonance of the ground state of paradichlorobenzene

from the ESR spectra as to the relative orientation of H_{SS}, H_Q and H_{HF}. Therefore, on the basis of single crystal ESR studies of other molecules in $\pi\pi^*$ triplet states,[27,42] it was assumed that the axis systems are coincident. In addition, Zeeman studies of the pure nuclear quadrupole resonance of pDB in its ground state have shown that the chlorine nuclear quadrupole principal axis system is within one degree of the C-Cl bond direction as determined from x-ray studies.[110,111] We have also made the assumption that the hyperfine interaction due to the four protons may be neglected. This is justified on the basis that the interaction would cause only a small broadening and shift of the transitions and could not be resolved within our experimental accuracy. Furthermore, no resolveable hyperfine interaction attributable to protons has been reported to date for ODMR experiments with zero external magnetic field.* The basis states used in calculating the spin Hamiltonian and the effect of H_Q and H_{HF} on the transition frequencies and intensities have been treated in detail in sections III and V-A and will therefore not be repeated here.

The total spin of the system is 4 and therefore we do not have Kramers degeneracy and must consider the 48 separate energy levels of the excited triplet state. The ODMR spectra were simulated by use of a computer program (see Appendix) that diagonalized the spin Hamiltonian and calculated the transition frequencies and intensities. The spectra were fitted by calculating the spectra for the ^{35}Cl-^{35}Cl species of pDB. After the best fit to these transitions was obtained, the nuclear quadrupole coupling constant of ^{35}Cl was multiplied by the ratio of the ^{37}Cl nuclear quadrupole

* However, Hutchison and his group have observed the proton hyperfine interaction in the $^3\pi\pi^*$ state of naphthalene using conventional ESR techniques.[124]

moment to the ^{35}Cl nuclear quadrupole moment (0.78815)[112] in order to obtain the ^{37}Cl nuclear quadrupole coupling constant. The ^{37}Cl hyperfine interaction was obtained in a similar fashion by multiplying the ^{35}Cl hyperfine interaction (A_{xx}) by the ratio of $\gamma_{^{37}Cl}$ to $\gamma_{^{35}Cl}$ (0.8322). The elements of H_{SS} used in simulating the spectra observed while monitoring the x trap emission are listed in Table 11 along with the approximate values of H_{SS} for the y trap and the values reported for benzene.[93] The best value of the ^{35}Cl nuclear quadrupole coupling constant was -64.50 MHz (^{37}Cl = -50.84 MHz) and for the ^{35}Cl hyperfine interaction A_{xx} = 22 MHz (^{37}Cl; A_{xx} = 18.3 MHz). The experimental and calculated ESR frequencies for the x trap of pDB are listed in Table 12. With the parameters used in the spin Hamiltonian all of the calculated transition frequencies are within experimental error. In order to observe the simultaneous chlorine and electron spin transitions it was necessary to use a large microwave field (approximately one watt). Since there are several transitions differing slightly in frequency that correspond to a particular type of transition (A, B, C, etc.), assigning one average frequency to a transition is difficult since the magnitude of the time dependent magnetic field and the relaxation rate constants are not known. Therefore a simple weighted average of the transitions corresponding to a particular type was made which introduces a small error in the calculated frequencies.

The observed and calculated chlorine ENDOR transitions are listed in Table 13. The ENDOR resonances associated with the D - E multiplet are due to transitions in the x and z triplet levels whereas those observed while saturating the D + E multiplet are due to transitions in

the y and z triplet levels. In addition to the linewidth of the ENDOR transitions the large time dependent magnetic fields used in the ENDOR experiments (approximately twenty watts) makes the proper weighting of the calculated ENDOR frequencies unknown. Therefore only the range of calculated ENDOR frequencies is listed in Table 13.

Discussion

From previous experimental[11,94] and theoretical[113-116] studies of aromatic molecules in $\pi\pi^*$ triplet states it is almost certain that in pDB the largest component of the electron spin-spin tensor in its principal axis system is along the molecular axis normal to the plane (x). Indeed this is what is observed for the $\pi\pi^*$ triplet state of benzene.[93] The ordering of the interaction along the two in-plane molecular axes is not immediately apparent. From the analysis of the PMDR spectra of pDB (which is treated in the following section) the component of the electron spin-spin interaction along the molecular z (or long in-plane axis) is assigned as the larger of the two in-plane components of the hyperfine tensor.

Since the zero field splitting parameters D and D* ($D^* = (D^2 + 3E^2)^{\frac{1}{2}}$) are primarily a function of the size of the π system involved in the excitation,[117] the value of these parameters for both pDB and benzene should be similar if pDB is a $\pi\pi^*$ triplet. As can be seen in Table 11 the values of D and D* for both traps of pDB differ from the corresponding values for benzene by only a few percent which confirms the assignment of the excited triplet state of pDB as a $\pi\pi^*$ state.

The zero field splitting parameter E which is a measure of the anisotropy of the triplet electron distribution in the molecular plane is however quite different for both molecules. If the benzene molecule possessed D_{6h} symmetry in the excited state, E must be zero by symmetry. The finite value of E for benzene has been explained by deGroot and van der Waals[101] on the basis of a distortion of the benzene ring from the symmetric D_{6h} benzene with bond lengths of 1.427 Å to a compressed D_{2h} benzene with four long bonds (1.448 Å) and two short bonds (1.381 Å). Godfrey, Kern, and Karplus[102] have evaluated the integrals exactly and have explained the observed zero field splitting by use of a symmetrical structure for the benzene molecule and adjusting the extent of configurational mixing. They also calculated the effect of adding a substituent along our z axis with 2 electrons in a p_x orbital and found that if the benzene configurations are assumed to maintain the same relative weights as undistorted benzene and if the small matrix elements between the charge transfer and the benzene configurations are neglected, the values of D, E and D* decrease linearly in magnitude with increasing charge transfer. As will be discussed in the next section, the value of the zero field splitting parameter E for pDB is of the opposite sign as that predicted by Godfrey, Kern and Karplus.[102] The largest in-plane zero field axis in pDB is along the molecular z axis while the theoretical studies predict the largest in-plane zero field axis along the molecular y axis.

The discrepancy between the zero field splitting of pDB and that predicted on the basis of treating the chlorines as a small perturbation of the excited state of benzene raises the possibility that the symmetry

of the excited state of pDB is different than that of the excited state of benzene. In any case the zero field tensor of pDB is consistent with a triplet spin distribution in which the spin density on the two carbon atoms to which the chlorines are bonded is much smaller than the spin density on the other four carbon atoms.

The value of the chlorine nuclear quadrupole coupling constant (e^2qQ) in the excited state of pDB is significantly reduced compared to the corresponding value for the ground state.

With the assumption that the asymmetry parameter η may be neglected, the value of e^2qQ for the ^{35}Cl nuclei of pDB in its excited triplet state at 1.3°K is -64.5 MHz. The measured pure nuclear quadrupole resonance frequency of pDB in its ground state at 4.2°K is 34.831 MHz which, if η is assumed to equal zero, corresponds to a value of e^2qQ of -69.662 MHz. The assumption that η may be neglected is justified on the basis that e^2qQ is not changed significantly for small value of η and for the ground state of pDB at room temperature η is only 0.08.[108] Referring to Figure 7, it may be seen that the assumption that the pure NQR transition frequency ν equals $|\frac{1}{2}e^2qQ|$ causes a positive error of less than 5% for $\eta \leq 0.5$. The sign of e^2qQ is not obtained from either the measurement of the pure NQR transition frequency or the spin Hamiltonian; however, from other theoretical and experimental studies e^2qQ for Cl is known to be negative for covalently bonded compounds.

The increase of 52 KHz in the pure NQR frequency of the ground state of pDB upon lowering the temperature of the sample from 77°K (ν = 34.779 MHz) to 4.2°K (ν = 34.831 MHz) is consistent with Bayer's theory[118]

which treats the temperature dependence of the NQR frequency in terms of the molecular torsional motions. The small change in the pure NQR transition frequency indicates that there is no major physical change in the environment of the chlorine nuclei in pDB upon cooling. Therefore the difference in e^2qQ between the ground and excited states of pDB is clearly due to a change in the electric field gradient (q) at the chlorines upon excitation. In contrast to the electron spin-spin and hyperfine interactions which are a function of the triplet electrons only, e^2qQ is independent of the spin of the electrons.

Since electrons in s orbitals have spherical symmetry, they do not contribute to the field gradient. A closed p shell also contributes nothing to the field gradient, and therefore following the analysis of Bersohn[103] the field gradient in pDB can be considered as arising from a hole in the p_z orbital and a partial hole in the p_x orbital. The total contribution is due to two axially symmetric tensors whose major axes are perpendicular. In Table 14, the contributions to the field gradients are expressed in terms of the number of holes in the p_x and p_z chlorine orbitals.

The difference in e^2qQ for the excited and ground state may be written,

$$\Delta e^2qQ = e^2(q_T - q_G)Q \qquad (6)$$

where q_T and q_G refer to the field gradient at the chlorines in the triplet and ground states of pDB respectively. Equation 6 may be expressed in terms of the number of holes in the p_z and p_x orbitals as

$$\Delta e^2qQ = e[(\sigma_T - \sigma_G) - \tfrac{1}{2}(\delta_T - \delta_G)]Q \qquad (7)$$

Since Δe^2qQ is negative, one of the following three conditions must be met, a) $\sigma_G > \sigma_T$, b) $\delta_T > \delta_G$, or c) $\sigma_G > \sigma_T$ and $\delta_T > \delta_G$. If σ_G is greater than σ_T, the number of holes has decreased along the carbon-chlorine bond, and therefore the chlorine nuclei are more successful in competing for electrons in the excited state. However since the sigma electrons are not involved in the excitation, this effect should be very small.

If δ_T is greater than δ_G, the out-of-plane chlorine p orbital has lost electrons. An increase in the number of holes in the p_x orbital would be the most likely explanation of the decrease in e^2qQ since the chlorine p_x orbitals are allowed by symmetry to interact with the carbon p_x orbitals. The increase in the number of holes in the chlorine p_x orbital can come about from either an increase in the double bond character of the C-Cl bond or a "bent" C-Cl bond. Bray, Barnes and Bersohn[104] have shown that although the overlap of the carbon and chlorine p_x orbitals is reduced with a bent C-Cl bond, the chlorine p_x orbitals may overlap with the carbon sigma system, consequently increasing the number of holes in the p_x orbital of chlorine (δ_T) relative to the number of holes in the p_x orbital in the ground state (δ_G). From the analysis of the zero field tensor it appears that the triplet electrons do not have a large spin density on the carbon atoms bonded to the chlorines. Therefore an appreciable increase in π bonding seems unlikely. This leaves us with the possibility of a bent C-Cl bond. This would require a small value for the chlorine hyperfine interaction since the C-Cl p_x overlap is reduced. The interpretation of the observed chlorine hyperfine interaction is limited since only one of the three components of the hyperfine tensor

was measured. The magnitude of the chlorine hyperfine interaction is a function of both the spin density on the chlorine and the ring carbon to which it is bonded.[105,106] However, we will limit our discussion to a simple analysis in which only the spin density on the chlorine is considered to contribute to the hyperfine interaction. The theoretical hyperfine interaction due to one unpaired electron in a carbon P orbital is 280 MHz.[89] Neglecting any isotropic contribution to the measured hyperfine interaction, the spin density in each chlorine p_x orbital is,

$$\rho \approx 22/280 = .08$$

where ρ is normalized to two. Although this is a very crude approximation, it is clear that the chlorines do not participate significantly in the excitation. This small value for ρ is also consistent with a bent C-Cl bond rather than an increased double bond character since in the latter case a significantly larger value of ρ would be expected.

Since all three of the parameters obtained from the spin Hamiltonian support the hypothesis that the C-Cl bond is bent, it seems the most reasonable conclusion. The molecule in the excited state may therefore exist in a cis (C_{2v}) or trans (D_{2h}) configuration. In order to resolve this question, the phosphorescence spectra have been analyzed by investigating the relative changes in the vibronic structure of the phosphorescence upon inducing ESR transitions between the three triplet sublevels. The result of this analysis is given in the following section.

Table 10

ESR Transitions in Paradichlorobenzene

Transition Type	Simultaneous Transitions	Molecular Species
A	Electron Spin	I, II, III
B	Electron and ^{35}Cl Spins	I, II
C	Electron and ^{37}Cl Spins	II, III
D	Electron, ^{35}Cl and ^{35}Cl Spins	I
E	Electron, ^{35}Cl and ^{37}Cl Spins	II
F	Electron, ^{37}Cl and ^{37}Cl Spins	III

Table 11

Zero Field Splitting Parameters (MHz)

	Paradichlorobenzene X Trap (1.3°K)	Paradichlorobenzene Y Trap (4.2°K)	Benezene-h_4 In Benzene-d_6 (1.95°K)+
X	-2988.75	-2967.7	-3159.8
Y	616.07	654.4	1769.4
Z	2372.68	2313.4	1385.0
$D^{\ddagger}$	4483.13	4451.6	4739.7
$E^{\ddagger}$	878.31	829.5	-192.2
D^{*}	4733.8	4677.7	4793.2

‡In order to be consistent with the standard ESR definitions we have defined

$$D = -3/2X \text{ and } E = 1/2(Z - Y)$$

+Data from reference 93 expressed in our axis system.

Table 12

Measured and Calculated ESR Transitions of the $^3\pi\pi^*$ State of Paradichlorobenzene (X Trap)

	Measured Frequency (MHz)	σ	Calculated Frequency	Classification
a) $\tau_x \rightarrow \tau_z$				
	5426.7	1.0*	5426.91	D
	5419.6	1.0*	5419.56	E
	5394.56	0.41	5394.62	B
	5387.86	0.41	5387.79	C
	5368.73	0.64	5368.89	E
	5362.20	0.34	5362.14	A
	5355.13	0.25	5355.12	E
	5336.67	0.24	5366.50	C
	5329.74	0.28	5329.75	B
	5303.8	1.0*	5304.11	E
	5296.5	1.0*	5297.35	D
b) $\tau_x \rightarrow \tau_y$				
	3636.03	.07	3636.13	B
	3629.65	.18	3629.56	C
	3611.18	.24	3611.04	E
	3604.19	.25	3604.10	A
	3597.69	.31	3597.43	E
	3578.90	.22	3578.89	C
	3571.88	.34	3571.99	B
c) $\tau_y \rightarrow \tau_z$				
	1791.1	1.5	1791.13	B
	1758.2	1.0	1758.05	A
	1724.5	1.5	1726.55	B

* Estimated value of σ

Table 13

Measured and Calculated Chlorine ENDOR Transitions of the $^{3}\pi\pi^{*}$ State of Paradichlorobenze (X Trap)

	Measured Frequency in MHz (±.05)	Calculated Frequency in MHz (range)
	$\tau_x \rightarrow \tau_z$ Manifold	
^{35}Cl	32.06; 32.96	31.56 - 33.03
^{37}Cl	25.12; 26.00	24.94 - 26.09
	$\tau_x \rightarrow \tau_y$ Manifold	
^{35}Cl	31.75; 33.13	31.53 - 32.94
^{37}Cl	24.94; 26.19	24.79 - 25.90

Table 14

Contributions to the Chlorine Nuclear Quadrupole Coupling Constant

Chlorine Orbital	No. of Holes	Contribution to V_{xx}	Contribution to V_{yy}	Contribution to V_{zz}
P_x	δ	δq	$-\delta q/2$	$-\delta q/2$
P_z	σ	$-\sigma q/2$	$-\sigma q/2$	σq

Total Contribution

$$V_{xx} = (\delta - \sigma/2)q$$

$$V_{yy} = -1/2(\delta + \sigma)q$$

$$V_{zz} = (\sigma - \delta/2)q$$

2. The PMDR Spectrum of Paradichlorobenzene

The experimental technique is essentially the same as that used in the ODMR experiments except that the phosphorescence spectrum is scanned while saturating one of the three microwave transitions. The microwave field is amplitude modulated and the resulting time-dependent change in intensity of the phosphorescence converted to DC by means of a lock-in amplifier. With this technique only the change in emission of two of the three triplet levels is detected while saturating any one of the three microwave transitions.

In addition to the previously reported exciton phosphorescence[71,97] of pDB (origin = 27890 cm^{-1}), emission from a shallow trap which will be referred to as the x trap (origin = 27868 cm^{-1}) and a deep trap which will be referred to as the y trap (origin = 27807 cm^{-1}) was observed. The pDB sample was found to be extremely sensitive to its recent thermal history. In order to observe the weak exciton phosphorescence it was necessary to cool the sample slowly to the temperature of liquid helium over a three hour period. The emission of both the exciton and the x trap was observed at 4.2°K with approximately equal intensity. Upon cooling the sample to 1.3°K only the x trap emission was observed. If the temperature of the pDB crystal was lowered to 4.2°K rapidly (approximately 20 minutes), exciton emission was not observed, but the emission from the y trap was observed in addition to that from the x trap. Upon cooling the sample below 4.2°K, the intensity of the x trap emission increased while the intensity of the y trap emission decreased until at 1.3°K only the x trap emission was observed. The y trap emission is

believed to be due to triclinic inclusions[119] in the monoclinic pDB lattice.[120] This was tested by preparing a sample of pDB which contained approximately 0.01 mole percent paradimethylbenzene as an impurity. Francis[121] has found from laser man studies that this impurity forces the pDB to remain in its triclinic crystalline form. Since the same phosphorescence origin as well as the same ESR transition frequencies (±20 MHz) were observed for both the y trap and the triclinic form of pDB, the y trap is due to triclinic inclusions.

An example of the usefulness of the PMDR technique is the resolution of the emission from the x and y traps. In Figure 46 is shown the first 300 Å portion of the phosphorescence spectrum of pDB at 1.95°K which is composed of both x and y trap emission. Since the ESR transition frequencies are slightly different for the two traps, the contribution to the phosphorescence spectrum due to only one of the traps may be obtained by saturating the ESR transition associated with the particular trap molecules while monitoring only the component of the phosphorescence emission that is changing in amplitude at the modulation frequency. An example of the spectra obtained from this experiment is shown in Figure 47. The emission from the y trap is no longer observed and the phosphorescence spectrum consists of only emission from the x trap.

In addition to resolving the emission from different molecular sites in the crystal, the use of the PMDR technique simplifies the analysis of the vibrational structure of the phosphorescence, and in favorable cases gives the orientation of the electron spin-spin tensor and the spacial symmetry of the excited state.

The phosphorescence spectrum of the x trap of pDB at 1.35°K obtained using 10μ slits is shown in Figure 48. In order to obtain a reasonable

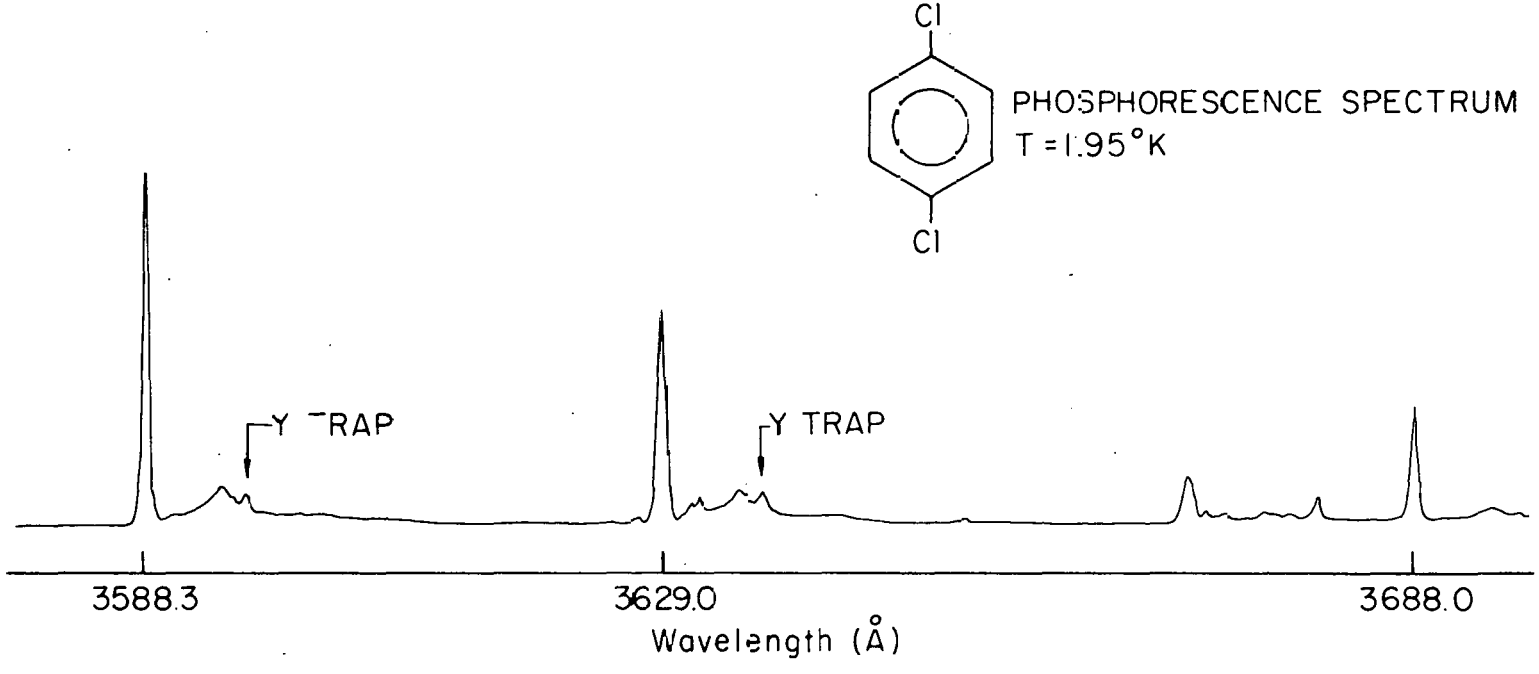

XBL 711-55

Figure 46

Phosphorescence spectrum of paradichlorobenzene

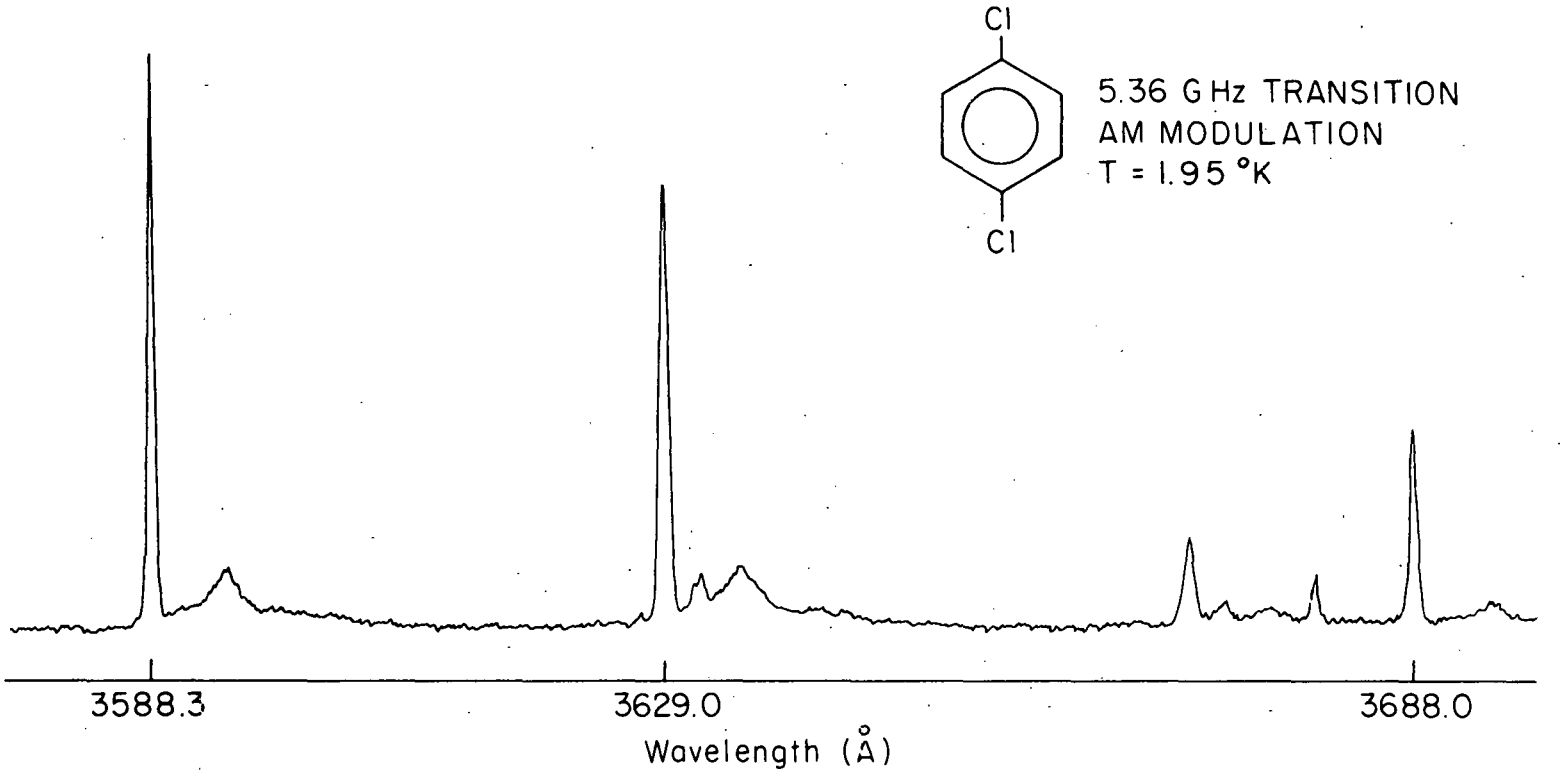

XBL 711-56

Figure 47

PMDR spectrum of the X trap emission of paradichlorobenzene

signal to noise ratio for the PMDR experiments, it was necessary to use 50μ slits resulting in a lower resolution spectrum. In Figure 49 the phosphorescence spectrum using 50μ slits (49a) and the PMDR spectra obtained with the same slit width while saturating the $\tau_x \rightarrow \tau_z$ (49b), $\tau_x \rightarrow \tau_y$ (49c) and $\tau_y \rightarrow \tau_z$ (49d) transitions are shown. All of the vibronic transitions increase in intensity for each of the PMDR experiments. Since a lock-in amplifier was used, any decrease in intensity while monitoring the emission to a vibrational level of the ground state would have caused the PMDR transition to go negative rather than positive. The relative increase in intensity of the vibronic band at 0-0 + 1583 cm^{-1} (denoted by * in Figure 49) compared to the origin is striking. The relative increase in intensity of the vibronic band is greatest while saturating the $\tau_x \rightarrow \tau_y$ transition (49c) while the relative increase in intensity of the origin is greatest for the $\tau_x \rightarrow \tau_z$ transition (49b). The other vibrations that have been assigned as a_g behave in a manner similar to the origin and therefore it is clear that the vibration at 0-0 + 1583 cm^{-1} is not an a_g vibration as previously assigned[71,97] since all vibrations with the same symmetry should maintain a constant intensity ratio within all three PMDR spectra. This vibration is therefore assigned b_{3g} symmetry since from laser Raman studies both a b_{3g} and an a_g vibration are observed at this energy.[122,123]

Analysis of the polarization of the absorption spectrum ($S_o \rightarrow T_1$) of pDB shows that the transition is primarily out-of-plane polarized which has been interpreted by Castro and Hochstrasser[71] as implying B_{2u} symmetry for the excited state. The three levels of a B_{2u} triplet transform as

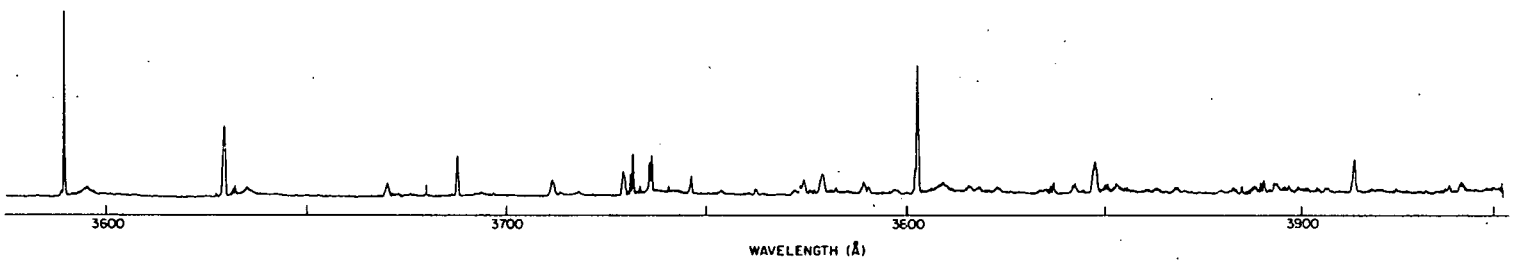

XBL 7012-7260

Figure 48

High resolution phosphorescence spectrumof the X trap emission of paradichlorobenzene at 1.3°K

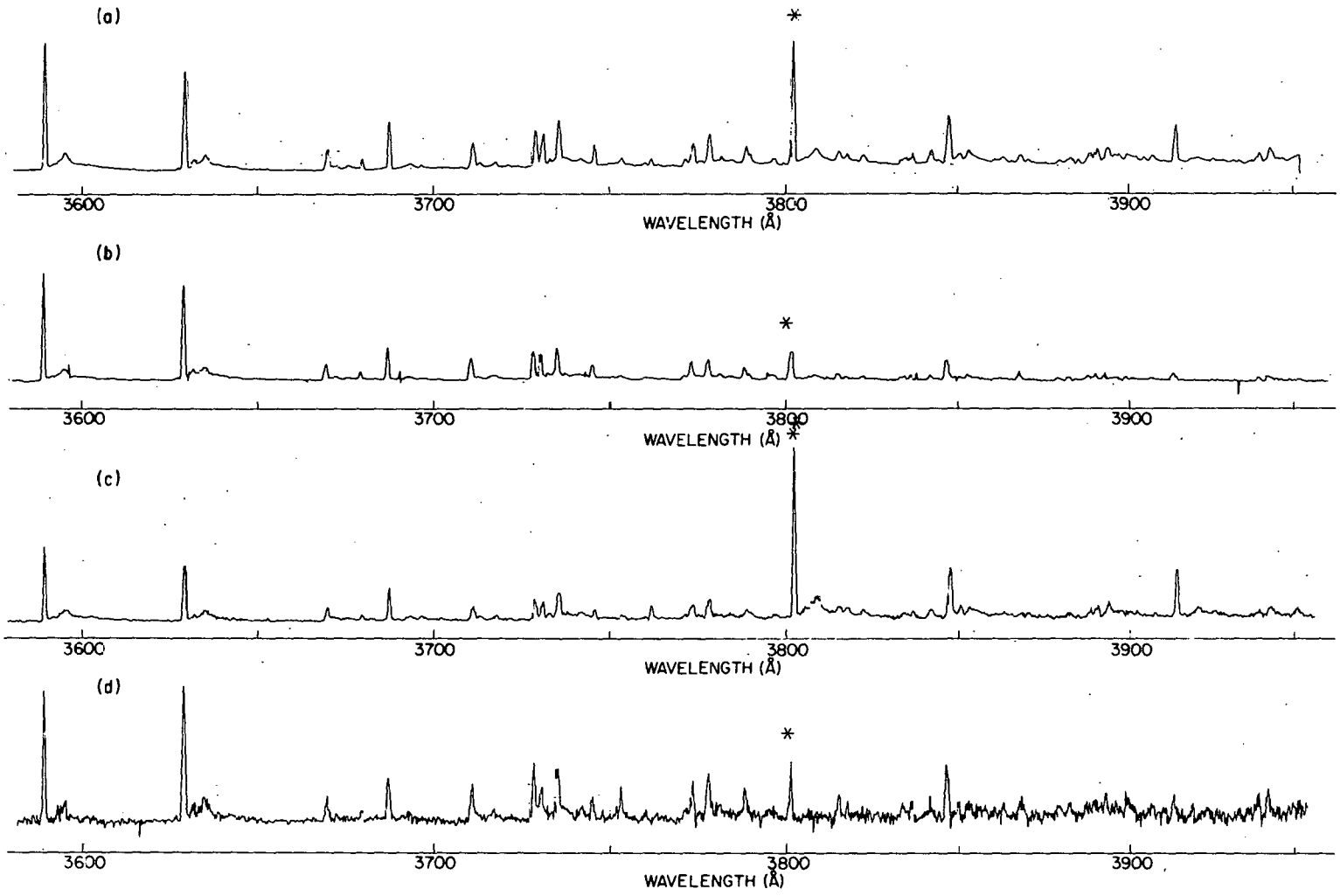

Figure 49

XBL 7012-7261

Phosphorescence spectra (a) and PMDR spectra obtained while saturating the $\tau_x \rightarrow \tau_z$ (b), $\tau_x \rightarrow \tau_y$ (c) and $\tau_y \rightarrow \tau_z$ (d) zero field transitions of paradichlorobenzene (X trap) at 1.3°K.

$$\tau_x = B_{3g} \times B_{2u} = B_{1u}$$
$$\tau_y = B_{2g} \times B_{2u} = A_u \qquad (8)$$
$$\tau_z = B_{1g} \times B_{2u} = B_{3u}$$

As is shown in Table 15 the emission to the b_{3g} vibrations must originate primarily from the τ_y triplet level since the emission is primarily x polarized. Since the largest relative intensity of the b_{3g} vibrations are obtained upon saturation of the ESR transition at ~ 3.6 GHz (see Figure 49c) that is between the frequency of the other two ESR transitions (~ 5.3 and 1.7 GHz), the τ_y level must be the lowest or middle triplet energy level. The possibility of the τ_y level as being either the highest or middle energy level is ruled out since this would require a larger value of E and correspondingly smaller value of D than is theoretically reasonable. As discussed in the previous section, the τ_x level is almost certainly the lowest in energy and therefore the energy of the triplet levels must be ordered,

$$E_z > E_y > E_x$$

The fact that the intensity of the entire phosphorescence spectrum increases for all three PMDR experiments requires that the triplet level which emits to the ground state with the fastest radiative rate constant have the smaller initial population. This further requires that the population and radiative rate constants of the triplet levels be ordered respectively $N_x > N_y > N_z$ and $K_z > K_y > K_z$ or vice versa.

Since there is a moderate amount of in-plane polarization, the contribution to the radiative rate constants of the three triplet levels due to other additional spin-orbit coupling must be included. The resulting polarization of the emission from the triplet levels to the ground vibrational states is given in Table 15. The emission intensity from any one triplet level may be written,

$$I_i = N_i \sum K_i^j \qquad (9)$$

where I_i in the intensity of emission from triplet level τ_i with population N_i, and K_i^j is the radiative rate constant for emission from τ_i with j polarization. The phosphorescence that is monitored is a summation of the emission from each of the triplet levels to a particular vibronic band (i.e., a_g, b_{2g}, or b_{3g}). The intensity of the phosphorescence in terms of the symmetry of the vibronic level that is monitored for the case of a B_{2u} triplet is given by

$$\begin{aligned} I_{a_g} &= N_x K_x^z + N_z K_z^x \\ I_{b_{2g}} &= N_x K_x^x + N_y K_y^y + N_z K_z^z \\ I_{b_{3g}} &= N_x K_x^y + N_y K_y^x \end{aligned} \qquad (10)$$

Upon saturation of one of the three microwave transitions, the population of the two levels connected by the microwave field are equalized (see Section II). The change in intensity of the phosphorescence is proportional to

$$\Delta I \approx (N_i - N_j)(K_j - K_i) \qquad (11)$$

However, if only the emission to a particular vibronic band is monitored, the emission from both of the levels that are connected by the microwave field may not be observed. In this case, the change in intensity of the phosphorescence when triplet levels i and j are connected by the microwave field and the emission from level i is not monitored is

$$\Delta I \approx (N_i - N_j)K_j \qquad (12)$$

In Table 16 the change in phosphorescence intensity is predicted for the $^3B_{2u}$ state of pDB upon saturating any one of the three zero field transitions while monitoring the emission to a particular vibration of the ground state with a_g, b_{2g} or b_{3g} symmetry. With the assumption that the populations are ordered $N_x > N_y > N_z$ and that all radiative rate constants from τ_z are greater than those from τ_y which are greater than those from τ_x, the change in phosphorescence is predicted to increase for six of the cases but decrease for the other three. Since the phosphorescence was observed to always increase, this assignment is clearly incorrect. However, if the molecule is distorted from D_{2h} to C_{2h} symmetry, the distinction between the x and z axes is lost and the triplet levels transform as

$$\begin{aligned} \tau_x &= B_g \times A_u = B_u \\ \tau_y &= A_g \times A_u = A_u \\ \tau_z &= B_g \times A_u = B_u \end{aligned} \qquad (13)$$

and the vibrations a_g, b_{2g} and b_{3g} transform as a_g, a_g and b_g respectively. The intensity of emission to the vibrational levels in this case is

$$I_{a_g} = N_x K_x^{xz} + N_y K_y^{y} + N_z K_z^{xz}$$
$$I_{b_g} = N_x K_x^{y} + N_y K_y^{xz} + N_z K_z^{y} \qquad (14)$$

In table 17 the change in intensity predicted for the distorted molecule is given. As can be seen in this case, the intensity of the phosphorescence always increases. If the molecule is distorted only two basic types of vibrational structures will be observed since both a_g and b_{2g} vibrations transform as a_g in C_{2h}. As can be seen in Table 18 the intensity ratio of the vibronic structure of the phosphorescence for the three PMDR experiments shows only two distinct types of vibrations. If the molecule is distorted, the transitions will be equally polarized along the x and z molecular axes. From the values of the squared directional cosines of pDB listed in Table 19, equal polarization along the x and z molecular axes gives a polarization ratio along the crystal axis of $I_c/I_b = 1.5$ as compared to the value of $I_c/I_b = 3.4$ for polarization along the molecular x axis only. The measured polarization ratio of I_c/I_b for the absorption origin is 2.9[97] and 3.1,[71] which is not inconsistent with the conclusion that pDB is distorted in its excited triplet state into a trans configuration.

In summary, the observed ODMR and PMDR spectra of pDB are consistent with the hypothesis that the excited triplet state of pDB is a $\pi\pi^*$ state and that the symmetry of the excited state is B_{2u}. From the assigned orientation of the zero field tensor, the spin density appears to be

localized primarily on the four carbons that are not bonded to the chlorines. The small value of the chlorine out-of-plane hyperfine element leads to the conclusion that the chlorines do not participate significantly in the excitation.

On the basis of the PMDR spectra and the reduced value of the chlorine nuclear quadrupole coupling constant as compared to the value for the ground state, it is hypothesized that the C-Cl bonds are bent and that the molecule possesses C_{2h} rather than D_{2h} spacial symmetry in the excited state.

The assignment of the symmetry of the excited triplet state of pDB as a B_{2u} state is somewhat disturbing in view of the small participation of the chlorines in the excitation and the accepted assignment of the first excited triplet state of benzene as a B_{1u} state.

Therefore two experiments are proposed to remove many of the assumptions made in the preceeding discussion. The measurement of the ODMR spectra in a magnetic field would give the orientation of the principal axis systems of H_{SS}, H_Q and H_{HF} and in addition permit the measurement of the two in-plane components of the chlorine hyperfine tensor. The use of a polarizer to separate the components of the phosphorescence spectra while performing the PMDR experiments would permit a more detailed analysis of the vibrational structure of the phosphorescence and consequently an unambiguous assignment of the symmetry of the excited triplet state of pDB.

Table 15

Polarization of the Phosphorescence

to the Ground State Vibrational Levels

$^3B_{2u}$ Levels	Polarization X	Y	Z	
τ_x	b_{2g}	b_{3g}	a_g	Symmetry of Ground State Vibrations
τ_y	b_{3g}	b_{2g}	b_{1g}	
τ_z	a_g	b_{1g}	b_{2g}	

Table 16

Predicted change in intensity of the phosphorescence for a molecule in a $^3B_{2u}$ state when monitoring the individual vibronic bonds of the phosphorescence*.

Vibrational Symmetry	Microwave Transition Saturated $\tau_x \rightarrow \tau_y$	$\tau_x \rightarrow \tau_z$	$\tau_y \rightarrow \tau_z$
a_g	$(N_y-N_x)K_x^z$ $< o$	$(N_x-N_z)(K_z^x-K_x^z)$ $> o$	$(N_y-N_z)K_z^x$ $> o$
b_{2g}	$(N_x-N_y)(K_y^y-K_x^x)$ $> o$	$(N_x-N_z)(K_z^z-K_x^x)$ $> o$	$(N_y-N_z)(K_z^z-K_y^y)$ $> o$
b_{3g}	$(N_x-N_y)(K_y^x-K_x^y)$ $> o$	$(N_z-N_x)K_x^y$ $< o$	$(N_z-N_y)K_y^x$ $< o$

*The change in intensity is based on the assignment $N_x > N_y > N_z$ and $K_z^i > K_y^i > K_x^i$.

Table 17

Predicted change in intensity of the phosphorescence for a distorted (C_{2h}) excited state.*

Vibrational Symmetry	Microwave Transition Saturated $\tau_x \rightarrow \tau_y$	$\tau_x \rightarrow \tau_z$	$\tau_y \rightarrow \tau_z$
a_g	$(N_x-N_y)(K_y^y-K_x^{xz})$ $> o$	$(N_x-N_z)(K_z^{xz}-K_x^{xz})$ $> o$	$(N_y-N_z)(K_z^{xz}-K_y^y)$ $> o$
b_g	$(N_x-N_y)(K_y^{xz}-K_x^y)$ $> o$	$(N_x-N_z)(K_z^y-K_x^y)$ $> o$	$(N_y-N_z)(K_z^y-K_y^{xz})$ $> o$

*The change in intensity is based on the assumption $N_x > N_y > N_z$ and $K_z^i > K_y^i > K_x^i$ or vice versa.

Table 18

Analysis of the PMDR Spectra of the X Trap Phosphorescence of Paradichlorobenzene (1.3°K)

$\bar{\nu}(\pm 5 cm^{-1})$	$\Delta\bar{\nu}$	Intensity* of PMDR While Saturating			Intensity Ratio		TYPE	Assignment*
		A $\tau_x \rightarrow \tau_z$	B $\tau_x \rightarrow \tau_y$	C $\tau_y \rightarrow \tau_z$	A/C	B/C		
27868		61	43	77	1.42	0.56	I	Trap origin
27823	45	6	7	13	0.86	0.54	I	Lattice (41 B_g)
27556	312	33	32	79	1.72	0.41	I	b_{2g} (306)
27538	330	7	7	10	1.00	0.70	I	a_g (327)
27504	364	8	10	15	0.80	0.67	I	312 + 46
27247	621	10	20	15	0.50	1.33	I	2 x 312
27115	753	19	10	26	1.90	0.38	I	a_g(744)
26938	931	13	8	23	1.63	0.35	I	3 x 312
26808	1061	17	14	35	1.21	0.40	I	755 + 313
26793	1075	16	12	20	1.33	0.60	I	a_g(1081)
26759	1109	19	18	31	1.06	0.58	I	a_g(1103)
26686	1182	10	7	15	1.43	0.47	I	a_g(1174)
26570	1298	2	10	1	0.20	10.0	II	b_{3g}(1293
26502	1366	4	5	8	0.80	0.63	I	
26487	1382	12	11	24	1.09	0.46	I	
26453	1415	12	14	28	0.86	0.50	I	
26285	1583	17	101	35	0.17	2.89	II	b_{3g}(1577)
26241	1627	3	15	0	0.20	∞	II	1583 + 46
26054	1814	5	7	13	0.71	0.54	I	
26016	1852	4	8	16	0.50	0.5	I	
25980	1888	13	32	33	0.41	0.97	I	
25695	2173	5	10	14	0.5	0.71	I	
25542	2326	6	31	17	0.19	1.82	II	1583 + 753

*Ground state values are given in parentheses (See reference 123).

Table 19

Squared Directional Cosines of the Molecular Axes with Respect to the Crystallographic Axes*

Paradichlorobenzene (133°K)

Molecular Axis	Crystallographic Axis		
	a	b	c
X	0	0.231	0.778
Y	0.472	0.412	0.116
Z	0.537	0.357	0.106

*From reference 71.

ACKNOWLEDGEMENTS

I would like to express my sincere appreciation to Professor C. B. Harris for his constant support and guidance throughout the course of this work. I am indebted to him for having shown me many fascinating and exciting aspects of science.

I would also like to thank Professor M. A. El-Sayed (University of California at Los Angeles) for supplying the samples of 8-chloroquinoline and 2-3 dichloroquinoxaline, and Professor A. H. Maki (University of California at Riverside) for supplying one of the pyrazine samples.

I would also like to express my appreciation to all of Professor Harris's graduate students and research associates for many stimulating discussions and especially Dr. A. H. Francis for his lucid explanations of the fundamentals of optical spectroscopy.

Thanks are also due to the many technical support groups at both the Chemistry Department and the Lawrence Radiation Laboratory and in particular the Chemistry Department machinists for their ability to fabricate equipment from only rudimentary instructions.

Finally I would like to thank my wife Barbara for her constant encouragement and support throughout the course of this work.

APPENDIX

Program ODMR

A. Description

This Fortran IV program written for the CDC 6600 computes the electron magnetic dipole allowed transition frequencies and probabilities as well as the energy levels for a spin system consisting of the triplet electrons and an arbitrary number of nuclei in the absence of an external magnetic field. The present form of the program accepts up to 4 different nuclear spins and will solve a spin Hamiltonian matrix up to 48×48. The number of nuclear spins may be increased to any necessary number by changing the dimensions of the appropriate matrices.

The program calculates the spin Hamiltonian matrix by evaluating the individual contributions from H_{SS}, H_Q and H_{HF} (see section III). The basis states of the spin Hamiltonian are the eigenstates of S_z for both the electron and nuclear spins. In order to allow for non-coincidence of the axis systems that diagonalize H_{SS}, H_Q and H_{HF}, a rotation of the nuclear quadrupole and/or nuclear hyperfine Hamiltonian axis systems about the y axis of H_{SS} is provided.

The individual matrix elements of H_{SS}, H_Q and H_{HF} are evaluated and collected into groups depending on the operators involved, such as S_zI_z, S_zI_+ etc. (see comment cards). The completed spin Hamiltonian is then diagonalized by subroutine HDIAG which was written by Marjorie Merwin, M.I.T., and converted for CDC 6600 operation by Bill Dempster, LRL Berkeley. The matrix multiplication necessary to compute the transition probabilities is performed by the Compass subroutine

FEMME (also written by Bill Dempster) which is approximately 5.5 times as fast as an equivalent Fortran subroutine. The frequencies and intensities, as well as the energy levels they connect, are then printed in order from the highest frequency transition to the lowest. In addition, the transitions are collected into groups differing in frequency by 0.05 MHz (see cards A-11 and A-279) and the weighted average of the transition frequencies and the summation of their intensities printed.

ENDOR transitions due only to the electron magnetic dipole operator are sorted into the triplet manifold in which they occur and also printed.

An option is provided to suppress printing of the matrix elements of the total spin Hamiltonian (OP1) as well as an option which permits only the weighted average of the transition frequencies to be printed (OP2).

B. Input Variables

Use one set of data cards for each calculation. For a definition of the terms used see section III.

CARD #1 (Format 3F10.3)

Col	1-10	X	H_{SS}
	11-20	Y	
	21-30	Z	

CARD #2 (Format 3I1)

Col 1 Number of nuclear spins

Col 2 If set equal to zero, the input spin Hamiltonian is not printed

Col 3 If set equal to zero, the complete list of transition frequencies is not printed

CARD #3 (Format 7F10.3, 2F5.0)

This card is necessary for each nuclear spin

Col 1-10 nuclear spin quantum number (I_z)

11-20 V_{xx}
21-30 V_{yy} } H_Q
31-40 V_{zz}

41-50 A_{xx}
51-60 A_{yy} } H_{HF}
61-70 A_{zz}

71-75 Rotation angle for H_Q about y axis of H_{SS} (in degrees)

76-80 Rotation angle for H_{HF} about y axis of H_{SS} (in degrees)

6789 Card

```
      PROGRAM ODMR (INPUT,OUTPUT,TAPE5=INPUT)                                   A    1
      DIMENSION A1(48),A(48,48),TK(48,48),EIVR(48,48)                           A    2
      DIMENSION E1(600,4),XXX(300,4)                                            A    3
      DIMENSION XM(5),YM(5),ZM(5),B(5),F(5),PH(5),X(5),J2(5),K2(5),IY(5)        A    4
      DIMENSION IZ(5),XA(5),AXX(5),AYY(5),QA(5),AS(5),S(5),S2(5),AZZ(5)         A    5
      DIMENSION C(5),C2(5),TH(5),Q(5)                                           A    6
      EQUIVALENCE (A,XXX),(E1,TK)                                               A    7
      REAL J2,K2                                                                A    8
      EE=SQRT(2.)                                                               A    9
      PI=3.14159265358979323846                                                 A   10
      RES=0.01                                                                  A   11
   10 CONTINUE                                                                  A   12
      CALL SECOND (ZAP)                                                         A   13
      READ 720, XM(1),YM(1),ZM(1)                                               A   14
      IF (EOF,5) 710,20                                                         A   15
   20 CONTINUE                                                                  A   16
      DO 30 L=1,15                                                              A   17
      B(L)=0.0                                                                  A   18
   30 CONTINUE                                                                  A   19
      DO 40 L=1,5                                                               A   20
      IZ(L)=1                                                                   A   21
   40 CONTINUE                                                                  A   22
      DO 50 I=1,600                                                             A   23
      DO 50 J=1,4                                                               A   24
      E1(I,J)=0.0                                                               A   25
   50 CONTINUE                                                                  A   26
      X(1)=1                                                                    A   27
      IY(1)=3                                                                   A   28
      D=-3*ZM(1)/2.                                                             A   29
      E=(YM(1)-XM(1))/2.                                                        A   30
      READ 730, N,OP1,OP2                                                       A   31
      N1=N+1                                                                    A   32
      DO 60 I=2,N1                                                              A   33
      READ 740, X(I),XM(I),YM(I),ZM(I),AXX(I),AYY(I),AZZ(I),TH(I),PH(I)         A   34
      THP=(TH(I)/180.)*PI                                                       A   35
      PHP=(PH(I)/180.)*PI                                                       A   36
      S(I)=SIN(THP)                                                             A   37
      C(I)=COS(THP)                                                             A   38
      B(I)=SIN(PHP)                                                             A   39
      F(I)=COS(PHP)                                                             A   40
      S2(I)=(B(I))*(B(I))                                                       A   41
      C2(I)=(F(I))*(F(I))                                                       A   42
      XA(I)=(X(I))*(X(I))+X(I)                                                  A   43
      Q(I)=ZM(I)                                                                A   44
      IF (Q(I).EQ.0.0) GO TO 60                                                 A   45
      QA(I)=Q(I)/(8*(X(I))**2-4*(X(I)))                                         A   46
      AS(I)=(XM(I)-YM(I))/ZM(I)                                                 A   47
   60 CONTINUE                                                                  A   48
      NZ=3                                                                      A   49
      DO 70 I=2,N1                                                              A   50
      IY(I)=2*(X(I))+1                                                          A   51
      NZ=NZ*IY(I)                                                               A   52
   70 CONTINUE                                                                  A   53
      IF (OP1.EQ.0) GO TO 80                                                    A   54
      PRINT 750, NZ,NZ                                                          A   55
   80 CONTINUE                                                                  A   56
      DO 90 I=1,NZ                                                              A   57
      DO 90 J=1,NZ                                                              A   58
```

```
      A(I,JJ)=0.                                                        A  59
      JK(I,JJ)=0.                                                       A  60
   90 CONTINUE                                                          A  61
      DO 100 I=1,N                                                      A  62
      MAP=I+1                                                           A  63
      DO 100 J=MAP,N1                                                   A  64
      IZ(I)=IZ(I)*IY(J)                                                 A  65
  100 CONTINUE                                                          A  66
      DO 35  II=1,NZ                                                    A  67
      DO 110 I=1,N1                                                     A  68
      MAX=(II-1)/IZ(I)                                                  A  69
      J2(I)=X(I)-MAX*(MAX/IY(I))*(IY(I))                                A  70
  110 CONTINUE                                                          A  71
      DO 33  JJ=II,NZ                                                   A  72
      DO 120 I=1,N1                                                     A  73
      MAX=(JJ-1)/IZ(I)                                                  A  74
      K2(I)=X(I)-MAX*(MAX/IY(I))*(IY(I))                                A  75
  120 CONTINUE                                                          A  76
      IF (J2(1).NE.K2(1)) GO TO 210                                     A  77
      DO 130 I=2,N1                                                     A  78
      K=I                                                               A  79
      IF (J2(I).NE.K2(I)) GO TO 150                                     A  80
  130 CONTINUE                                                          A  81
C                     ********** SZ IZ **********                      A  82
      DO 140 I=2,N1                                                     A  83
      A(II,JJ)=A(II,JJ)+(QA(I)/2.)*(3*(J2(I))**2-XA(I))*((3.-AS(I))*(C(I  A  84
     1))**2+AS(I)-1)+(J2(1))*(J2(I))*((AZZ(I))*(C2(I))+(AXX(I))*(S2(I)))  A  85
  140 CONTINUE                                                          A  86
      A(II,JJ)=A(II,JJ)+(D*((J2(1))**2-(2./3.)))                        A  87
      GO TO 320                                                         A  88
  150 CONTINUE                                                          A  89
      IF (J2(K).NE.(K2(K)+1)) GO TO 180                                 A  90
      L=K+1                                                             A  91
      IF (L.GT.N1) GO TO 170                                            A  92
      DO 160 I=L,N1                                                     A  93
      IF (J2(I).NE.K2(I)) GO TO 320                                     A  94
  160 CONTINUE                                                          A  95
C                     ********** SZ I+ **********                      A  96
  170 CONTINUE                                                          A  97
      A(II,JJ)=A(II,JJ)+(QA(K)/2.)*(K2(K)+J2(K))*(SQRT(XA(K)-(K2(K))*(J2  A  98
     1(K))))*((C(K))*(S(K)))*(AS(K)-3.)+(J2(1))*(SQRT(XA(K)-(K2(K))*(J2(  A  99
     2K))))*(AZZ(K)-AXX(K))*(B(K))*(F(K))                               A 100
      GO TO 320                                                         A 101
  180 CONTINUE                                                          A 102
      IF (J2(K).NE.(K2(K)+2)) GO TO 320                                 A 103
      L=K+1                                                             A 104
      IF (L.GT.N1) GO TO 200                                            A 105
      DO 190 I=L,N1                                                     A 106
      IF (J2(I).NE.K2(I)) GO TO 320                                     A 107
  190 CONTINUE                                                          A 108
C                     ********** SZ I+**2 **********                   A 109
  200 CONTINUE                                                          A 110
      A(II,JJ)=(QA(K)/4)*(SQRT((XA(K)-(K2(K))**2-K2(K))*(XA(K)-(J2(K))*(  A 111
     1K2(K))-J2(K))))*(3*(S(K))**2+AS(K)*((C(K))**2+1))                 A 112
      GO TO 320                                                         A 113
  210 CONTINUE                                                          A 114
      IF (J2(1).NE.(K2(1)+1)) GO TO 300                                 A 115
      DO 220 I=2,N1                                                     A 116
```

```
      K=I                                                                A 117
      IF (J2(I).NE.K2(I)) GO TO 240                                      A 118
  230 CONTINUE                                                           A 119
C                     ********** S+ IZ **********                       A 120
      DO 230 I=2,M                                                       A 121
      A(II,JJ)=A(II,JJ)+FF*(K2(I))*(P(I))*(F(I))*(AZZ(I)-AXX(I))         A 122
  230 CONTINUE                                                           A 123
  240 CONTINUE                                                           A 124
      IF (J2(K).EQ.(K2(K)+1)) GO TO 270                                  A 125
      L=K+1                                                              A 126
      IF (L.GT.M1) GO TO 260                                             A 127
      DO 250 I=L,M1                                                      A 128
      IF (J2(I).NE.K2(I)) GO TO 320                                      A 129
  250 CONTINUE                                                           A 130
C                     ********** S+ I+ **********                       A 131
  260 CONTINUE                                                           A 132
      A(II,JJ)=A(II,JJ)+(((AXX(K))*(C2(K))+(AZZ(K))*(S2(K))-AYY(K))/4.)* A 133
     1FF*(SQRT(XA(K)-(K2(K))*(J2(K))))                                   A 134
      GO TO 320                                                          A 135
  270 CONTINUE                                                           A 136
      IF (J2(K).NE.(K2(K)-1)) GO TO 320                                  A 137
      L=K+1                                                              A 138
      IF (L.GT.M1) GO TO 290                                             A 139
      DO 280 I=L,M1                                                      A 140
      IF (J2(I).NE.K2(I)) GO TO 320                                      A 141
  280 CONTINUE                                                           A 142
C                     ********** S+ I- **********                       A 143
  290 CONTINUE                                                           A 144
      A(II,JJ)=A(II,JJ)+(((AXX(K))*(C2(K))+(AZZ(K))*(S2(K))+AYY(K))/4.)* A 145
     1FF*(SQRT(XA(K)-(K2(K))*(J2(K))))                                   A 146
      GO TO 320                                                          A 147
  300 CONTINUE                                                           A 148
      IF (J2(1).NE.(K2(I)+2)) GO TO 320                                  A 149
      DO 310 I=2,M1                                                      A 150
      IF (J2(I).NE.K2(I)) GO TO 320                                      A 151
C                     ********** S+=2 **********                        A 152
  310 CONTINUE                                                           A 153
      A(II,JJ)=A(II,JJ)+F                                                A 154
  320 CONTINUE                                                           A 155
  330 CONTINUE                                                           A 156
      IF (OP1.EQ.0) GO TO 360                                            A 157
      DO 350 I=1,NZ                                                      A 158
      DO 350 J=I,NZ                                                      A 159
      IF (A(I,J).EQ.0.0) GO TO 340                                       A 160
      PRINT 760, I,J,A(I,J)                                              A 161
  340 CONTINUE                                                           A 162
  350 CONTINUE                                                           A 163
      CALL SECOND (ZAP)                                                  A 164
      PRINT 850, ZAP                                                     A 165
  360 CONTINUE                                                           A 166
      CALL PRTAG (A,NZ,0,EIVR,NP,48)                                     A 167
      IF (OP1.EQ.0) GO TO 370                                            A 168
      PRINT 770, NP                                                      A 169
      CALL SECOND (ZAP)                                                  A 170
      PRINT 850, ZAP                                                     A 171
  370 CONTINUE                                                           A 172
      PRINT 780, N                                                       A 173
      PRINT 790, D,E,XM(1),YM(1),ZM(1)                                   A 174
```

```
      DO 380 I=2,N1                                                    A 175
      J=I-1                                                            A 176
      PRINT 800, J,X(I),Q(I),AS(I),XM(I),YM(I),ZM(I)                   A 177
      PRINT 810, AXX(I),AYY(I),AZZ(I),TH(I),PH(I)                      A 178
  380 CONTINUE                                                         A 179
      PRINT 820                                                        A 180
      DO 390 I=1,NZ                                                    A 181
      PRINT 830, I,A(I,I)                                              A 182
  390 CONTINUE                                                         A 183
      DO 400 I=1,NZ                                                    A 184
      A1(I)=A(I,I)                                                     A 185
  400 CONTINUE                                                         A 186
      N3=NZ/3                                                          A 187
      N2=2*N3                                                          A 188
      DO 410 I=1,NZ                                                    A 189
      DO 410 J=1,NZ                                                    A 190
      A(I,J)=0.0                                                       A 191
  410 CONTINUE                                                         A 192
      DO 420 I=1,N3                                                    A 193
      J=I+N2                                                           A 194
      A(I,I)=1.                                                        A 195
      A(J,J)=-1.                                                       A 196
  420 CONTINUE                                                         A 197
      DO 430 I=1,N2                                                    A 198
      J=N3+I                                                           A 199
      A(I,J)=FF                                                        A 200
  430 CONTINUE                                                         A 201
      CALL FEMME (A,EIVR,TK,NZ,NZ,48)                                  A 202
      DO 440 I=1,NZ                                                    A 203
      DO 440 J=1,NZ                                                    A 204
      A(I,J)=EIVR(J,I)                                                 A 205
  440 CONTINUE                                                         A 206
      DO 450 I=1,NZ                                                    A 207
      DO 450 J=1,NZ                                                    A 208
      EIVR(I,J)=A(I,J)                                                 A 209
      A(I,J)=0.0                                                       A 210
  450 CONTINUE                                                         A 211
      CALL FEMME (EIVR,TK,A,NZ,NZ,48)                                  A 212
      DO 460 I=1,NZ                                                    A 213
      DO 460 J=1,NZ                                                    A 214
      A(I,J)=ABS(A(I,J)*A(J,I))                                        A 215
  460 CONTINUE                                                         A 216
      CALL SECOND (ZAP)                                                A 217
      PRINT 850, ZAP                                                   A 218
      II=0                                                             A 219
      DO 500 I=1,NZ                                                    A 220
      J=I+1                                                            A 221
      IF (J.GT.NZ) GO TO 490                                           A 222
      DO 480 K=J,NZ                                                    A 223
      IF (A(I,K).LE.1.0E-9) GO TO 470                                  A 224
      II=II+1                                                          A 225
      IF (II.GT.599) GO TO 510                                         A 226
      E1(II,1)=ABS(A1(I)-A1(K))                                        A 227
      E1(II,2)=A(I,K)                                                  A 228
      E1(II,3)=I                                                       A 229
      E1(II,4)=K                                                       A 230
  470 CONTINUE                                                         A 231
  480 CONTINUE                                                         A 232
```

```
 490 CONTINUE                                                          A 233
 500 CONTINUE                                                          A 234
     GO TO 520                                                         A 235
 510 CONTINUE                                                          A 236
     PRINT 840                                                         A 237
 520 CONTINUE                                                          A 238
     DO 560 K=1,II                                                     A 239
     EMAX=0.0                                                          A 240
     DO 550 I=K,II                                                     A 241
     IF (EMAX-E1(I,1)) 530,530,540                                     A 242
 530 CONTINUE                                                          A 243
     EMAX=E1(I,1)                                                      A 244
     MI=I                                                              A 245
 540 CONTINUE                                                          A 246
 550 CONTINUE                                                          A 247
     TEMP1=E1(K,1)                                                     A 248
     TEMP2=E1(K,2)                                                     A 249
     TEMP3=E1(K,3)                                                     A 250
     TEMP4=E1(K,4)                                                     A 251
     E1(K,1)=E1(MI,1)                                                  A 252
     E1(K,2)=E1(MI,2)                                                  A 253
     E1(K,3)=E1(MI,3)                                                  A 254
     E1(K,4)=E1(MI,4)                                                  A 255
     E1(MI,1)=TEMP1                                                    A 256
     E1(MI,2)=TEMP2                                                    A 257
     E1(MI,3)=TEMP3                                                    A 258
     E1(MI,4)=TEMP4                                                    A 259
 560 CONTINUE                                                          A 260
     IF (OP2.EQ.0) GO TO 580                                           A 261
     PRINT 860                                                         A 262
     DO 570 I=1,II                                                     A 263
     IF (E1(I,1).LT.0.1) GO TO 570                                     A 264
     LEV1=E1(I,3)                                                      A 265
     LEV2=E1(I,4)                                                      A 266
     PRINT 870, LEV1,LEV2,E1(I,1),E1(I,2)                              A 267
 570 CONTINUE                                                          A 268
 580 CONTINUE                                                          A 269
     PRINT 880, PES                                                    A 270
     PRINT 890                                                         A 271
     TEMP2=0.0                                                         A 272
     TEMP1=0.0                                                         A 273
     II=II-1                                                           A 274
     NP=1                                                              A 275
     DO 630 I=1,II                                                     A 276
     J=I+1                                                             A 277
     AXE=E1(I,1)-E1(J,1)                                               A 278
     IF (AXE.LE.AFS) GO TO 590                                         A 279
     GO TO 600                                                         A 280
 590 NP=NP+1                                                           A 281
     IF (NP.EQ.2) JR=I                                                 A 282
     GO TO 620                                                         A 283
 600 IF (NP.EQ.1) JR=I                                                 A 284
     NP=I                                                              A 285
     DO 610 JM=JR,MR                                                   A 286
     TEMP1=TEMP1+E1(JM,1)                                              A 287
     TEMP2=TEMP2+E1(JM,2)                                              A 288
 610 CONTINUE                                                          A 289
     TEMP1=TEMP1/NP                                                    A 290
```

```
      PRINT 900, TEMP1,TEMP2,NP                                          A 291
      NP=1                                                               A 292
      TEMP1=0.0                                                          A 293
      TEMP2=0.0                                                          A 294
  620 CONTINUE                                                           A 295
  630 CONTINUE                                                           A 296
      N3=NZ/3                                                            A 297
      K=0                                                                A 298
      II=II+1                                                            A 299
      DO 660 I=1,II                                                      A 300
      LEV1=E1(I,3)                                                       A 301
      LEV2=E1(I,4)                                                       A 302
      NL1=(LEV1-1)/N3                                                    A 303
      NL2=(LEV2-1)/N3                                                    A 304
      IF (NL1.EQ.NL2) GO TO 640                                          A 305
      GO TO 650                                                          A 306
  640 CONTINUE                                                           A 307
      K=K+1                                                              A 308
      XXX(K,1)=E1(I,1)                                                   A 309
      XXX(K,2)=E1(I,2)                                                   A 310
      XXX(K,3)=E1(I,3)                                                   A 311
      XXX(K,4)=E1(I,4)                                                   A 312
  650 CONTINUE                                                           A 313
  660 CONTINUE                                                           A 314
      PRINT 910                                                          A 315
      DO 700 I=1,3                                                       A 316
      N1=(I-1)*N3+1                                                      A 317
      N2=I*N3                                                            A 318
      PRINT 920, N1,N2                                                   A 319
      PRINT 930                                                          A 320
      DO 690 J=1,K                                                       A 321
      LEV1=XXX(J,3)                                                      A 322
      LEV2=XXX(J,4)                                                      A 323
      IF (LEV1.GE.N1.AND.LEV1.LE.N2) GO TO 670                           A 324
      GO TO 680                                                          A 325
  670 IF (XXX(J,1).LE.0.1) GO TO 680                                     A 326
      PRINT 940, LEV1,LEV2,XXX(J,1),XXX(J,2)                             A 327
  680 CONTINUE                                                           A 328
  690 CONTINUE                                                           A 329
  700 CONTINUE                                                           A 330
      GO TO 10                                                           A 331
  710 CONTINUE                                                           A 332
C                                                                        A 333
C                                                                        A 334
  720 FORMAT(3E10.3)                                                     A 335
  730 FORMAT(3I1)                                                        A 336
  740 FORMAT(7E10.4,2E5.0)                                               A 337
  750 FORMAT(1H1,*THIS MATRIX SHOULD HAVE BEEN DIMENSION *,I3,* X *,I3)  A 338
  760 FORMAT(10X,2I5,E10.3)                                              A 339
  770 FORMAT(//,10X,*NP=*,I5)                                            A 340
  780 FORMAT(1H1,*INPUT PARAMETERS, TRIPLET PLUS *,I1,* NUCLEAR FUNCTION A 341
     1(S)*)                                                              A 342
  790 FORMAT(//,10X,*D=*,F9.3,7X,*E=*,F9.3,6X,*X=*,F9.3,6X,*Y=*,F9.3,6X, A 343
     1*Z=*,F9.3)                                                         A 344
  800 FORMAT(//,10X,*N=*,I1,5X,*S=*,F4.1,5X,*Q=*,F7.3,5X,*AS=*,F6.2,5X,*V A 345
     1XX=*,F7.3,5X,*VYY=*,F7.3,5X,*VZZ=*,F7.3)                           A 346
  810 FORMAT(26X,*AXX=*,F6.1,5X,*AYY=*,F6.1,5X,*AZZ=*,F6.1,4X,*THETA=*,F A 347
     15.1,6X,*PSI=*,F6.1)                                                A 348
  820 FORMAT(///,10X,*LEVEL     ENERGY (MHZ)*,///)                       A 349
  830 FORMAT(/,10X,I3,*X,F10.3)                                          A 350
  840 FORMAT(//,*WARNING E1 MATRIX NOT LARGE ENOUGH*)                    A 351
  850 FORMAT(//,10X,*CP=*,F9.3)                                          A 352
  860 FORMAT(1H1,12X,*TRANSION*,7X,*FREQUENCY*,5X,*INTENSITY*,///)       A 353
  870 FORMAT(/,11X,I3,*  -*,I3,6X,F10.3,5X,E10.3)                        A 354
  880 FORMAT(1H1,10X,*TRANSISTIONS COLLECTED INTO GROUPS WITH A FREQUENC A 355
     1Y DIFFERENCE LESS THEN OR EQUAL TO *,F8.5,* MHZ*)                  A 356
  890 FORMAT(///,12X,*FREQUENCY*,5X,*INTENSITY*,5X,*NUMBER*,///)         A 357
  900 FORMAT(10X,F10.3,5X,E10.3,7X,I3,//)                                A 358
  910 FORMAT(1H1)                                                        A 359
  920 FORMAT(5/,10X,*ENDOR TRANSISTIONS ASSOCIATED WITH LEVELS*,I3,* TO  A 360
     1*,I3,* INCLUSIVE*,///)                                             A 361
  930 FORMAT(10X,*LEVEL 1     LEVEL 2     FREQUENCY     INTENSITY*,///)  A 362
  940 FORMAT(13X,I3,8X,I3,5X,F10.3,5X,E10.3,///)                         A 363
      END                                                                A 364-
```

```
      FORTRAN IV SUBROUTINE HDIAG(H,N,IEGEN,U,NR,NDIMEN)                B    1
      DIMENSION H(NDIMEN,1),U(NDIMEN,1),X(48),IQ(48)                    B    2
      IF (IEGEN) 50,10,50                                               B    3
   10 DO 40 I=1,N                                                       B    4
      DO 40 J=1,N                                                       B    5
      IF (I-J) 30,20,30                                                 B    6
   20 U(I,J)=1.0                                                        B    7
      GO TO 40                                                          B    8
   30 U(I,J)=0.0                                                        B    9
   40 CONTINUE                                                          B   10
      N2=(2*N)/3                                                        B   11
   50 NR=0                                                              B   12
      IF (N-1) 430,430,60                                               B   13
   60 NM1=N-1                                                           B   14
      DO 80 I=1,NM1                                                     B   15
      X(I)=0.0                                                          B   16
      IPL1=I+1                                                          B   17
      DO 80 J=IPL1,N                                                    B   18
      KILL=I-J                                                          B   19
      IF (KILL.EQ.N2) GO TO 70                                          B   20
      IF (X(I)-ABS(H(I,J))) 70,70,80                                    B   21
   70 X(I)=ABS(H(I,J))                                                  B   22
      IQ(I)=J                                                           B   23
   80 CONTINUE                                                          B   24
      RAP=.1640400000000000000                                          B   25
      HDTEST=1.0E307                                                    B   26
   90 DO 120 I=1,NM1                                                    B   27
      IF (I-1) 110,110,100                                              B   28
  100 IF (XMAX-X(I)) 110,120,120                                        B   29
  110 XMAX=X(I)                                                         B   30
      IPIV=I                                                            B   31
      JPIV=IQ(I)                                                        B   32
  120 CONTINUE                                                          B   33
      IF (XMAX) 430,430,130                                             B   34
  130 IF (HDTEST) 150,150,140                                           B   35
  140 IF (XMAX-HDTEST) 150,150,180                                      B   36
  150 HDIMIN=ABS(H(1,1))                                                B   37
      DO 170 I=2,N                                                      B   38
      IF (HDIMIN-ABS(H(I,I))) 170,170,160                               B   39
  160 HDIMIN=ABS(H(I,I))                                                B   40
  170 CONTINUE                                                          B   41
      HDTEST=HDIMIN*RAP                                                 B   42
      IF (HDTEST-XMAX) 180,430,430                                      B   43
  180 NR=NR+1                                                           B   44
      TANG=SIGN(2.0,(H(IPIV,IPIV)-H(JPIV,JPIV)))*H(IPIV,JPIV)/(ABS(H(IPI  B   45
     1V,IPIV)-H(JPIV,JPIV))+SQRT((H(IPIV,IPIV)-H(JPIV,JPIV))**2+4.0*H(IP  B   46
     2IV,JPIV)**2))                                                     B   47
      COSINE=1.0/SQRT(1.0+TANG**2)                                      B   48
      SINE=TANG*COSINE                                                  B   49
      HII=H(IPIV,IPIV)                                                  B   50
      H(IPIV,IPIV)=COSINE**2*(HII+TANG*(2.0*H(IPIV,JPIV)+TANG*H(JPIV,JPI  B   51
     1V)))                                                              B   52
      H(JPIV,JPIV)=COSINE**2*(H(JPIV,JPIV)-TANG*(2.0*H(IPIV,JPIV)-TANG*H  B   53
     1II))                                                              B   54
      H(IPIV,JPIV)=0.0                                                  B   55
      IF (H(IPIV,IPIV)-H(JPIV,JPIV)) 190,200,200                        B   56
  190 HTEMP=H(IPIV,IPIV)                                                B   57
      H(IPIV,IPIV)=H(JPIV,JPIV)                                         B   58
```

```
      H(JPIV,JPIV)=HTEMP                                                B  59
      HTEMP=SIGN(1.0,-SINE)*COSINE                                      B  60
      COSINE=ABS(SINE)                                                  B  61
      SINE=HTEMP                                                        B  62
  200 CONTINUE                                                          B  63
      DO 270 I=1,NM11                                                   B  64
      IF (I-IPIV) 220,270,210                                           B  65
  210 IF (I-JPIV) 220,270,220                                           B  66
  220 IF (IQ(I)-IPIV) 230,240,230                                       B  67
  230 IF (IQ(I)-JPIV) 270,240,270                                       B  68
  240 K=IQ(I)                                                           B  69
      HTEMP=H(I,K)                                                      B  70
      H(I,K)=0.0                                                        B  71
      IPL1=I+1                                                          B  72
      X(I)=0.0                                                          B  73
      DO 260 J=IPL1,N                                                   B  74
      IF (X(I)-ABS(H(I,J))) 250,250,260                                 B  75
  250 X(I)=ABS(H(I,J))                                                  B  76
      IQ(I)=J                                                           B  77
  260 CONTINUE                                                          B  78
      H(I,K)=HTEMP                                                      B  79
  270 CONTINUE                                                          B  80
      X(IPIV)=0.0                                                       B  81
      X(JPIV)=0.0                                                       B  82
      DO 400 I=1,N                                                      B  83
      IF (I-IPIV) 280,400,320                                           B  84
  280 HTEMP=H(I,IPIV)                                                   B  85
      H(I,IPIV)=COSINE*HTEMP+SINE*H(I,JPIV)                             B  86
      IF (X(I)-ABS(H(I,IPIV))) 290,300,300                              B  87
  290 X(I)=ABS(H(I,IPIV))                                               B  88
      IQ(I)=IPIV                                                        B  89
  300 H(I,JPIV)=-SINE*HTEMP+COSINE*H(I,JPIV)                            B  90
      IF (X(I)-ABS(H(I,JPIV))) 310,400,400                              B  91
  310 X(I)=ABS(H(I,JPIV))                                               B  92
      IQ(I)=JPIV                                                        B  93
      GO TO 400                                                         B  94
  320 IF (I-JPIV) 330,400,360                                           B  95
  330 HTEMP=H(IPIV,I)                                                   B  96
      H(IPIV,I)=COSINE*HTEMP+SINE*H(I,JPIV)                             B  97
      IF (X(IPIV)-ABS(H(IPIV,I))) 340,350,350                           B  98
  340 X(IPIV)=ABS(H(IPIV,I))                                            B  99
      IQ(IPIV)=I                                                        B 100
  350 H(I,JPIV)=-SINE*HTEMP+COSINE*H(I,JPIV)                            B 101
      IF (X(I)-ABS(H(I,JPIV))) 310,400,400                              B 102
  360 HTEMP=H(IPIV,I)                                                   B 103
      H(IPIV,I)=COSINE*HTEMP+SINE*H(JPIV,I)                             B 104
      IF (X(IPIV)-ABS(H(IPIV,I))) 370,380,380                           B 105
  370 X(IPIV)=ABS(H(IPIV,I))                                            B 106
      IQ(IPIV)=I                                                        B 107
  380 H(JPIV,I)=-SINE*HTEMP+COSINE*H(JPIV,I)                            B 108
      IF (X(JPIV)-ABS(H(JPIV,I))) 390,400,400                           B 109
  390 X(JPIV)=ABS(H(JPIV,I))                                            B 110
      IQ(JPIV)=I                                                        B 111
  400 CONTINUE                                                          B 112
      IF (IEGEN) 90,410,90                                              B 113
  410 DO 420 I=1,N                                                      B 114
      HTEMP=U(I,IPIV)                                                   B 115
      U(I,IPIV)=COSINE*HTEMP+SINE*U(I,JPIV)                             B 116
  420 U(I,JPIV)=-SINE*HTEMP+COSINE*U(I,JPIV)                            B 117
      GO TO 90                                                          B 118
  430 RETURN                                                            B 119
      END                                                               B 120-
```

```
                                ENTRY FEMME
                        *     THIS IS ASCENT SUBROUTINE FEMME(A,B,C,N,NC,L)
                         FEMME  BSSZ 1          .VERY HIGH SPEED MATRIX MULTIPLICATION,SAME AS
                  0000000 +     ENT    EQU  FEMME
56440                           SA4 B4         .FETCH N      .THE FOLLOWING FORTRAN
     56560                      SA5 B6         .FETCH L      .   DIMENSIONA(L,1),B(L,1),C(L,1)
          27604                 PX6 X4                       .   IF(N .LE. 0) RETURN
               56150            SA1 B5         .FETCH NC     .   IF(NC .LE. 0) RETURN
14711                           RX7 -X1                      .   DO 3 I = 1,N
     5170000020 +               SA7 MNC        .SAVE -NC     .   DO 2 J = 1,NC
               27005            PX0 X5                       .   C(I,J) = 0.
42206                           DX2 X0*X6                    .   DO 1 K = 1,N
     14122                      BX1 -X2                      .   C(I,J) = C(I,J)+A(I,K)*B(K,J)
          63610                 SB6 X1         .B6 HAS -N*L  . 1 CONTINUE
               27307            PX3 X7                       . 2 CONTINUE
63440                           SB4 X4         .B4 HAS N     . 3 CONTINUE
     42203                      DX2 X0*X3                    .   RETURN
          63720                 SB7 X2         .B7 HAS -NC*L.   END
               56110            SA1 B1         .INITIALIZE A1 AND X1
54220                           SA2 B2         .INITIALIZE A2 AND X2
     6110000001                 SB1 1          .B1 HAS 1
0741000000 +                    LT  B4,B1,ENT  .IF N .LE. 0 RETURN
          67537                 SB5 B3-B7
               63350            SB3 X5         .B3 HAS L
57051                           SA0 B5-B1      .INITIALIZE A0
     63570                      SB5 X7         .TEMPORARILY SET B5 TO -NC
          14544                 BX5 -X4        .INITIALIZE I COUNTER TO -N
               76710            SX7 B1         .X7 HAS 1
0650000000 +                    GE  B5,B0,ENT  .IF NC .LE. 0, RETURN
          67234                 SB2 B3-B4      .B2 HAS L-N
54470                    L1     SA4 A7         .INITIALIZE X4 TO -NC (I COUNTER)
     36557                      IX5 X5+X7      .INCREMENT I
          74007                 SX0 A0+B7
               53001            SA0 X0+B1      .A0 HAS THE ADDRESS OF C(I,1)
43600                    L2     MX6 0          .INITIALIZE C(I,J) TO ZERO
     66500                      SB5 B0         .INITIALIZE B5 (K COUNTER)
          46000                 NO
               36447            IX4 X4+X7      .INCREMENT J
40312                    L3     FX3 X1*X2      .A(I,K)*B(K,J)
     54113                      SA1 A1+B3      .FETCH A(I,K+1) FOR NEXT CYCLE
          66551                 SB5 B5+B1      .INCREMENT K
               30063            FX0 X6+X3      .C(I,J) + A(I,K)*B(K,J)
24600                           NX6 X0         .NORMALIZE SUM
     54221                      SA2 A2+B1      .FETCH B(K+1,J) FOR NEXT CYCLE
          0754000013 +          LT  B5,B4,L3   .TEST K
54520                           SA6 A0         .STORE SUM IN C(I,J)
     54116                      SA1 A1+B6      .READJUST A1 TO ADDRESS OF A(I,1)
          54222                 SA2 A2+B2      .SET A2 TO ADDRESS OF B(1,J+1)
               54003            SA0 A0+B3      .A0 NOW HAS ADDRESS OF C(I,J+1)
0314000012 +                    NZ  X4,L2      .TEST J
          54111                 SA1 A1+B1      .SET A1 TO ADDRESS OF A(I+1,1)
               54227            SA2 A2+B7      .SET A2 TO ADDRESS OF B(1,1)
0315000011 +                    NZ  X5,L1      .TEST I
          0400000000 +          EQ  B0,B0,ENT
                         MNC    BSSZ 1
                                END
```

References

1. S. P. McGlynn, T. Azumi and M. Kinoshito, Molecular Spectroscopy of the Triplet State (Prentice Hall Inc., 1969).

2. R. S. Becker, Theory and Interpretation of Fluorescence and Phosphorescence (Wiley Interscience, John Wiley & Sons, Inc., 1969).

3. S. K. Lower and M. A. El-Sayed, Chem. Rev., 66, 199 (1966).

4. M. S. DeGroot, I. A. M. Hesselmann and J. H. van der Waals, Mol. Phys., 12, 259 (1967).

5. G. N. Lewis and M. J. Kasha, J. Am. Chem. Soc. 66, 2100 (1944).

6. G. N. Lewis and M. J. Kasha, J. Am. Chem. Soc. 67, 994 (1945).

7. G. N. Lewis and M. Calvin, J. Am. Chem. Soc. 67, 1232 (1945).

8. G. N. Lewis, M. J. Kasha, and M. Calvin, J. Chem. Phys. 17, 804 (1949).

9. H. F. Hameka, thesis, Leiden (1956).

10. C. A. Hutchison and B. W. Mangum, J. Chem. Phys. 29, 952 (1958).

11. C. A. Hutchison and B. W. Mangum, J. Chem. Phys. 34, 908 (1961).

12. Ph. Kottis and R. Lefelivre, J. Chem. Phys. 39, 393 (1963).

13. Ph. Kottis and R. Lefelivre, J. Chem. Phys. 41, 379 (1964).

14. S. Geschwind, G. E. DeVlin, R. L. Cohen, and S. R. Chinn, Phys. Rev. 137, A1087 (1965).

15. J. Brossel and A. Kastler, Compt. Rend. 229, 1213 (1949).

16. J. Brossel and F. Bitter, Phys. Rev. 86, 308 (1952).

17. M. J. Scharnoff, J. Chem. Phys. 46, 3263 (1967).

18. A. L. Kwiram, Chem. Phys. Letters 1, 272 (1967).

19. J. Schmidt, I. A. M. Hesselmann, M. S. DeGroot and J. H. van der Waals, Chem. Phys. Letters 1, 434 (1967).

20. J. Schmidt and J. H. van der Waals, Chem. Phys. Letters 2, 640 (1968).

21. R. W. Brandon, R. E. Gerkin and C. A. Hutchinson, Jr., J. Chem Phys. 41, 3717 (1968).

22. J. Schmidt and J. H. van der Waals, Chem Phys. Letters 3, 546 (1969).

23. D. S. Tinti, M. A. El-Sayed, A. H. Maki and C. B. Harris, Chem. Phys. Letters 3, 343 (1969).

24. C. B. Harris, D. S. Tinti, M. A. El-Sayed and A. H. Maki, Chem. Phys. Letters 4, 409 (1969).

25. I. Y. Chan, J. Schmidt and J. H. van der Waals, Chem. Phys. Letters 4, 269 (1969).

26. M. J. Buckley, C. B. Harris, and A. H. Maki, Chem. Phys. Letters 4, 591 (1970).

27. M. J. Buckley and C. B. Harris, Chem. Phys. Letters 5, 205 (1970).

28. T. S. Kuan, D. S. Tinti and M. A. El-Sayed, Chem. Phys. Letters 4, 507 (1970).

29. M. A. El-Sayed, D. S. Tinti and E. M. Yee, J. Chem. Phys. 51, 5721 (1969).

30. M. A. El-Sayed, D. S. Tinti and O. V. Owens, Chem. Phys. Letters 3, 339 (1969).

31. M. A. El-Sayed, J. Chem. Phys. 52, 6438 (1970).

32. M. Schwoerer and H. C. Wolf, Molecular Crystals 3, 177 (1967).

33. M. A. El-Sayed and O. F. Kalman, J. Chem. Phys. 52, 4903 (1970).

34. M. Sharnoff, J. Chem. Phys. 51, 451 (1969).

35. M. Sharnoff, Symposium of the Faraday Society, No. 3, Magneto Optical Effects (1969).

36. D. Owens, M. A. El-Sayed and S. Ziegler, J. Chem. Phys. 52, 4315 (1970).

37. M. Sharnoff, Chem. Phys. Letters 2, 498 (1968).

38. L. Cheng and A. L. Kwiram, Chem. Phys. Letters 4, 457 (1969).

39. J. Schmidt, W. S. Veeman and J. H. van der Waals, Chem. Phys. Letters 4, 341 (1969).

40. R. W. Brandon, R. E. Gerkin and C. A. Hutchison, Jr., J. Chem. Phys. 37, 447 (1962).

41. C. A. Hutchison, Jr., Phys. Soc. Japan. 17, Suppl. B-1, 458 (1962).

42. J. S. Vincent and A. H. Maki, J. Chem. Phys. 39, 3088 (1963).

43. J. S. Vincent and A. H. Maki, J. Chem. Phys. 42, 865 (1965).

44. O. H. Griffith, J. Phys. Chem. 69, 1429 (1965).

45. S. W. Charles, P. H. H. Fisher and C. A. McDowell, Mol. Phys. 9, 517 (1965).

46. R. W. Brandon, G. L. Closs and C. A. Hutchison, Jr., J. Chem. Phys. 37, 1878 (1962).

47. R. W. Brandon, G. L. Closs, C. E. Davoust, C. A. Hutchison, Jr., B. E. Kohler and R. Silbey, J. Chem. Phys. 43, 2006 (1965).

48. C. A. Hutchison, Jr., J. Phys. Chem. 71, 203 (1967).

49. J. Ph. Grivet and J. M. Lhoste, Chem. Phys. Letters 3, 445 (1969).

50. J. S Vincent, J. Chem. Phys. 47, 1830 (1967).

51. W. S. Veeman and J. H. van der Waals, Chem. Phys. Letters 7, 65 (1970).

52. M. D. Fayer, D. A. Yuen and C. B. Harris, J. Chem Phys.,

53. C. B. Harris, J. Chem. Phys., in press.

54. D. Haarer and H. C. Wolf, Mol. Cryst. and Liq. Cryst. 10, 359 (1970).

55. J. Ph. Grivet, Chem. Phys. Letters 4, 104 (1969).

56. H. F. Hameka in The Triplet State (proc. International Symposium on the Triplet State, 1967)(Cambridge University Press, 1967) p. 25.

57. A. Carrington and A. D. McLachlan, Introduction to Magnetic Resonance (Harper and Row, 1967) p. 117.

58. T. P. Das and E. L. Hahn, Nuclear Quadrupole Resonance Spectroscopy, (Academic Press, New York/London, 1958).

59. M. H. Cohen and F. Reif, Solid State Physics V.5 (Academic Press, New York/London, 1957).

60. C. P. Slichter, Principles of Magnetic Resonance (Harper and Row, New York, 1963).

61. A. Abragam, The Principles of Nuclear Magnetism, (Oxford University Press, 1961).

62. E. A. C. Lucken, Nuclear Quadrupole Coupling Constants (Academic Press, New York/London, 1969).

63. M. S. de Groot, I. A. M. Hesselmann, J. Schmidt and J. H. van der Waals, Mol. Phys. 15, 17 (1968).

64. K. J. Standley and R. A. Vaughon, Electron Spin Relaxation Phenomena in Solids (Adam Hilger Ltd., London, 1969).

65. A. Abragam and B. Bleaney, Electron Paramagnetic Resonance of Transition Ions (Oxford University Press, 1970).

66. M. A. El-Sayed, D. S. Tinti and E. M. Yee, J. Chem. Phys. 51, 5721 (1970).

67. M. A. El-Sayed, D. S. Tinti and D. V. Owens, Chem. Phys. Letters 3, 339 (1969).

68. E. Gilmore, G. Gibson and D. McClure, J. Chem. Phys. 20, 829 (1952); 23, 399 (1955).

69. D. S. McClure, J. Chem. Phys. 17, 665 (1949).

70. D. S. McClure, J. Chem. Phys. 17, 905 (1949).

71. G. Castro and R. M. Hochstrasser, J. Chem. Phys. 46, 3617 (1967).

72. R. H. Webb, Rev. Sci. Instr. 33, 732 (1962).

73. M. Kasha, J. Opt. Sci. Am., 38, 929 (1948).

74. F. E. Terman, Electronic and Radio Engineering, (McGraw-Hill, 1955), p. 313.

75. B. H. Smith, Lawrence Radiation Laboratory Engineering Note, EE-1187 (1967).

76. A. H. Francis and C. B. Harris, Chem. Phys. Letters, in press.

77. M. Tinkham and M. W. P. Strandberg, Phys. Rev. 97, 937 (1955).

78. M. S. de Groot, I. A. M. Hesselmann and J. H. van der Waals, Mol. Phys. 10, 91 (1965).

79. S. L. Segal, R. G. Barnes and P. J. Bray, J. Chem. Phys. 25, 1286 (1956).

80. M. Dewar and E. Lucken, J. Chem. Soc. (London) 2653 (1958).

81. K. K. Innes, J. P. Byrne and I. G. Ross, J. Mol. Spectr. 22, 125 (1967).

82. L. Goodman and M. Kasha, J. Mol. Spectr. 2, 58 (1958).

83. J. E. Parkin and K. K. Innes, J. Mol. Spectr. 15, 407 (1965).

84. V. G. Krishna and L. Goodman, J. Chem. Phys. 36, 2217 (1962).

85. R. M. Hochstrasser and T. S. Lin, Symposium of the Farady Society, No. 3, Magneto Optical Effects (1969).

86. W. R. Moomaw and M. A. El-Sayed, J. Chem. Phys. 48, 2502 (1968).

87. H. Sternlicht, J. Chem. Phys. 38, 2316 (1963).

88. E. Schempp and P. J. Bray, J. Chem. Phys. 46, 1186 (1967).

89. P. B. Asycough, Electron Spin Resonance in Chemistry, Methuen and Co. Ltd. London (1967).

90. M. A. El-Sayed, W. R. Moomaw and D. S. Tinti, J. Chem. Phys. 50, 1888 (1969).

91. J. Higuchi, J. Chem. Phys. 39, 1339 (1963).

92. E. Clementi, J. Chem. Phys. 46, 4737 (1967).

93. M. S. De Groot, I. A. M. Hesselman and J. H. van der Waals, Mol. Phys. 16, 45 (1969).

94. N. Hirota, C. A. Hutchison, Jr., and P. Palmer, J. Chem. Phys. 40, 3717 (1964).

95. A. D. McLachlan, Mol. Phys. 5, 51 (1962).

96. C. L. Talcott and R. J. Myers, Mol. Phys. 12, 549 (1967).

97. G. A. George and G. C. Morris, Mol. Cryst. Liquid Cryst. 10, 187 (1970). 187 (1970).

98. R. R. Gilman and J. De Heer, J. Chem. Phys. 52, 4287 (1969).

99. P. G. Russell and A. C. Albrecht, J. Chem. Phys. 41, 2536 (1964).

100. M. D. Fayer and C. B. Harris, Inorg. Chem. 8, 2792 (1969).

101. M. S. De Groot and J. H. van der Waals, Mol. Phys. 6, 545 (1963).

102. M. Godfrey, C. W. Kern and M. Karplus, J. Chem. Phys. 44, 4459 (1966).

103. R. Bersohn, J. Chem. Phys. 22, 2078 (1954).

104. P. J. Bray, R. G. Barnes and R. Bersohn, J. Chem. Phys. 25, 813 (1956).

105. H. R. Falle, G. R. Luckhurst, A. Horsfield and M. Ballester, J. Chem. Phys. 50, 258 (1969).

106. D. Pooley and D. H. Whiffen, Spectrochim.Acta, 18, 291 (1962).

107. D. R. Kearns, J. Chem. Phys. 36, 1608 (1962).

108. A. C. Albrecht, J. Chem. Phys. 33, 157 (1960).

109. A. C. Albrecht, J. Chem. Phys. 38, 354 (1963).

110. C. Dean and R. V. Pound, J. Chem. Phys. 20, 195 (1952).

111. C. Dean, Thesis, Harvard University (1952).

112. C. H. Townes, Handbuch der Physik, edited by S. Flügge (Springer Verlag, Berlin, 1958), Vol. 38, p. 444.

113. M. Gouterman and W. Moffitt, J. Chem. Phys. 30, 1107 (1959).

114. M. Gouterman, J. Chem. Phys. 30, 1369 (1959).

115. H. Hamika, J. Chem. Phys. 31, 815 (1963).

116. Y. N. Chiu, J. Chem. Phys. 39, 2736 (1963).

117. A. Carrington and A. D. McLachlan, op.cit., p. 125-126.

118. H. Bayer, Z. Physik, 130, 227 (1951).

119. G. A. Jeffery and W. J. McVeagh, J. Chem. Phys. 23, 1165 (1955).

120. E. Frasson, C. Garbuguo and S. Bezzi, Acta Cryst. 12, 126 (1959).

121. A. H. Francis, Univ. of Calif. (Berkeley), personal communication (1970).

122. S. Saeki, Bull. Chem. Soc. Japan, 34, 1858 (1961).

123. M. Suzuki and M. Ito, Spectrochim. Acta, 25A, 1017 (1969).

124. C. A. Hutchison, Jr., J. V. Nicholas and G. W. Scott, J. Chem. Phys. 53, 1906 (1970).

TECHNICAL INFORMATION DIVISION
LAWRENCE RADIATION LABORATORY
UNIVERSITY OF CALIFORNIA
BERKELEY, CALIFORNIA 94720